A DNAZYME-LINKED SIGNAL AMPLIFICATION ASSAY

FOR BACTERIAL BIOSENSING

A DNAZYME-LINKED SIGNAL AMPLIFICATION ASSAY

FOR BACTERIAL BIOSENSING

By ALEXA MAINGUY, B.Sc. (Honours)

A Thesis Submitted to the School of Graduate Studies in Partial Fulfillment of the Requirements for the Degree Master of Science

MASTER OF SCIENCE (2021) McMaster University

(Chemical Biology) Hamilton, ON

TITLE: A DNAzyme-Linked Signal Amplification Assay For Bacterial Biosensing

AUTHOR: Alexa M. Mainguy, B.Sc. (Honours) (Queen's University)

SUPERVISOR: John D. Brennan

NUMBER OF PAGES: 96

ABSTRACT

RNA-cleaving DNAzymes (RCDs) are a class of functional nucleic acids that can bind various targets ranging in size from small molecules to large proteins, which results in activation of cleavage activity. The activation of RCDs results in the cleavage of a ribonucleotide site in an otherwise all-DNA substrate, leading to two cleavage fragments. In this work, a previously identified DNAzyme that binds to a protein biomarker endogenous to *Helicobacter pylori* (J99) crude extracellular matrix was evaluated for coupling to an isothermal amplification method termed rolling circle amplification (RCA) as a way to improve the originally reported detection limit. Three RCD constructs were designed with the goal of generating a cleavage fragment that could act as a primer to initiate RCA. The first method used the original HP DNAzyme, which liberated a short cleavage fragment that could be used as a primer. However, the primer fragment was rapidly digested by the bacterial matrix, preventing RCA. A second method evaluated use of a circularized substrate and separate RCD to generate a primer, however this system was not capable of generating a cleavage fragment. A final method redesigned the original RCD to move the substrate region from the 3' to the 5' end of the RCD, causing the longer RCD-containing fragment to be the primer for RCA. In this case, target-triggered cleavage was observed and the resulting primer was sufficiently resistant to digestion to allow its use as a primer for RCA. Preliminary characterization of the rearranged RCD showed that it retained selectivity similar to the original RCD, but that the cleavage rate was slower. In addition, the RCA based reaction, while successful, did not produce improved detection sensitivity relative to unamplified assays. Methods to further improve RCA performance are discussed for future work.

ACKNOWLEDGEMENTS

This work was completed during the COVID-19 pandemic, which prevented me from accessing the laboratory for approximately 6 months. The literature review (Chapter 2) served as an alternative sub-project during that time. I would like to thank Dr. John D. Brennan for his guidance and expertise while completing my graduate work within his lab. Dr. Brennan, in conjunction with my other committee member Dr. Yingfu Li, provided useful advice and insight into my project. I can't thank the other members of the Brennan group enough, both past and present – Dr. Michael Wolfe, Dr. Monsur Ali, Dr. Saeed Mohammadi, Dr. Julijana Milojevic, Steffi Ende. Special thanks to Dr. Roger Bialy, my favourite co-author and MVP lab mate. I would also like to thank the staff members of the Biointerfaces Institute for their knowledge, patience, and help in the lab. Special thanks to Dawn White for all her patience and generosity for helping me in the second half my thesis, specifically. I would be remiss if I didn't mention my friends, family, and boyfriend for their support over these ~~two~~ *three* years – thank you for putting up with me! Thank you to my parents for your support during this last year especially. I couldn't have done it without all of you. Lastly, thanks to Tammy Feher for all your help organizing all of my meetings.

"Science is… whatever we want it to be." *Dr. Spacemen, 30 Rock*

TABLE OF CONTENTS

LIST OF FIGURES

LIST OF TABLES

LIST OF ABBREVIATIONS

ATP	adenosine 5’-triphosphate
AuNPs	gold nanoparticles
CEM	crude extracellular matrix
DABCYL	4-(dimethylaminoazo)benzene-4-carboxylic acid
DNA	deoxyribonucleic acid
dNTPs	2’-deoxyribonucleoside 5’-triphosphates
dPAGE	denaturing polyacrylamide gel electrophoresis
dsDNA	double stranded DNA
FNAs	functional nucleic acids
FS28	ribonucleotide containing fluorogenic substrate
HRCA	hyperbranched rolling circle amplification
ITA	isothermal amplification
LFD	lateral flow device
MB	molecular beacon
MW	molecular weight
nt	nucleotide
POC	point of care
PON	point of need
PCR	polymerase chain reaction
PEG	polyethylene glycol
rA	riboadenosine
RCA	rolling circle amplification
RCD	RNA cleaving DNAzyme
RNA	ribonucleic acid
SELEX	systematic evolution of ligands by exponential enrichment
ssDNA	single stranded DNA
T4 PNK	T4 polynucleotide kinase
TSB	tryptic soy broth
UBT	urea breath test
WHO	world health organization

CHAPTER 1 | INTRODUCTION

Infectious pathogens and the diseases they cause are a great threat to human life throughout the world – a statement that rings especially true in light of the current coronavirus pandemic. Unlike some other human diseases, infectious diseases have unique characteristics that make them great targets for both prevention and eradication in part because a single agent perpetuates the disease.[1] Bacterial infections are a subset of infectious diseases, which are propagated by pathogenic bacteria. Even more frightening is the perniciousness of bacterial infections, especially with the increasing incidence of antimicrobial resistance, sometimes called antibiotic resistance. This leaves a substantial gap in the treatment options for bacterial diseases, increasing the likelihood of their spread. As such, rapid and sensitive detection of bacterial species is essential to mitigating and tracking spread of pathogenic disease globally and is commonly used for human and public health, biosecurity, and food and water safety.[1]

Helicobacter pylori is a pathogenic bacterium and known carcinogen that colonizes in the stomach, in severe cases escalating to dyspepsia, peptic ulcers, or gastric cancer.[2] With an overall prevalence of 44.3% in the world population, the world's highest infection rates are found in the developing world including the Caribbean and Latin America. [2,3] Testing methods for *H. pylori* infection are important for initial diagnosis, but also in monitoring the success of eradication therapy as is recommended in all cases of infection.[3] More and more of cases with treatment failure can be attributed to an increased incidence of antibacterial resistant *H. pylori* strains,[4] further highlighting the importance of post-treatment testing.

While invasive diagnostic methods like endoscopic biopsy and subsequent histology are highly accurate, non-invasive methods are required to allow faster testing times, greater simplicity and lower overall test cost.[4] Additionally, non-invasive methods are preferred for

post-treatment success monitoring. Two of the gold standards for non-invasive detection are the stool antigen test and urea breath test, [5,6] though these tests are regularly administered in clinical settings and not at the point of care (POC). In addition, current rapid antigen tests show poor sensitivity,[5] while urea breath tests require either scintillation counting or mass spectrometry to detect the exhaled products of urea hydrolysis (typically radiolabelled or isotopically labelled carbon dioxide).[6] As a result, novel methods of bacterial detection that can compete with conventional multi-day laboratory testing are sorely needed. One approach to developing new bacterial detection systems is to design simple bioassays and biosensors that meet the ASSURED criteria, being: Affordable, Sensitive, Specific, User-friendly, Rapid and robust, Equipment-free and Deliverable to end-users, particularly those in low-resource countries or in locations apart from the traditional hospital/laboratory setting. As shown in Figure 1.1, a typical biosensor is comprised of a biological agent used as a molecular recognition element (MRE), and a tranducer that can convert binding of a target to the bioreceptor.

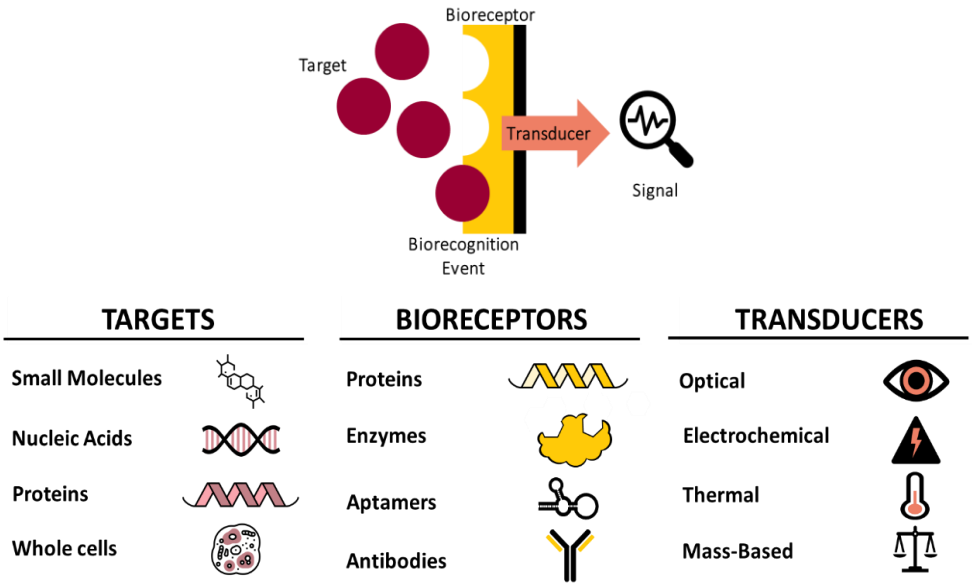

Figure 1.1.General design components shared by analytical bioassays. Several examples of potential targets, bioreceptors, and transducing methods are included. Figure by the author.

Functional nucleic acid (FNA)-based assays and FNA-based sensors use FNAs as a bioreceptors and have increased in popularity in point-of-care applications in the fields of environmental monitoring,[7] diagnostics,[8] and other small molecule detection.[9,10] FNAs can be selected for targets ranging in size from small molecules to proteins to whole cells, a diversity that highlights the power of the systematic evolution of ligands by exponential enrichment (SELEX) method.[11–13] Aptamers are a specific class of FNA, single-stranded DNA or RNA probes that undergo intra-nucleotide binding and non-covalent target binding to give aptamers a defined tertiary structure[14,15] that is adopted upon binding to the target in a similar induced fit model as antibodies, earning aptamers the nickname "chemical antibodies".[16] Deoxyribozymes (DNAzymes) are FNAs that are selected for their catalytic ability after binding to a target, using this reaction monitor biorecognition. [17–21] The first DNAzyme reported by Breaker and Joyce reported the cleavage of a ribonucleoside-containing DNA sequence,[21] and have since grown widely in their use.[22] DNAzymes can be classified as *cis* (Figure 1.2A) when the catalytic and substrate sequences are linked, or *trans* (Figure 1.2B) where they are two separate sequences. DNAzymes can similarly be incorporated as an MRE in lieu of an aptamer, utilizing the DNAzyme's catalytic action for target detection. There are less than ten examples if directly selected aptazymes, with others being developed using discovery-based SELEX strategies. [22]

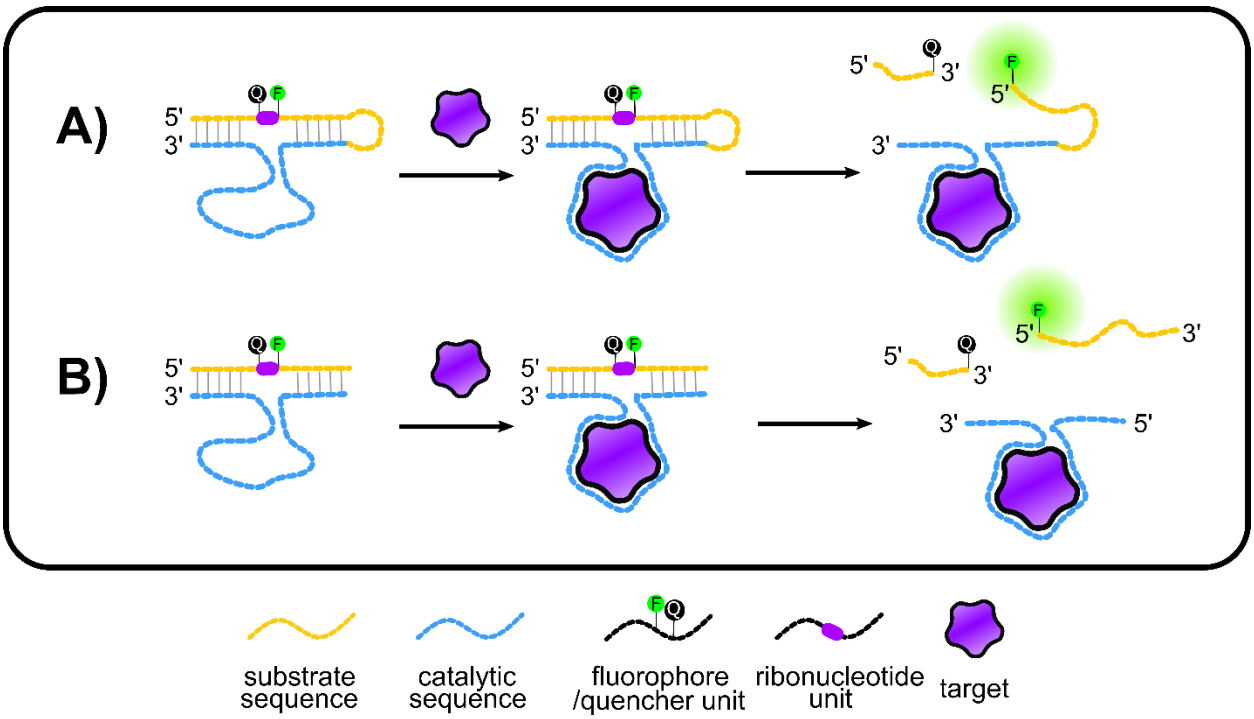

Figure 1.2. A) The catalytic and cleavage action of *cis*-RCD. B) The catalytic and cleavage action of a *trans*-RCD.

Previously, our laboratory reported an RNA-cleaving DNAzyme (RCD) assay capable of sensitive detection of *H. pylori* in human stool samples with minimal sample processing.[15] The RCD contains both a target recognition region, which allows target-mediated activation of catalytic activity, and a substrate region containing a ribonucleotide that can be cleaved by the DNAzyme to produce two cleavage fragments (Figure 1.3A).[17–21,23] A highly specific HP-activated RCD was generated using the crude extracellular matrix (CEM) of the bacterium, producing cleavage at the ribonucleotide unit in the chimeric DNA substrate strand, a common strategy in RCD design.[1] This ribonucleotide unit (riboadenosine, rA) was flanked by a fluorophore (fluorescein-dT) and quencher (dabcyl-dT), allowing for easy detection of the bacterium based on dequencing of fluorescence upon cleavage[13,14,16] producing a simple

fluorimetric assay with a detection limit of 10^4 CFU/mL (Figure 1.3B), a marked improvement over the LOD of the commercial LFD (10^7 CFU/mL).

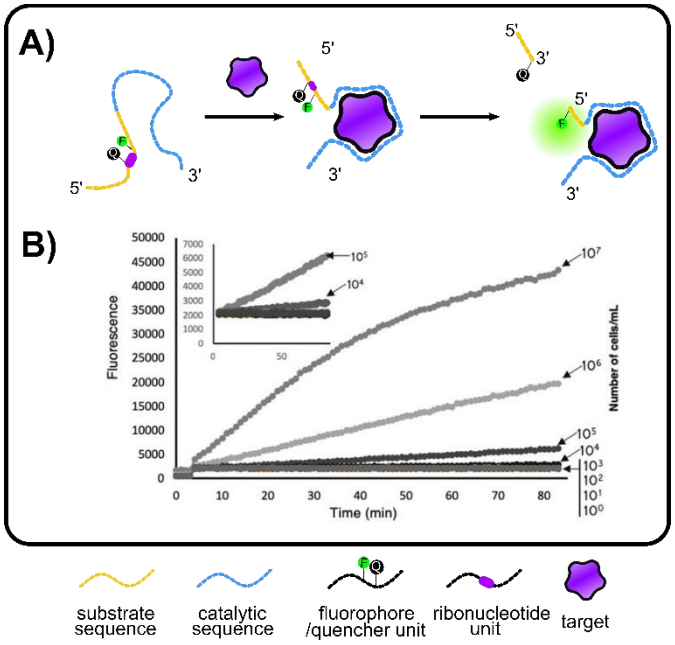

Figure 1.3. A) A figure depicting the schematic of *cis*-RCD cleavage, resulting in dequenching and an increase in fluorescence. B) Kinetic fluorescence data of *cis*-RCD cleavage from [5].

One method that can be used to improve the detection limit of assays that incorporate functional nucleic acids as MREs is to use a nucleic acid amplification step to amplify the ultimate signal. The most common nucleic acid amplification strategy is the polymerase chain reaction (PCR), a common biochemical method of increasing sensitivity of biomarker detection. PCR utilizes a DNA polymerase and several thermocycling steps to allow for the replication of a known sequence. Specific temperature requirements and instrumentation precludes its use in point of care (POC) testing and renders the method incompatible with ASSURED assays.[24,25] In the early 1990s, similar enzymatic methods of amplification without temperature cycling began to emerge, where amplification reactions that occur at a single temperature, producing an isothermal amplification (ITA) method. A number of ITA methods have emerged in the last 30

years.[26–31] These methods range in their mode of operation from DNA replication, enzymatic degradation and enzyme-free nucleic acid assembly.[24] Specifically, for POC applications methods that operate at room temperature are especially useful.

Rolling circle amplification (RCA) is an isothermal amplification methods method that can be performed at room temperature making it amenable to POC tests in ambient environments (Figure 1.4). [8–10] RCA is triggered by a short, complementary, single stranded nucleic acid primer. An engineered circular nucleic acid is hybridized to the primer which is subsequently extended by a DNA or RNA polymerase using deoxyribonucleoside triphosphates (dNTPs). [9,10] Standard RCA involves linear amplification of the primer to produce long single stranded nucleic acid strands comprised of repeating units complimentary to the sequence found on the circular DNA template,[8] resulting in tens to hundreds of repeats per primer. Several reports have described the integration of DNAzymes with RCA (see Chapter 2 for a full review of this field), and thus the goal of this thesis was to evaluate the use of the HP DNAzyme for regulation of RCA so as to produce a HP assay with improved sensitivity relative to the originally reported

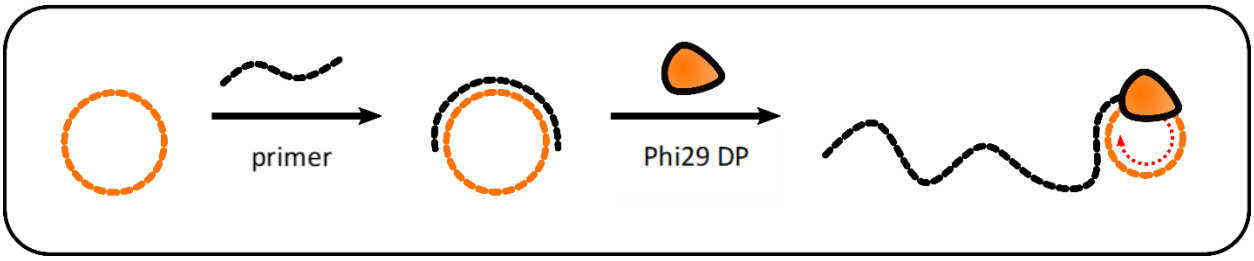

Figure 1.4. Schematic depicting the process for rolling circle amplification (RCA).

assay.

Chapter 2 of my thesis serves as a detailed review of FNA-based bioassays and biosensors that utilize RCA as an isothermal amplification step. In this chapter, we highlight the

key considerations for bioassay and biosensor design, including target-triggered biorecognition, signal amplification, and detection strategy, including strategies for incorporating RCA with DNAzymes. From there, we detail progress in the field over the last decade, highlighting our peers that have developed robust and practical assays that take real-world limitations into account.

This is followed by a description of the key methods used to integrate the HP DNAzyme with RCA. The first method explored a RCD design very similar to the original work, where a small RCD cleavage fragment would initiate amplification. A second method evaluated a *trans*-RCD arrangement to minimize issues with endogenous nucleases that could result in nucleic acid digestion. Finally, we explored a new RCD design that moved the substrate region of the *cis*-RCD to the 3' end of the sequence. In each case the ability of the RCD to produce cleavage fragments, and the ability of cleavage fragments to initiate RCA were investigated. Issues related to variations in the concentration of DNAzyme targets as a function of HP culturing conditions were also investigated. A final RCA-based assay for HP using the rearranged HP DNAzyme is then described for amplified fluorescence detection of *H. Pylori*. The thesis concludes with a discussion of remaining challenges and future work remaining to develop a working sensor for HP.

REFERENCES

[1] A. S. Fauci, D. M. Morens, *N. Engl. J. Med.* **2012**, *366*, 454–461.

[2] M. Zamani, F. Ebrahimtabar, V. Zamani, W. H. Miller, R. Alizadeh-Navaei, J. Shokri-Shirvani, M. H. Derakhshan, *Aliment. Pharmacol. Ther.* **2018**, *47*, 868–876.

[3] J. K. Y. Hooi, W. Y. Lai, W. K. Ng, M. M. Y. Suen, F. E. Underwood, D. Tanyingoh, P. Malfertheiner, D. Y. Graham, V. W. S. Wong, J. C. Y. Wu, F. K. L. Chan, J. J. Y. Sung, G. G. Kaplan, S. C. Ng, *Gastroenterology* **2017**, *153*, 420–429.

[4] K. Sugano, J. Tack, E. J. Kuipers, D. Y. Graham, E. M. El-Omar, S. Miura, K. Haruma, M. Asaka, N. Uemura, P. Malfertheiner, T. Azuma, F. Bazzoli, F. K. L. Chan, M. Chen, N. Chiba, T. Chiba, L. G. Vas Coelho, F. Di Mario, K. M. Fock, Y. Fukuda, R. M. Genta,

K. L. Goh, P. H. Katelaris, M. Kato, T. Kawai, R. Kushima, V. Mahachai, T. Matsuhisa, H. Miwa, K. Murakami, C. A. O'Morain, M. Rugge, K. Sato, T. Shimoyama, T. Sugiyama, H. Suzuki, K. Yagi, M. S. Wu, M. Ito, N. Kim, T. Furuta, F. Mégraud, A. Shiotani, T. Kamada, *Gut* **2015**, *64*, 1353–1367.

[5] M. M. Ali, M. Wolfe, K. Tram, J. Gu, C. D. M. Filipe, Y. Li, J. D. Brennan, *Angew. Chemie Int. Ed.* **2019**, *58*, 9907–9911.

[6] F. Mégraud, *J. Pediatr.* **2005**, *146*, 198–203.

[7] E. M. McConnell, J. Nguyen, Y. Li, *Front. Chem.* **2020**, *8*, 434.

[8] L. Wang, R. Wang, H. Wei, Y. Li, *World J. Microbiol. Biotechnol.* **2018**, *34*, 149.

[9] M. Citartan, S. C. B. Gopinath, J. Tominaga, S. C. Tan, T. H. Tang, *Biosens. Bioelectron.* **2012**, *34*, 1–11.

[10] D. Li, L. Liu, Q. Huang, T. Tong, Y. Zhou, Z. Li, Q. Bai, H. Liang, L. Chen, *World J. Microbiol. Biotechnol.* **2021**, *37*, 45.

[11] D. L. Robertson, G. F. Joyce, *Lett. to Nat.* **1990**, *344*, 467–468.

[12] A. D. Ellington, J. W. Szostak, *Nature* **1990**, *346*, 818–822.

[13] C. Tuerk, L. Gold, *Science (80-.).* **1990**, *249*, 505–510.

[14] A. D. Ellington, J. W. Szostak, E. AD, S. JW, A. D. Ellington, J. W. Szostak, E. AD, S. JW, *Nature* **1990**, *346*, 818–22.

[15] C. Tuerk, L. Gold, *Science (80-.).* **1990**, *249*, 505–510.

[16] M. Bauer, M. Strom, D. S. Hammond, S. Shigdar, *Molecules* **2019**, *24*, 4377.

[17] R. R. Breaker, *Nat. Biotechnol.* **1997**, *15*, 427–431.

[18] G. F. Joyce, *Annu. Rev. Biochem.* **2004**, *73*, 791–836.

[19] Y. Li, R. R. Breaker, *Curr. Opin. Struct. Biol.* **1999**, *9*, 315–323.

[20] B. Cuenoud, J. W. Szostak, *Nature* **1995**, *375*, 611–614.

[21] R. R. Breaker, G. F. Joyce, *Chem. Biol.* **1994**, *1*, 223–229.

[22] E. M. McConnell, I. Cozma, Q. Mou, J. D. Brennan, Y. Lu, Y. Li, *Chem. Soc. Rev.* **2021**, DOI 10.1039/D1CS00240F.

[23] I. Cozma, E. M. McConnell, J. D. Brennan, Y. Li, *Biosens. Bioelectron.* **2021**, *177*, 112972.

[24] Y. Zhao, F. Chen, Q. Li, L. Wang, C. Fan, *Chem. Rev.* **2015**, *115*, 12491–12545.

[25] P. Craw, W. Balachandran, *Lab Chip* **2012**, *12*, 2469–2486.

[26] J. C. Guatelli, K. M. Whitfield, D. Y. Kwoh, K. J. Barringer, D. D. Richman, T. R. Gingeras, *Proc. Natl. Acad. Sci.* **1990**, *87*, 1874–1878.

[27] G. T. Walker, M. S. Fraiser, J. L. Schram, M. C. Little, J. G. Nadeau, D. P. Malinowski, *Nucleic Acids Res.* **1992**, *20*, 1691–1696.

[28] K. Nagamine, K. Watanabe, K. Ohtsuka, T. Hase, T. Notomi, *Clin. Chem.* **2001**, *47*, 1742–1743.

[29] O. Piepenburg, C. H. Williams, D. L. Stemple, N. A. Armes, *PLoS Biol.* **2006**, *4*, 1115–1121.

[30] A. Fire, S. Q. Xu, *Proc. Natl. Acad. Sci.* **1995**, *92*, 4641–4645.

[31] J. Compton, *Nature* **1991**, *350*, 91–92.

CHAPTER 2 | LITERATURE REVIEW

Author's Preface

Roger Bialy was responsible for the review structure, and wrote the first draft of the manuscript. He wrote the content and designed the figures for the Introduction and Regulation sections of the review. He compiled the data and generated the summary tables included in this review.

I wrote the content and designed the figures for the Amplification section of the review. Roger Bialy, and I both co-wrote the content and co-designed the figures for the remaining sections of the review. Dr. Brennan, Roger Bialy, and I provided editorial input for all sections of the review. Dr. Brennan and Dr. Li provided editorial input to generate the final draft of the paper.

This review has been included in the format dictated by Chemical Society Reviews for eventual submission in the near future.

Design Strategies for Functional Nucleic Acid Biosensors Utilizing Rolling Circle Amplification

Roger M. Bialy,[a] Alexa Mainguy,[a] Yingfu Li,*[ab] and John D. Brennan*[a]

[a] R. M. Bialy, A. Mainguy, Prof. Dr. Y. Li, Prof. Dr. J. D. Brennan
Biointerfaces Institute, McMaster University
1280 Main Street West, Hamilton, ON, L8S 4O3, Canada
E-mail: brennanj@mcmaster.ca
[b] Prof. Dr. Y. Li
Department of Biochemistry and Biomedical Sciences, McMaster University
1280 Main Street West, Hamilton, ON, L8S 4K1, Canada
E-mail: liying@mcmaster.ca

Abstract: Functional nucleic acids (FNA), including DNA aptamers and DNAzymes, are finding increasing use as molecular recognition elements (MRE) for point of care (POC) devices. An ongoing challenge in the development of FNA-based POC sensors is the ability to achieve detection of low levels of analyte without compromising assay time and ease of use. Rolling circle amplification (RCA) is a leading nucleic acid (NA) isothermal amplification (ITA) method which can be coupled with FNAs for the ultrasensitive detection of non-NA targets. Herein we examine the key considerations required when designing FNA-coupled biosensors utilizing RCA. Specifically, we describe methods for using FNAs as inputs to regulate RCA, various modes of RCA amplification, and methods to detect the output of the RCA reaction, along with how these can be combined to allow detection of non-NA targets. Recent progress on development of portable POC devices that incorporate RCA is then described, followed by a summary of key challenges and opportunities in the field.

1. Introduction

Modern nucleic acid biosensors (NABs) have found widespread use as they provide many advantages over traditional diagnostic methods.[1–3] NABs can provide processing times of minutes to hours, are substantially smaller and more affordable relative to traditional instrument-based methods, and are often semi-automated, requiring minimal user training. These make them excellent candidates for applications at the point of care (POC). A key advantage of NABs is the ability to integrate nucleic acid amplification strategies, which can significantly improve the limit of detection.[4–6] However, sample preparation remains a major issue for such biosensors, as extraction of NAs (DNA, RNA, or miRNA) from a biological sample is non-trivial and often requires several laborious and time-consuming extraction procedures. Furthermore, many important clinical and environmental sensing applications do not have a relevant NA target. Hence, there has been a significant amount of research devoted to methods that can utilize readily accessible non-NA targets, such as metal ions, small molecules, and proteins, while retaining the advantages offered by NA amplification to lower the detection limit for such species. In this review, we describe methods to utilize functional nucleic acids (FNAs) in combination with isothermal NA amplification via rolling circle amplification (RCA) as a platform for ultrasensitive detection of non-NA targets, with an emphasis on sensors that are suitable for point-of-care (POC) applications.

Functional nucleic acids, which are either NA aptamers or (deoxy)ribozymes (RNAzymes or DNAzymes), have seen widespread use as molecular recognition elements (MREs) for the selective detection of non-NA targets.[3,7–13] While both RNA aptamers and ribozymes are present in nature, no naturally occurring DNA aptamers or DNAzymes have been found to date.[14,15] Hence, all such species have been generated using artificial *in vivo* selection methods.

The first reported selection of a DNA aptamer was in 1990, with three different groups independently reporting the discovery of DNA aptamers using a using a process known as SELEX (Systematic Evolution of Ligands by Exponential Enrichment).[16–18] This Darwinian-type process of selection,[19] and variations of it,[20] have led to the discovery of aptamers for a variety of targets, including small molecules, proteins, viruses and cells, typically with picomolar to micromolar binding affinities.[17,18,21–30] These single-stranded NA probes typically undergo substantial conformational changes upon non-covalent target binding, producing a defined tertiary structure based on an induced fit with the target, earning aptamers the nickname "chemical antibodies".[17,18,31] Aptamers can be incredibly selective, with the theophylline aptamer able to distinguish between theophylline and caffeine – a single methyl group difference – with 1000-fold selectivity,[22] and the anti-platelet-derived growth factor (PDGF) aptamer binding the PDGF-BB isoform with 700-fold selectivity over the PDGF-AA isoform.[21] Even enantiomers can be differentiated with the L-adenosine aptamer showing over 1700-fold chiral discrimination over D-adenosine.[32]

The first selection of a DNAzyme was conducted in 1994, when Joyce's group reported on the first RNA cleaving DNAzyme, which catalyzed the transesterification reaction of the phosphodiester bond of RNA.[33] Since this time, many other DNAzymes have been discovered[11,34] with various catalytic abilities including nucleic acid ligation,[35,36] hydrolysis,[37–39] phosphorylation,[40] capping,[41] deglycosylation[42] and peroxidation.[43] DNAzymes can either be natively active in the buffer conditions, or an aptamer domain can be incorporated into the DNAzyme as the MRE allosterically activating the catalytic domain upon target binding (often referred to as aptazymes). Many aptazymes such as the ATP aptazyme, are rationally designed to link a target binding event with catalytic activity through a communication module.[1,44] More recently, aptazymes have been directly selected against bacterial or mammalian cellular media to

produce MREs that are selective against desired bacteria or cancer cells.[45,46] Together, the breadth of DNA aptamers and DNAzymes has made FNAs a particularly useful set of MREs for the development of POC diagnostic tests.[47–49]

While FNAs represent a novel category of MRE, in many cases their affinity constants are not sufficient to allow detection of trace levels of targets. Indeed, achieving ultrasensitive detection of analytes in a manner that meets the World Health Organization (WHO) ASSURED criteria (Affordable; Sensitive and Specific enough to provide useful information; User-friendly; Rapid and robust; Equipment-free, and; Deliverable to the end-user)[50–53] remains a major challenge in the field of POC diagnostics.[4,6,53,54] To address this issue, binding of a target to a FNA can be coupled to one of several DNA amplification methods to increase sensitivity and drive down detection limits. Though there are non-enzymatic DNA amplification methods, improvements to sensitivity can be limited.[55] As a result, sensors that utilize FNAs for target recognition commonly incorporate an enzymatic NA amplification method to retain sensitivity that is otherwise lost to miniaturization and simplification.

The most common enzymatic DNA amplification method is the polymerase chain reaction (PCR),[56] however the need for thermocycling makes this method incompatible with simple point-of-care assays.[57] Over the past 30 years a number of isothermal amplification (ITA) methods have been developed to overcome this limitation. These include strand displacement amplification (SDA),[4,6,58,59] recombinase-polymerase amplification (RPA),[60–62] loop-mediated amplification (LAMP),[63–66] helicase dependent amplification (HDA),[67–70] and hybridization chain reaction (HCR).[55,71,72] While these are powerful amplification methods, and often provide exponential amplification, many of these require multiple enzymes or primers, complicated sequence design, and operate at elevated temperatures (typically 30 – 65 °C) making them difficult to apply in simple POC assays or devices which aim to operate in an equipment-free manner.

Rolling circle amplification (RCA) is another ITA method that has received significant attention for biosensing applications as described in recent reviews.[73–79] Replication of DNA around a circular template is a naturally occurring process which normally involves circular plasmids that are typically thousands of nucleotides in length.[80] However, the CTs used in RCA are often synthesized to be less than one hundred nucleotides long rather than several thousands of nucleotides found in DNA plasmids. In fact, the first literature examples of circular oligonucleotides with open, unpaired structures that showed potential as substrates for polymerases were not reported until 1990,[81,82] and it was not until 1995 that the Fire group reported on the replication of DNA using short synthetic nucleotide CTs.[80] Shortly thereafter, Kool *et al.* suggested its possible application in NA amplification.[83] Since this time, extensive advancements have been made in the use of RCA for detection of nucleic acid targets, including improvements in regulation methods, polymerase selection, amplification methods, and detection strategies. For more extensive information on the history of RCA, readers are referred to early reviews on the field.[73,80,84]

In contrast to other ITA methods, RCA requires only a single enzyme, a single primer and can be done at room temperature, making it well suited for utilization in simple, equipment-free POC devices. RCA is unique among ITA methods in that it utilizes a circular DNA template (CT) rather than a linear one. In the presence of deoxyribonucleotide triphosphates (dNTPs), and the CT, a DNA polymerase (typically phi29 DNA polymerase (phi29 DP)) amplifies a complementary linear DNA or RNA primer. As the template is circular, the resultant RCA product (RP) generated is a series of tens to thousands of concatemeric single-stranded DNA copies that are complementary to the CT. As described below in Sections 3 and 4, it is also possible to encode a variety of sequences into the RP to allow subsequent reactions that can improve either amplification efficiency or detection sensitivity, allowing this method to achieve single molecule detection limits.[85–88]

RCA has been extensively used as an amplification tool for the detection of NA targets,[73–75] and has the specificity to detect single nucleotide polymorphisms (SNPs).[87,89–91] However, the use of RCA for the amplified detection of non-NA species requires careful consideration of three main components: 1) molecular recognition in a manner that triggers RCA; 2) the nature of the amplification reaction, and; 3) the method to transduce the RCA output into a measurable signal. While there are examples of RCA reactions that utilize antibodies as MREs,[92–97] in this review we will focus on FNAs as MREs to trigger RCA, and will describe how the CT sequence can be used to modulate the triggering, amplification efficiency, and output of the RCA reaction (Figure 2.1). We also describe simple POC devices that integrate FNA-based MREs with RCA-enabled amplification and detection systems, with a focus on devices that meet the ASSURED criteria. Particular emphasis is placed on electrochemical and paper-based biosensing approaches as these devices meet the ASSURED criteria,[48,53,98,99] and allow for sensitive and robust analyte detection.

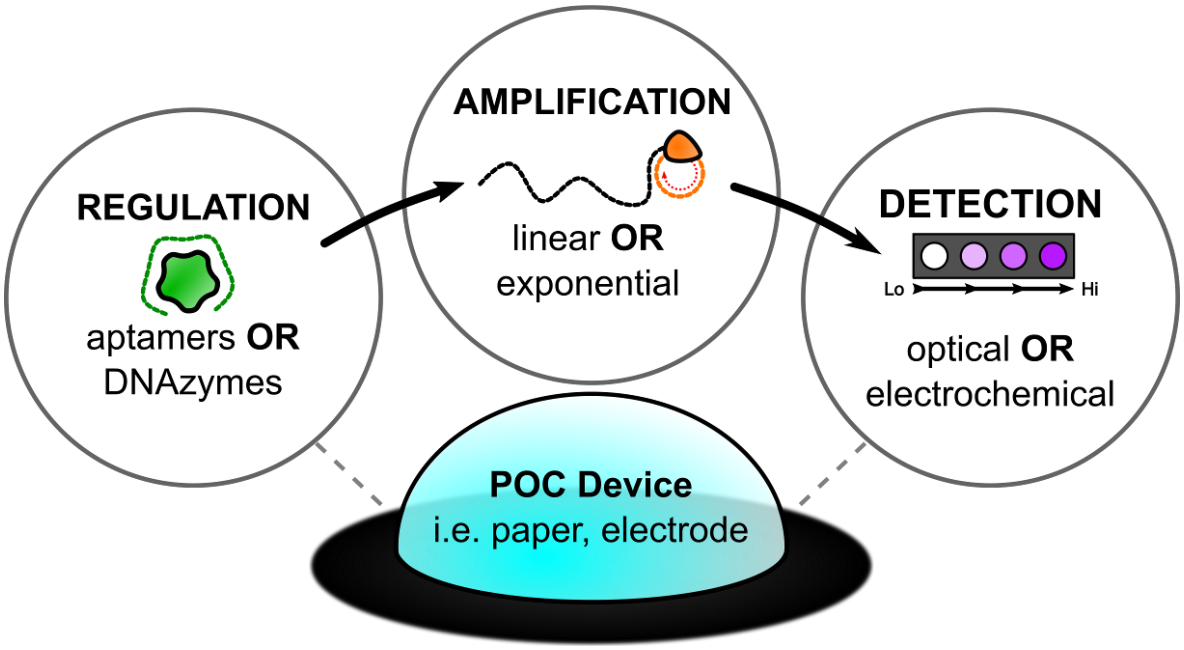

Figure 2.1. Overview of the three overarching ways that rolling circle amplification (RCA) can be manipulated. (A) Regulation, which governs how a non-nucleic acid target can be integrated as a regulator for RCA; (B) Amplification, and the different strategies that determine efficiency of amplicon generation; (C) Detection, which covers the various strategies for optically quantifying the amount of RCA product generated; (D) On paper, which focuses on how all three aspects can be incorporated on a paper-based surface for POC biosensing...

2. Regulation of RCA by FNAs

Controlling the initiation of the RCA reaction can be achieved by regulating the availability of at least one of the four essential components of RCA: the primer, CT, a DNA polymerase (phi29 DP unless otherwise indicated), or dNTPs. To date, no methods have been reported that involve the modulation of DP or dNTP availability to regulate RCA. Though the primer and CT are NA strands, FNAs act as a powerful bridge to allow non-NA targets to regulate NA strand availability. Here we will focus on techniques that specifically regulate the availability of either the primer strand or the CT with a focus on methods that best satisfy the ASSURED criteria.

2.1. Primer Regulation

The complementary binding of a NA primer to the CT to form a primer-CT complex is a fundamental requirement for RCA. The primer can be as short as six nucleotides in length,[100] though longer primers will improve selectivity and the efficiency of initiating the RCA process.[101] Once bound, the phi29 DP will elongate the primer along the CT from the 3' end, eventually displacing the primer after a revolution around the CT. This allows multiple copies of the antisense RP to be generated as identical repeating units. Binding of a target to a FNA can be used to alter that availability of the primer, and thus regulate the initiation of RCA, by three different methods. These include using: i) a target-binding event to trigger the release of a primer strand from a FNA, ii) binding of a target to an aptamer that acts as a primer to control primer-CT hybridization, or, iii) a target-activated RNA cleaving DNAzyme (RCD) to liberate an otherwise blocked primer. These methods are described in detail in the following sections.

2.1.1 Primer Regulation using Structure-Switching Aptamers

Structure-switching aptamers are designed to switch between a duplex form, which has a short NA strand hybridized across the aptamer domain and a primer extension, and a complex formed between the target and aptamer, which displaces the hybridized NA strand.[102–105] While often used to directly generate fluorescence signals based on displacement of adjacent quencher- and fluorophore-labelled strands,[102–105] this method can also be used as a means to initiate RCA by using the displaced NA strand as the RCA primer. For example, Hu *et al.* utilized the thrombin-binding structure switching aptamer to regulate RCA in this manner.[106] In this case, the aptamer released an RCA primer upon target binding, which was first captured at its 5' end by an immobilized DNA probe (Figure 2.2A). Following a washing step, addition of CT and phi29 DP to the captured primer allowed for target-mediated RP generation from the 3' terminus.

More recently, Liu *et al.* designed a tripartite structure-switching system for the detection of PDGF, which elegantly combined the essential RCA components together in a manner that eliminated the need for washing steps (Figure 2.2B).[107] The system was comprised of a primer strand with the 5'-end hybridized to a CT and the 3'-end hybridized to an anti-PDGF aptamer. Without target present, the aptamer blocked phi29 DP from initiating RCA on the primer. However, addition of PDGF triggered a structure-switch and released the aptamer. This allowed the 3' end of the primer to hybridize to the CT to generate a fully complementary primer sequence that could be used to initiate RCA.

A notable drawback of structure-switching aptamers is that hybridizing DNA strands to the aptamer sequence can affect its apparent binding affinity.[102] For example, Nutiu *et al.* reported that both the anti-thrombin and anti-ATP structure-switching aptamers showed a marked increase in the apparent dissociation constant (60-fold higher for the ATP aptamer). In addition, optimization of such systems requires extensive manipulation of the sequence of the displaced NA to ensure that it is easily released from the aptamer upon

target binding, but also has sufficient affinity for the CT to allow facile initiation of RCA.

To overcome this issue, it is possible to perform the structure-switching using graphene oxide (GO) rather than DNA-DNA duplexes (Figure 2.2C). GO exhibits properties that can be tuned to retain single-stranded or double-stranded DNA on its surface.[108] Structure-switching from GO using an aptamer was first demonstrated by Lu *et al.* in 2009 for the detection of thrombin.[109] In this case, the adsorbed aptamer is displaced from the GO surface upon binding the target to form a DNA-target complex. Liu *et al.* built upon this initial report by demonstrating GO-linked RCA for the detection of thrombin.[110] Reduced graphene oxide (rGO) was reported to perform better than its GO counterpart at releasing the thrombin-bound aptamer from the surface while preventing non-specific desorption of the aptamer. To initiate RCA, the aptamer had a 3' primer extension that could bind to a CT even when the aptamer was bound to its target, allowing the released aptamer to act as the linear primer. This approach has been used to develop RCA-linked assays for a variety of other targets, including PDGF and *C. difficile* glutamate dehydrogenase (GDH).[110–114] A drawback of this method is the potential for readsorption of the liberated aptamer onto the rGO surface. This necessitates removal of rGO by centrifugation[110,111] or the use of a paper-based assay to allow migration of the aptamer-target complex away from the immobilized rGO and into a zone containing the CT[112] (as described in section 5) for regulation of primer availability.

It is also possible to use an unmodified aptamer complexed to a CT to provide a structure switching system that controls RCA. In this method, reported in 2010 by Cheng *et al.* for the colorimetric detection of VEGF,[115] the VEGF aptamer was covalently immobilized on a glass slide and hybridized to a CT. Addition of the target displaced the CT, which was subsequently washed away. As such, the addition of target lead to the prevention of RCA, producing a "signal-off" sensor.

A simplified one-pot version of the RCA inhibition assay was reported by Bialy *et al.* recently, which removed the need for aptamer immobilization and washing steps. The assay is based on pre-incubation of the target with the aptamer, which forms a complex that blocks the 3' end of the aptamer, preventing it from binding to a subsequently added CT containing the anti-sense sequence to the aptamer and thus inhibiting RCA (Figure 2.2D).[101] An important advantage of this method is that the affinity of the aptamer is not affected as is the case for displacement of a hybridized CT. However, the use of an inhibition mechanism results in the signal decreasing as target concentration increases, which leads to a poorer detection limit. In addition, it is important to carefully design the aptamer sequence to avoid background binding of the aptamer-target complex to the CT.

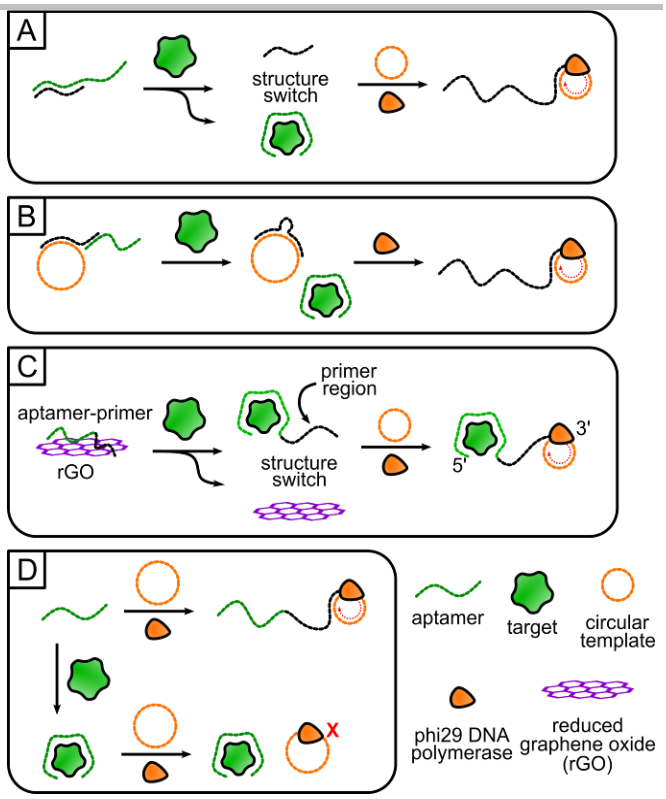

Figure 2.2. RCA-linked FNABs utilizing structure-switching. (A) Traditional structure-switching; (B) Tripartite structure-switching; (C) Structure-switching using reduced graphene oxide material; (D) Target-mediated inhibition of structure-switching.

2.1.2 Integration of native phi29 DP 3'-exonuclease activity

While phi29 DP is primarily used as a polymerase, the enzyme also has native 3' exonuclease activity as part of its proofreading mechanism. Liu *et al.* made use of this feature to regulate primer availability with a one-pot assay based on the tripartite structure-switching system outlined above (Figure 2.3A).[116] In this case, RCA was regulated by binding the aptamer partially to the CT and partially to a primer, such that the aptamer blocked the 3' end of the primer. The 3' end of the aptamer was capped with an inverted dT nucleotide to prevent 3'-exonuclease activity on the aptamer itself. In the absence of target, RCA was prevented owing to blocking of the 3' end of the primer. Upon target binding, the aptamer was displaced and the phi29 DP could then trim the 3' overhang of the primer (which was complementary to the aptamer rather than the CT) via 3'-exonuclease digestion to generate a fully complementary primer which could initiate RCA.

A further example utilized the 3'-exonuclease strategy with a supramolecular aptamer (or split aptamer) for the detection of ATP (Figure 2.3B).[117] Here, the first subunit (SA1) of the ATP aptamer contains an extended 5'-end region complementary to a CT. The second subunit (SA2) of the ATP aptamer contains the second half of the ATP aptamer on the 5'-end, a short region complementary to the CT in the center of the strand, and a 3'-end that is not complementary to the CT. In this format, SA1 stays hybridized with the circular template, and SA2 is unable to interact with the duplex. An inverted dT nucleotide on the 3'-end prevents phi29 DP from digesting SA1 and thus no RP can be generated. However, the addition of ATP causes SA1 and SA2 to orient in close proximity and form the ATP aptamer,

which brings SA2 close enough to the CT to stabilize the otherwise weak interaction. Addition of phi29 DP allows digestion of the 3'-end of SA2 and initiates the RCA reaction at the middle point of the SA2 strand.

Our group recently reported a simplified approach for utilizing the 3'-exonuclease activity of phi29 DP without requiring inverted dTs or complex structure-switching systems (Figure 2.3C).[118] In this approach, pre-incubation of the target with an aptamer forms a complex that protects the aptamer from 3'-exonuclease activity. The aptamer contains a toehold extension at its 5'-end, allowing liberation of the aptamer by a CT through toehold-mediated strand displacement (TMSD), which then initiates RCA. In the absence of target, the aptamer is digested and thus RCA does not occur. The method works well for low target concentrations. However, TMSD is not able to displace the target when at high concentrations, leading to blocking of phi29 processing by the target, inhibiting RCA.

Another method to modulate the interaction of a primer with a CT it by using a phi29 nuclease activity to act on a hairpin containing both the aptamer and primer.[119] In this case, the hairpin contains three regions: an aptamer region on the 5'-end, a primer region in the middle, and a blocking region at the 3'-end that forms a weak hairpin with the aptamer region (Figure 2.3D). Without target, the blocking region could be extended along the hairpin using Klenow Fragment to strengthen the hairpin and shield the primer from being used for RCA. In the presence of target the hairpin is disrupted and Klenow Fragment cannot extend the hairpin, thereby allowing the primer region to hybridize to the CT. Addition of phi29 DP digests the excess blocking region nucleotides to produce a complementary primer that can initiate RCA.

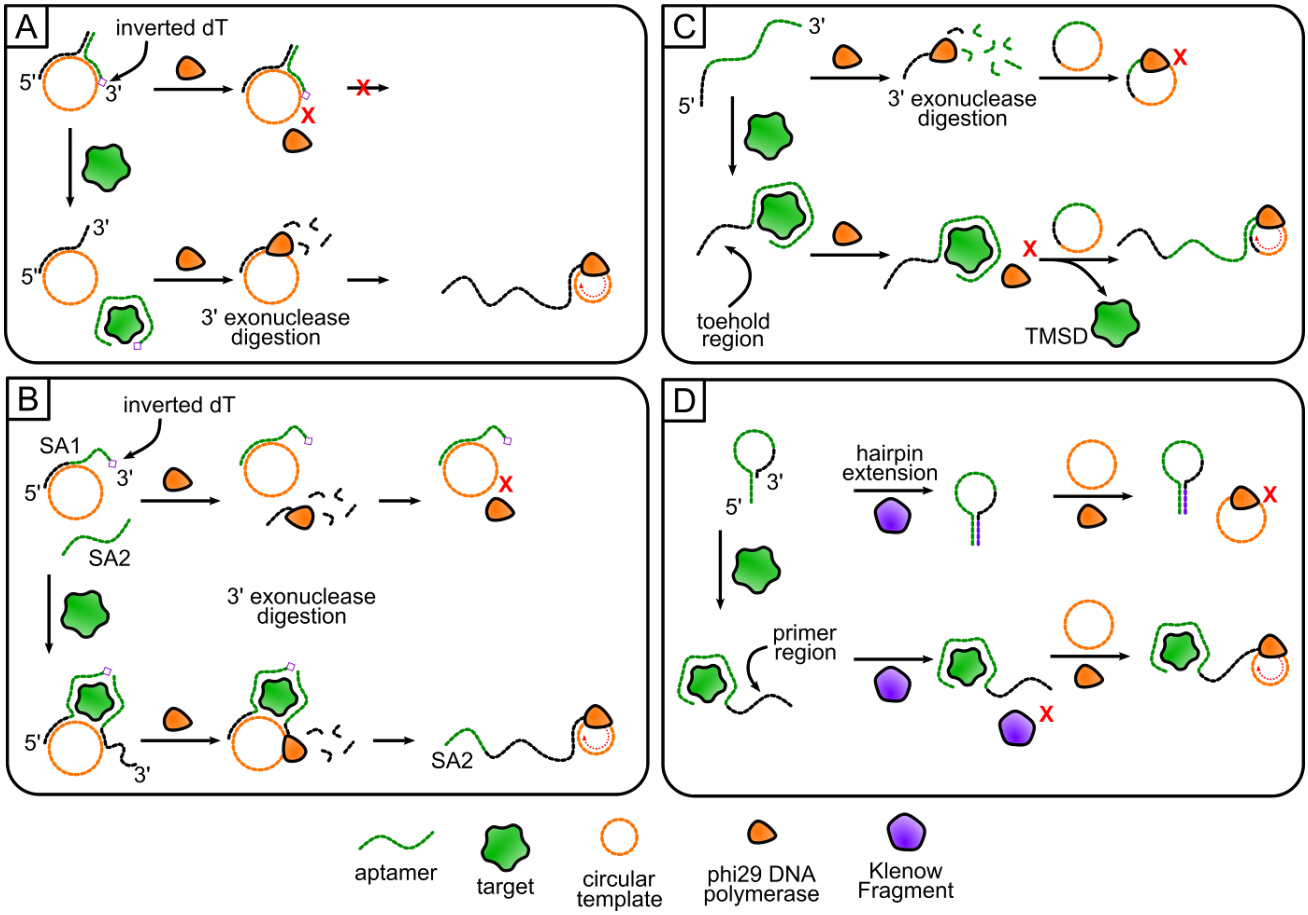

Figure 2.3. Enzyme-assisted regulation of primer availability. (A)-(C) RCA FNABs incorporating native 3'-exonuclease activity of phi29 DP. (A) Tripartite structure-switching; (B) Supramolecular (split aptamer) variant; (C) Toehold-mediated strand displacement; (D) Hairpin formation via Klenow Fragment.

2.1.3 DNAzyme Mediated Primer Regulation

RNA-cleaving DNAzymes (RCD) are another MRE that can be used to modulate RCA via primer regulation, which is achieved through the target-dependent activation of the DNAzyme to allow catalysis of the cleavage reaction involving a DNA substrate containing an embedded ribonucleotide cleavage site. This reaction results in the production of specific cleavage fragments that can be used as primers to control the RCA reaction.

The first example of this method utilized the coupling of an RCD with RCA for the detection of ATP.[120] The substrate was designed such that the RCA primer region was upstream of the ribonucleic acid linker, so that phi29 DP was unable to access the primer and initiate RCA. Addition of ATP activated DNAzyme catalysis to cleave the ribonucleic acid linker within the substrate (Figure 2.4A), producing a DNA fragment with a free 3' terminus. After treatment with polynucleotide kinase (PNK) to remove the 2,3-cyclic phosphate (a by-product of the RCD cleavage reaction), this primer was able to hybridize with a CT to trigger RCA, allowing for amplified detection of ATP.

In contrast with the first example, it is possible to use a pre-formed tripartite complex to avoid the need for separate addition of the CT

(Figure 2.4B). In this case,[121] a primer was designed such that the 5'-end hybridized to a CT and the 3'-terminal region contained a ribonucleic acid linker bound to an RCD specific for *E. coli*. The presence of *E. coli* activated the DNAzyme and triggered cleavage of the ribonucleic acid linker. Subsequent 3'-exonuclease digestion by phi29 DP removed the 3'-overhang and allowed RCA to proceed to produce an easily detected reaction product.

In both examples described above, access to the primer strand by phi29 DP specifically required a cleavage reaction to liberate the primer, and thus RCA could not be initiated unless both the DNAzyme and phi29 DP enzymatic functions worked in unison to liberate the primer strand. This is in stark contrast to structure-switching aptamers described above, where access to the primer is typically only gated by one layer of control (DNA-DNA hybridization or DNA-rGO adsorption). As a result, the use of RCDs provides a highly specific approach to primer regulation of RCA activity.

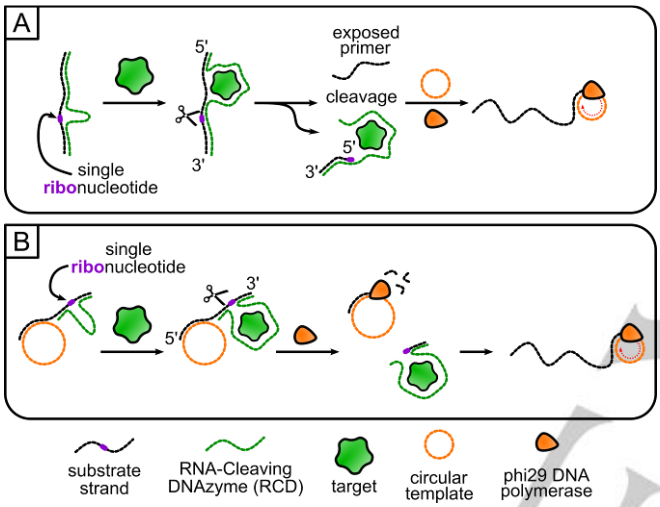

Figure 2.4. RCA FNABs utilizing RNA-cleaving DNAzymes (RCDs). (A) Traditional RCD-mediated cleavage; (B) Tripartite RCD utilizing 3'-exonuclease activity of phi29 DP.

2.2. Circle Regulation

FNAs can also be used to regulate the availability of the CT instead of the primer. RCA requires the presence of a circularized template to generate long, concatemeric reaction products, as only trace amounts of monomeric RP can be generated when using phi29 DP with a linear template.[122,123] The three primary strategies for regulating CT availability involve: 1) using a FNA to control the formation of a circularized template from a linear DNA precursor strand; 2) integrating the aptamer directly into the CT to modulate the ability of phi29 DP to generate RP, or; 3) enabling access to the CT through the use of an RCD.

2.2.1 Circle ligation method

In 1994, Nilsson *et al*. reported on the concept of using a ligase to circularize a linear NA strand in the presence of a target NA that hybridizes to the linear strand to guide ligation, denoted as the padlock probe (PLP) method.[124] This ligation reaction can only occur in the presence of a ligation strand which has segments that are complementary to the 5'-end and 3'-end of the linearized padlock probe, ensuring high selectivity. Lizardi *et al.* built on this work in 1998 by utilizing the ligated padlock probe as a CT for RCA, creating the first CT-regulated RCA system.[85] Since then, PLP-linked RCA has developed into the most common method for CT regulation of the reaction, providing for ultrasensitive[85–88] and selective[85,87,89–91] NA detection. The method has also been utilized using aptamers as ligation strands to allow detection of non-NA targets.[125–141] Below, the key advances in aptamer-linked, PLP-regulated RCA are described.

PLP-linked RCA modulated by an aptamer was first demonstrated by Yang *et al.* in 2007 for the detection of PDGF.[125] Here, the PDGF aptamer was elongated at both the 3' and 5' ends to include carefully designed sequences that only permitted the formation of a ligation junction in the presence of PDGF (Figure 2.5A). Without PDGF, the terminal ends were hybridized to the aptamer domain, and thus unavailable to bind to the linearized CT. The addition of PDGF caused a conformational switch in the aptamer that released the terminal ends, allowing formation of a junction that could be ligated in the presence of T4 DNA ligase. Addition of a separate primer strand then initiated RCA.

An alternative approach is to use a structure-switching aptamer where target binding leads to the release of a ligation strand which doubles as the primer (Figure 2.5B). Ma *et al.* used this approach for the detection of cocaine.[135] The cocaine aptamer was immobilized on a magnetic bead and hybridized to a ligation strand. Addition of cocaine lead to the liberation of the ligation strand. After magnetic separation to remove the unreacted duplexes, a linear template and T4 DNA ligase was added to form a CT for subsequent amplification. A similar approach was used by Tong *et al.* except that the structure-switching aptamer (in this case for ochratoxin A) was reacted with its target in solution to liberate a linear template (Figure 2.5C), while the ligation strand was immobilized on a magnetic bead with the 3' end at the distal end. In this way, the ligation strand could act as a primer to allow the RCA reaction to be run directly on the bead and allow RP to be easily extracted from solution.

The ligation strand (and primer) can also be integrated within the aptamer.[130–132] Jiang *et al.* tethered a ligation strand to the 3'-end of an aptamer in a sandwich assay for the detection of *E. coli*.[130] In this approach, *E. coli* cells were captured on a PDMS surface with a dendrimer and the modified aptamer was introduced to form a sandwich complex (Figure 2.5D). Addition of a linear CT precursor and T4 DNA ligase allowed for CT formation and subsequent RCA elongation from the 3'-end of the aptamer. The aptamer strand can also be designed to act as the ligation strand without any 3' modifications (Figure 2.5E).[132] To demonstrate this approach, gastric cancer exosomes were incubated with the aptamer and a filter membrane was used to discard unbound aptamer. Next, the aptamer-exosome complex was heat denatured to release the aptamer. The liberated aptamer subsequently served as the ligation strand for CT formation and as the primer for RP generation.

A potential drawback of current aptamer-modulated PLP methods include the requirement of an additional enzyme, and the need for additional separation or washing steps to remove unreacted ligation templates. In addition, many examples perform the ligation and amplification reactions separately rather than in one-pot, limiting their use in simple POC devices.

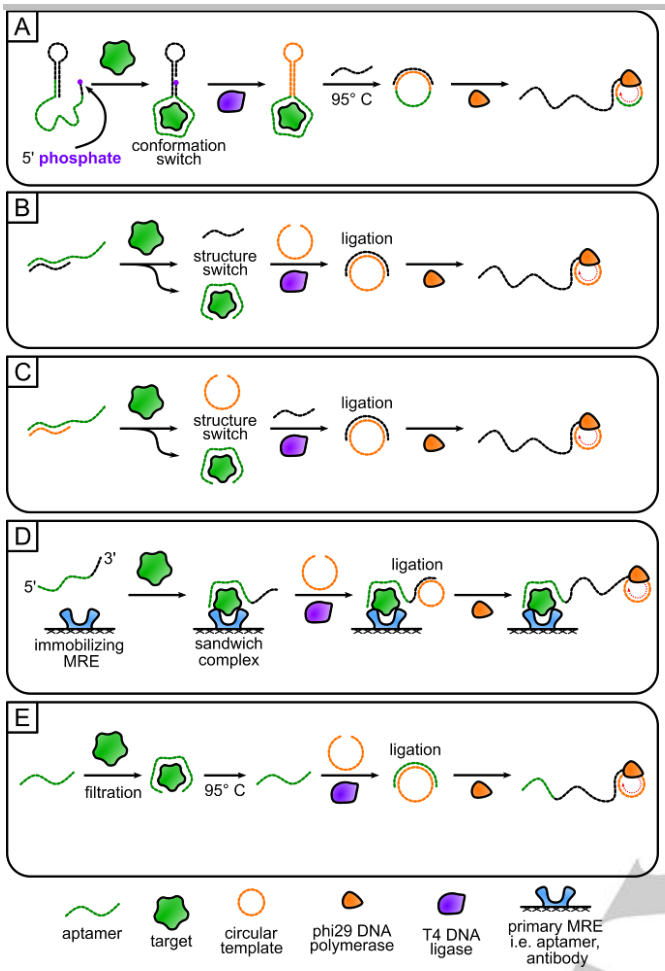

Figure 2.5. RCA-linked FNABs utilizing padlock probes for regulation of circular template. (A) Conformational structure-switching; (B) Structure-switching to release a ligation strand; (C) Structure-switching to release a linearized circular template; (D) Sandwich assay with ligation strand tethered to aptamer; (E) Dual-function DNA acting as aptamer and ligation strand

2.2.2 Circular Aptamers

An emerging method to modulate the CT is to incorporate the sequence of the FNA, and specifically an aptamer, directly into the CT sequence to regulate the RCA reaction. As noted below, most circularized aptamers were initially generated as linear species, since most SELEX methods used to find novel aptamers utilize linear NA libraries.[113] Importantly, the linear aptamer sequence can simply be inserted into the CT, while retaining any primer binding or detection sequences encoded within the circle. As the circle lacks both 3' and 5' ends, circularized aptamers (denoted as captamers) are resistant to exonuclease degradation, making them particularly suitable for applications involving biological samples.[113,142]

The first example of using captamers to regulate RCA was demonstrated by Di Giusto *et al.* for the detection of thrombin in a proximity extension assay.[143] In this approach, two aptamers were used, one of which had a 3' extension to act as a primer for RCA, and another that was embedded into a CT with a region that was complementary to the primer. As both aptamers could bind to different regions of thrombin, target binding brought the aptamer and captamer together, initiating RCA. To prevent non-specific amplification in the absence of thrombin, the complementary region was 6 base pairs, which is sufficiently short to prevent non-specific hybridization.

The circular nature of captamers allows also for their incorporation into intramolecular structure-switching strategies for RP regulation. Zhao *et al.* converted a linear aptamer for lipopolysaccharides (LPS) into a captamer by embedding the aptamer, along with a primer-binding region, within a CT (Figure 2.6A).[144] In the absence of target, the captamer formed a dumbbell shape through intramolecular hybridization, limiting access to the primer-binding region. Upon addition of LPS, the captamer adopted an extended conformation that exposed the primer-binding region, allowing for subsequent binding to a primer and RP generation.

The Liu group demonstrated the ability to use captamers to develop a structure-switching system, where PDGF binding could cause displacement of the circularized PDGF aptamer from rGO (Figure 2.6B).[114] Once displaced, the complex between the captamer and PDGF was removed from the rGO through centrifugation, and then the supernatant containing the liberated captamer was mixed with primer, allowing for RP generation. Though this method required a centrifugation step to isolate the liberated CT, it should also be amenable to paper-based spatial separation from rGO, as has been demonstrated with linear aptamers (see Section 5 for more details).[112]

While circularizing linear aptamers into CTs is relatively straightforward, the CT sequences must be carefully designed to prevent altering the native activity of the aptamer and its ability to switch between duplex and complex conformations. Recently, our group successfully conducted a SELEX experiment using a circular library and isolated a novel glutamate dehydrogenase (GDH) captamer which was only active in the circular form.[113] Importantly, this captamer showed lower affinity for recombinant GDH (rGDH) relative to native GDH (nGDH), a key target for *C. difficile* detection (Figure 2.6C). This allowed the development of a competitive assay wherein the GDH captamer was first incubated with rGDH-coated magnetic beads to form a captamer-rGDH complex. Addition of nGDH caused release of the captamer from the bead, and after removal of MBs, the liberated captamers were able to bind to an added primer to allow for nGDH-mediated RCA.

As was the case for PLP-mediated RCA, most of the examples above required a separation step, making them challenging to implement in POC tests. To overcome this issue, a method was developed using a CT-integrated aptamer to modulate the RCA reaction upon target binding by blocking the ability of phi29 DP to read through the CT (Figure 2.6D). A PDGF aptamer was incorporated within a CT and it was observed that phi29 DP was unable to displace the bound protein and thus read through the aptamer sequence, thereby inhibiting the RCA reaction when the protein was bound.[145] In this instance, and also with a thrombin-targeting system[145,146], no modifications of the PDGF or thrombin aptamers were required, thus making the method generalizable. In addition, no separation steps were required, making the assay much simpler. On the other hand, the assay operates as a "turn-off" signalling system, which generally tends to have poorer detection limits relative to "turn-on" systems.

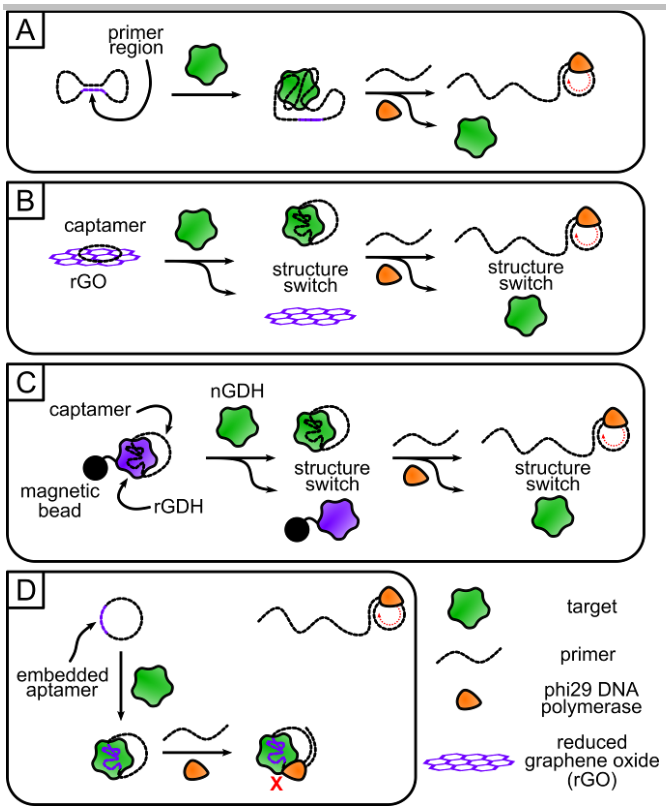

Figure 2.6. RCA-linked FNABs utilizing structure-switching for regulation of circular template. (A) Intramolecular structure-switching; (B) Structure-switching using reduced graphene oxide material; (C) Structure-switching using recombinant analyte (GDH); (D) Target-mediated inhibition of structure-switching.

2.2.3 DNAzyme Regulation of CTs

The use of DNAzymes to modulate the formation or accessibility of a CT is less prevalent than CT modulation by aptamers, however, there have been some interesting approaches, as noted below. The first example used a DNAzyme with ligase activity to regulate the formation of a CT from a linear DNA sequence (Figure 2.7A).[147] Similar to a PLP ligation approach, the Ellington group used a ligase DNAzyme that formed a hairpin loop when bound to ATP. The ends of the hairpin mimicked a ligation strand, bringing the two ends of the linearized CT together such that DNAzyme catalyzed ligation could occur. This DNAzyme ligase approach did not require an additional protein enzyme, as the linearized form of the CT was functionalized with a 3'-phosphorothioate and 5'-iodine residue.

Another approach to regulate CT formation utilized a DNAzyme with kinase activity, denoted as Dk2, to facilitate the ligation of a circular template in the presence of GTP (Figure 2.7B).[148] In this strategy, the DNAzyme was used as the linearized form of the CT. In the presence of GTP, the DNAzyme catalyzed a self-phosphorylation reaction wherein GTP transferred a phosphate to the 3' end of the DNAzyme. Circular ligation was carried out using T4 DNA ligase and a splint oligonucleotide complementary to the 5' and 3' ends of Dk2. The splint oligonucleotide also acted as a primer to allow RCA to proceed around the newly formed CT, allowing for sensitive detection of GTP as a target.

An issue with the use of DNAzymes to perform CT ligation is the poor diversity of targets that can activate such DNAzymes (generally NTPs such as ATP or GTP), and thus act as targets for sensing, thereby limiting the potential of this method for biosensing. An alternative strategy is to use a DNAzyme to modulate the accessibility of a CT, usually by liberating it from a constrained configuration. As an example, a Pb^{2+}-specific RCD was used to liberate a NA that served as a ligation strand for PLP ligation (Figure 2.7C).[149] The ribonucleotide-containing substrate strand was first hybridized to the DNAzyme. The presence of Pb^{2+} activated the DNAzyme, and cleaved the ribonucleotide junction in the substrate strand, with the cleaved fragment dissociating from the DNAzyme and acting as a ligation template to allow T4 ligase catalyzed ligation to form a circular template suitable for RP generation. Importantly, the diversity of RCDs makes this a more versatile method for sensing, as there are numerous targets that can activate RCDs.[1,150]

In addition to ligation methods, it is also possible to use RCDs to modulate the accessibility of a preformed CT. Liu *et al.* showed that it was possible to produce a circularized ribonuclotide-containing substrate that was strongly interlocked with the CT by using the CT as the ligation strand to circularize the substrate. By including a sufficiently long section that could hybridize to the CT, phi29 DP was prevented from reading through the hybridized section, and thus neither circle could be used to initiate RCA (Figure 2.7D).[151] In the presence of the RCD, the addition of the target (in this case *E. coli*) activated the RCD, which could cleave the ribonucleotide junction, linearizing the substrate strand. The phi29 DP was then able to trim the free 3' end of the substrate strand, which could then serve as a primer for RP generation.

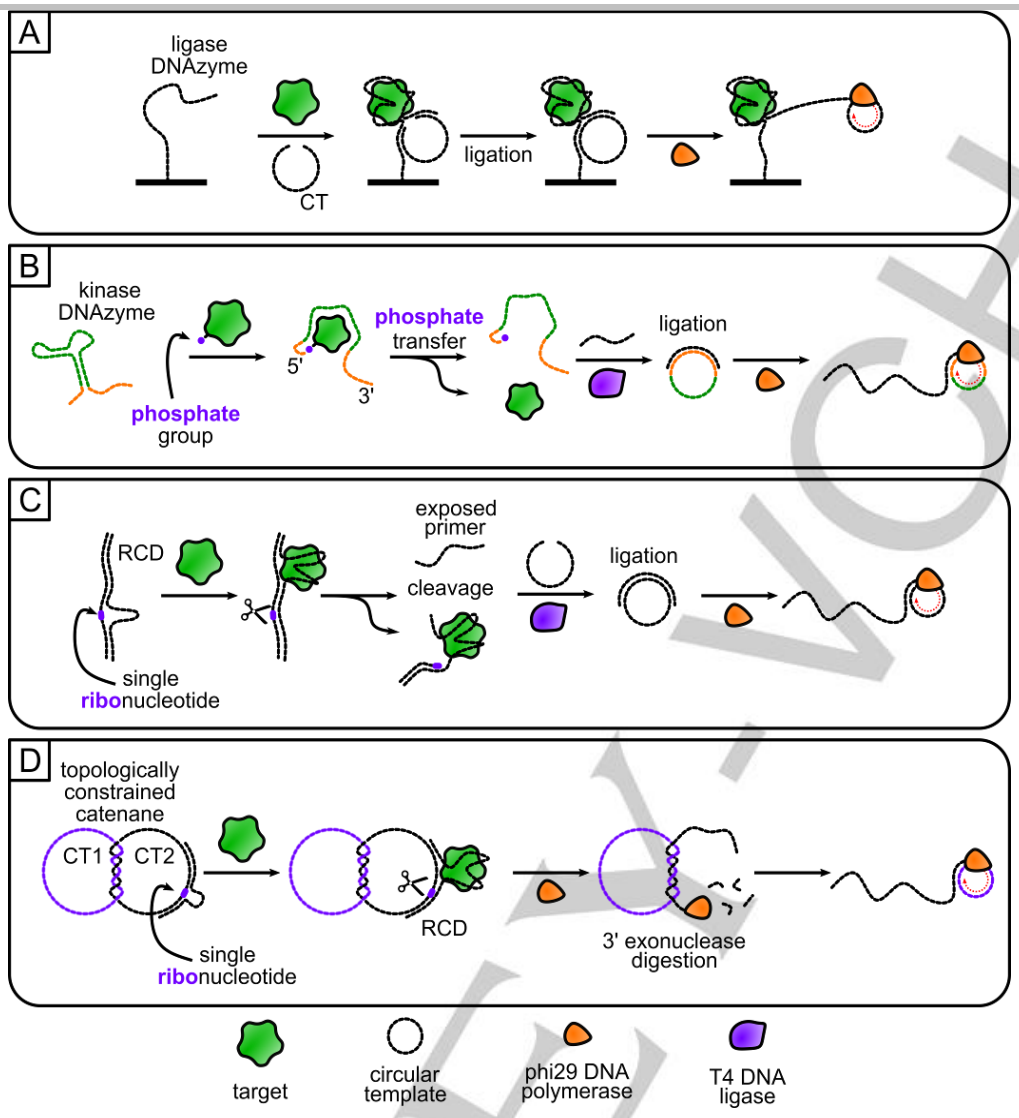

Figure 2.7. RCA FNABs utilizing DNAzymes for regulation of circular template. (A) Ligase DNAzyme-mediated; (B) Kinase DNAzyme-mediated; (C) RCD-mediated with CT ligation step; (D) RCD-mediated utilizing catenane approach and 3'-exonuclease activity of phi29 DP.

3. Amplification Methods

The heart of the RCA process is the ability to produce long concatenated DNA products by round-by-round amplification around a CT. Since its introduction in 1995, several groups have investigated the effects of different polymerases and CTs on RCA efficiency. As noted below, optimization of the polymerase and the CT sequence can improve the rate of RP production by up to an order of magnitude. However, more recent improvements have incorporated various feedback processes to produce exponential RCA, which can improve the rate of RCA by several orders of magnitude relative to linear RCA, depending on the specific method used. Below, we provide an overview of both linear and exponential RCA methods, with a focus on their performance, ease of use, and utility for point-of-care sensing.

3.1. Linear amplification

The earliest examples of RCA as an amplification method involved a polymerase simply extending the primer around the CT

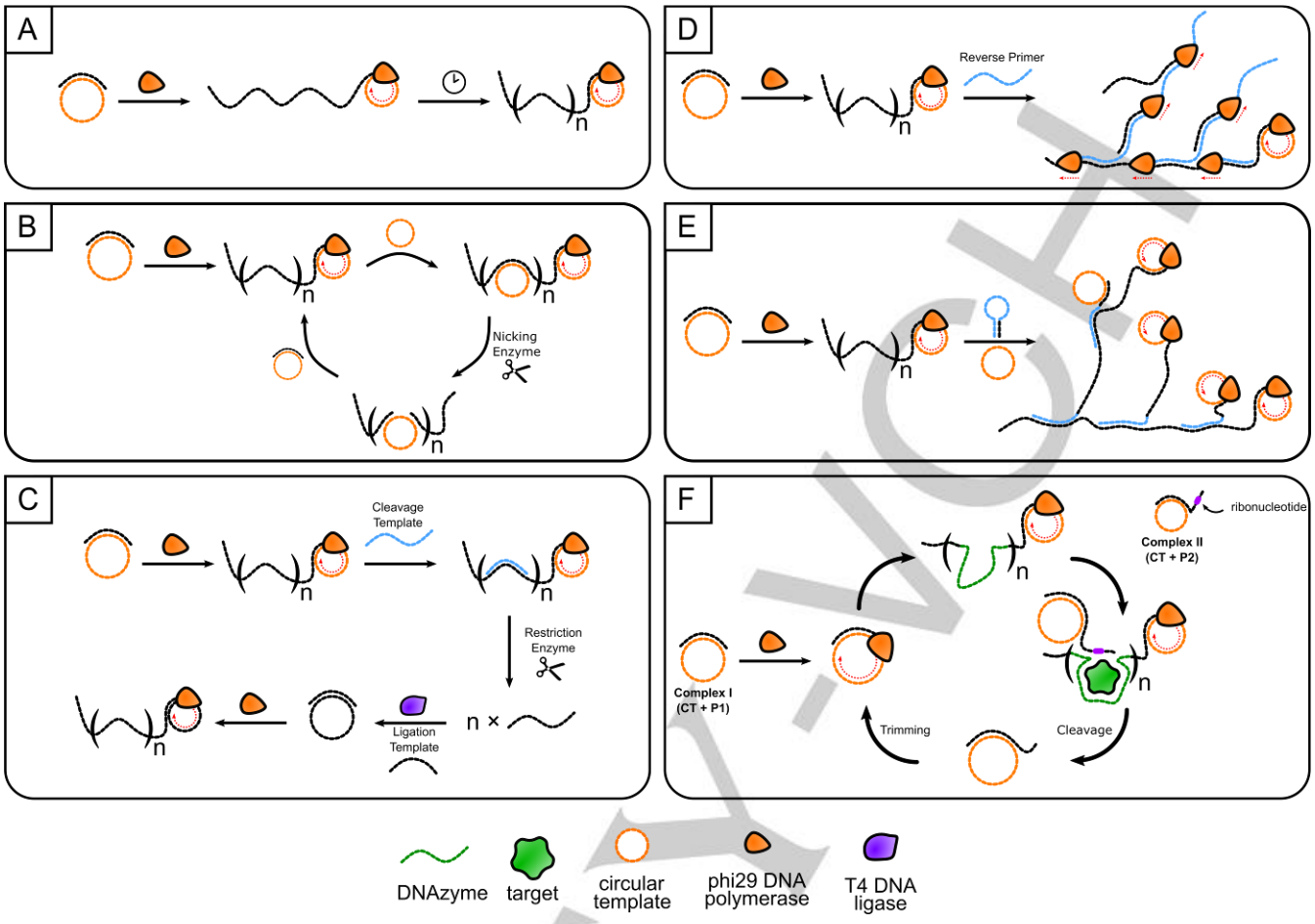

Figure 2.8. Schematic illustrations for linear amplification and two methods of exponential amplification. (A) Linear RCA (B) Nicking Endonuclease RCA (C) Circle-to-circle (C2C) RCA (D) Hyperbranched RCA (E) Dendritic RCA (F) DNAzyme Feedback Amplification.

to produce long, concatenated reaction products that increased linearly in concentration with time (Figure 2.8A). Early work aimed at evaluating the effect of polymerases on RCA efficiency have demonstrated that several replicating polymerases can be used to drive RCA, including *Bst* DNA polymerase and Klenow Fragment (-exo), though phi29 DP has emerged as the preferred polymerase owing to several key features.[152,153] For example while most polymerases require accessory proteins to assist with clamping the enzyme to DNA,[154,155] phi29 DP requires no assistance.[156,157] Phi29 DP also possesses the highest reported processivity of a polymerase, at greater than 70 kilobases in 40 minutes,[122,156] and excellent proof-reading ability,[158,159] with an error rate of only 1 in 10^4 to 10^6 bases.[160] In addition, as noted above, phi29 DP displays 3' to 5' exonuclease activity for single-stranded DNA,[161,162] providing an alternative avenue for designing input strategies. Phi29 DP also does not require the help of any helicase proteins as it exhibits excellent strand displacement properties.[123] Finally, and perhaps most importantly for POC testing, phi29 DP can operate at room temperature, unlike *Bst* DNA polymerase and Klenow Fragment (KF), both of which require elevated temperatures to operate. These factors have helped make phi29 DP a powerful polymerase for simple and effective RCA applications, particularly those that are amenable to POC sensing applications.[73,74,152,153]

Optimization of the circular template (CT) length and sequence can also be used to improve the efficiency and rate of RCA. Li *et al.* showed that DNA coding strategies can be employed to design optimal circular DNA templates generated through *in vitro* selection.[111] Amplification efficiency was maximized for certain CT nucleobase compositions, with a strong bias towards adenosine and cytosine-rich CT sequences, which comprised 85.4% of the nucleotides in the top 10 most efficient sequences. The optimized CT yielded detection limits that were an order of magnitude better than obtained with unoptimized CTs, producing the lowest reported LOD for aptameric thrombin detection at 1 pM. CT length may also be modified to impact amplification efficiency when care is taken to modulate the conformational strain in the CT.[163] Joffroy *et al.* observed that RCA amplification efficiency was maximized when a CT contained an odd number of helical half turns instead of an even number (~10.3 base pairs per turn) and the conformational strain was maximized. Simulations showed that sequences with maximized CT strain outperformed minimized sequences, amplifying up to 6-fold better. Amplification efficiency was also improved as the overall size of the CT was decreased, stressing the importance of minimizing overall CT length.

In addition to optimizing the polymerase and CT, there are additional modifications that can be made to improve the rate of linear RCA. For example, incorporating multiple primer regions to facilitate multiply primed RCA can increase amplification more than three-fold in some applications[152]. Multiply primed RCA uses several primers complementary to different unique regions along the CT, allowing each to initiate RCA concurrently. Incorporation of PEG 4000 at concentrations from 10 - 20% can also improve RP generation and

uniformity, particularly when RCA is performed on a solid surface.[164] Liu *et al*. observed that generating RCA on a nitrocellulose surface also led to improved RCA efficiency.[98] In each case, the authors attributed the improvement in RCA rates to a molecular crowding effect, which increased local concentrations of RCA reagents.

The final method to increase RP concentration, and hence decrease limits of detection when using linear RCA, is to increase reaction time, though this can be a challenge for rapid monitoring applications. Hence, even when optimized, linear RCA methods can provide at most 1000-fold amplification within 1 h.[85] Even so, this amplification factor may be adequate in cases where only moderate improvements in LOD are needed relative to unamplified assays. Hui *et al*.'s paper-based ATP and GDH aptasensors achieved sensitive fluorogenic detection in stool samples without any amplification.[112] To allow for equivalent detection sensitivity using equipment-free detection, the assay incorporated RCA to allow for colorimetric detection, which was as sensitive as the unamplified fluorogenic assay when using an amplification time of 1 hour.

3.2. Exponential RCA (E-RCA)

Although many assays can be achieved using linear RCA methods, in cases where ultrasensitive detection or more rapid generation of detectable RP concentrations is required it is necessary to implement exponential methods of RCA (E-RCA). Examples include detection of pathogens of both bacterial and viral origin,[165] where detection of as low as 1 organism is required,[166] and early detection of disease biomarkers, which are present at low concentrations.[167] Monitoring of the response to targeted therapies,[168] which is a cornerstone of precision medicine,[169,170] can also make use of these ultrasensitive approaches. In many cases, it is necessary to detect the analytes in complex biological samples, including blood, faeces, saliva or sputum, which may require sample dilution to reduce the effects of interferants within the matrix, further reducing analyte concentration.[171] In such cases amplification levels of 10^6 to 10^9 may be required, which requires exponential amplification systems to be achieved in a timely fashion.

In the case of RCA, exponential amplification is achieved through the use of various feedback processes which allow for cross-amplification. This is typically accomplished by incorporating some means to generate additional primers after the initial linear amplification step begins. Specific methods to produce E-RCA are described below, with emphasis on specific design considerations and their potential for use in simple POC sensors.

3.2.1 Enzyme-Assisted Exponential Amplification

Several exponential RCA methods utilize a secondary enzyme in addition to phi29 DP to process the RCA product in a manner that can generate new primers to allow cross-amplification. Examples include nicking RCA and circle-to-circle (C2C) amplification (Figure 2.8B and Figure 2.8C, respectively), both of which employ additional enzymes to achieve E-RCA. Nicking RCA, also known as primer-generation RCA, uses nicking endonucleases to monomerize the long concatemeric RP, thereby generating new monomeric primers to initiate amplification on other CTs. The nicking site is engineered in the CT so that the nicking enzyme can cleave along the complementary RCA product.[172] Nicking RCA can also incorporate multiple antisense nicking sites into the CT to yield different unique monomers, as shown by Li *et al.* in their exonucleolytic digestion-assisted E-RCA strategy.[173] By incorporating two nicking sites, one complementary repeat of the CT can be cleaved into two linear pieces. The first acts as a primer to initiate exponential amplification, and the second forms a G-quadruplex structure that can be probed fluorescently (see Section 4). Incorporation of the exponential primer feedback can improve the LOD of targets by as much as five orders of magnitude relative to unamplified detection, and 2-4 orders of magnitude better than for linear RCA.[83,116,173]

C2C amplification is another multi-enzyme E-RCA method, first reported by Nilsson *et al.* as an extension of their work on padlock probes.[90] C2C amplification consists of two primary steps. First, linear RCA proceeds in the presence of a primer to generate a long RCA concatemer. This RCA concatemer is then monomerized by a restriction enzyme, and then following heat inactivation of the restriction enzyme, each monomer is circularized using T4 ligase to act as a new CT. In this work, Nilsson and co-workers showed a sensitivity improvement of nine orders of magnitude in under an hour in comparison to the analogous linear RCA reaction, though the multi-step process and need for heating make the method difficult to implement in simple POC assays.

It is also possible to integrate non-RCA isothermal amplification methods in combination with RCA to achieve exponential amplification. This approach has been demonstrated with exponential amplification methods including loop-mediated isothermal amplification (LAMP),[174,175] catalytic hairpin amplification (CHA)[176,177] and strand-displacement amplification (SDA).[178,179] In most cases, linear RCA is used as the primary amplification method, and the concatenated RP is used directly as the input to supply primers for the subsequent exponential ITA scheme. These assays can increase assay sensitivity 1000-fold compared to their original ITA methods[174] but in most cases these secondary ITA methods require operation at elevated temperatures, making them challenging to integrate into POC sensors. In addition, incorporation of additional enzymes can impact the storage considerations, making NAs a more chemically and thermally robust alternative. These methods also increase the complexity of the assay, as the initial amplification is often performed prior to initiating the second amplification step, requiring significant user intervention to control reaction timing.

3.2.2 Hyperbranched RCA (H-RCA)

Hyperbranched RCA (H-RCA), sometimes referred to as ramification amplification,[180] can produce exponential RCA at room temperature without requiring additional enzymes (Figure 2.8D). First introduced by Lizardi *et al.* to detect point mutations in human genomic DNA,[85] this has emerged as the most popular method of E-RCA. H-RCA employs two unique primers: one complementary to the CT, and the other complementary to a region of the amplicon. After the first primer is elongated by phi29 DP, the second primer binds to the RP and initiates a secondary amplification complementary to the RP. This creates a branched system of replication where the linear RP is used as the template for exponential amplification. Some assays opt to use *Bst* DP instead of phi29 DP for H-RCA as this DP shows excellent strand displacement and processivity but does not exhibit 3' exonuclease activity.[181,182] H-RCA has been paired with a number of FNAs[116,128,132,181–185] including DNAzymes.[151] Typically, H-RCA methods can improve amplicon production, and hence detection limits, by as much as 10^4 relative to linear RCA,[116] with detection limits being several orders of magnitude below the affinity constants for the aptamer MRE. However, attaching such ultrasensitive detection limits can require reaction times of up to 3 h or more.[116]

H-RCA is also amenable to pairing with nicking enzyme amplification to yield netlike H-RCA (N-RCA) for cubic amplification.[186] This method can improve sensitivity by more than an

order of magnitude compared to H-RCA, and has been used to detect both NA[187] and protein[188] targets, but has yet to be paired with FNA-based detection.

For detection methods that benefit from a uniform RP sequence, dendritic RCA can be incorporated as a variation on H-RCA.[189] A caveat for H-RCA is that the second RP is generated by amplification of the first RP, making two complementary RP strands. In dendritic RCA, an additional hairpin sequence is included which is complementary to both the RP and CT. Upon RP generation, this hairpin sequence unfolds, exposing the stem region which can subsequently be amplified by the same CT or by a secondary CT (Figure 2.8E).[190] In contrast to H-RCA, as the RP is exclusively generated using CTs throughout, the length of the RPs are limited by the kinetics of the polymerase rather than the length of the template RP being used.[85] Importantly, this dendritic RCA method retains the ability to encode the CT to allow generation of various RP outputs for strategic downstream sensing, which is not possible with traditional H-RCA.[190,191] Dendritic RCA has been used to detect NAs[189,190] and very recently expanded to the non-NA target PDGF-BB.[107]

3.2.3 DNAzyme Feedback Amplification

DNAzyme Feedback Amplification (DFA) is a recently reported method that utilizes RCA initiated generation of a DNAzyme to achieve E-RCA[121,192] (Figure 2.8F). The CT encodes a DNAzyme in the RP and is bound to a DNA primer (P2), found in Complex II, that includes a 3' overhang containing a substrate for a RCD, and an inverted 3' dT to prevent phi29 DP from acting as a 3'-exonuclease to trim the overhang. Amplification is initiated when an appropriate primer (P1), found in Complex I, is produced via target-modulated primer generation by the FNA, as described in Section 2. The primer can bind to excess free CT to initiate linear amplification, which produces a RCD as a repeating unit in the RP. This RCD then cleaves P2 at the RNA junction, leaving the DNA overhang, which is acted upon by PNK to produce an unblocked 3' terminus. The exonuclease activity of phi29 DP then trims the overhang and proceeds to generate the mature primer P1 that can initiate RCA to produce more RP, resulting in cross-feedback amplification.

DFA is an interesting case of a multi-enzyme E-RCA method, where the second enzyme is a DNAzyme rather than a protein enzyme. This method specifically highlights the power of RCA assays to produce the secondary enzyme directly, which can be used to achieve exponential amplification through a cross-feedback mechanism.

DFA is versatile in that any RCD for a NA or non-NA target could potentially be incorporated into the assay framework. Thus far, DFA has been used to detect miR-21, an RNA target, by using the miRNA target as a primer and the Mg^{2+}-sensitive MgZ as the RCD.[121] Detection of *Escherichia coli* (*E. coli*) was also achieved by making two alterations to Complex I. First, P1 was redesigned to contain a 3' overhang with a ribonucleotide, like Complex II. Second, the DNAzyme EC1 was added to the system to bind the overhang region and cleave the P1 ribonucleotide only in the presence of *E. coli*, which is a means of FNA-triggered primer generation. The CT still produced the MgZ DNAzyme, which could cleave the substrate on complex II, producing exponential amplification. Such an approach allowed single cell detection limits for *E. coli*. By modifying the substrate in Complex I as was done for E. coli detection, DFA has been extended to the detection of miRNA cancer biomarkers in liquid biopsy samples, with the output linked to a glucose meter (see Section 4)[193] and further modified for Pb^{2+} detection in river water samples using a Pb^{2+}-DNAzyme.[194] While DFA is a potentially powerful E-RCA method, it should be noted that the ribonucleotide-containing DNA sequences in Complex II are susceptible to nuclease degradation,[195] potentially making the DFA system less suitable for some POC applications, such as those that use complex samples that may contain ribonucleases.

3.3 Pre-amplified RP as MREs

Integrating an amplification step into an assay is not always required to reap some of the benefits of RCA. The production of substantially elevated localized concentrations of DNA has allowed for the visualization of single molecules of long RCA-derived amplicons.[84,85,196] In several assays, the RP has been used as a pre-amplified sequence not dependent on the presence of target, but instead generated to act as a MRE.[197–199] Further, using pre-amplified RP eliminates any time restrictions posed on the assay thus sidestepping the need to optimize the amplification efficiency. Other creative uses of RCA amplicons as MREs or as a polymeric biomaterials have been thoroughly discussed in a recent review found here.[200]

In one example, Gu *et al.* generated a competitive structure-switching assay for the detection of okadaic acid (OA) where the the pre-amplified RP is introduced to the reaction, using the aptamer region as an anchor.[201] The competitive binding assay with the OA aptamer causes a structure-switch and releases the RP from the surface which could be extracted from the supernatant and detected downstream. Achieving a LOD of 1 pg/mL (1.24 pM), the authors observed that incorporation of this pre-amplified RCA improved the LOD 50-fold compared to an unamplified capture strand.

Aptameric RP was used by Zhao *et al.* to create a 3D-DNA network of RP capable of binding to target surface proteins on potentially cancerous cells for capture and quantification.[199] This approached engineered 2 functional sites into the CT used to generate the DNA network, giving it two roles within the assay. First functional site, the target aptamer antisense sequence was incorporated into the CT. Generated aptameric RP is then capable of binding to the protein PTK-7, a cancer marker. The second, an encoded restriction site, allowing for release of captured cells upon addition of the restriction enzyme. The authors note that in theory, by incorporating different restriction sites, cells could theoretically be analysed sequentially upon each RE addition to the 3D network. These two functional sites enable both target recognition as well as detection.

Li *et al.* investigated the degree of amplification required to maximize the surface capture potential of aptamer-containing RPs for *E. coli* detection.[202] Here, the authors compared functionalizing a PDMS surface using dendrimers coated with either single unit aptamers, or with RPs generated at varying amplification times. Interestingly, they observed that maximum retention of *E. coli* was achieved after 2 hours of RCA as higher degrees of amplification led to decreased capture capacity which the authors attribute to non-specific intramolecular interactions within the RP. Further, not only was capturing efficiency lost but specificity was adversely affected too with amplification times at 12 hours showing poor target capture and little to no specificity.

In a contrasting approach, Carrasquilla *et al.* used an inkjet printer to deposit RP directly on cellulose to generate a localized scaffold of highly concentrated DNA for enhanced analyte detection.[197] This printed RP "bioink" acted in the same way as a long-chained aptamer might, with each repeat unit capable of aptamer binding. When printed onto the paper surface, the authors found the bioink was was too large to migrate across a cellulose surface but could still retain aptameric function in the presence of analyte. In contrast, monomeric aptamers were not able to perform due to their propensity to be displaced from

the cellulose surface during sample addition. Inkjet printing can be a convenient form of assay development, as it allows for the incorporation of internal references and multiplexed detection.

Liu and co-workers compared the analytical performance of an immobilized monomeric aptamer (1D) relative to a concatemer of aptamer strands (2D), or a superstructure known as a DNA nanoflower (NF)[203] comprised of several concatemers of aptamer strands (3D).[198] The surface density of the aptamers within the 3D amplicon was 4.6 to 8.1-fold higher than the 1D and 1.9 to 3.1-fold higher than the 2D variants. This enhanced localization of aptameric units improved the signal-to-noise ratio of the thrombin-binding system of the 3D construct by over four-fold relative to the 1D construct. Further, the 3D variant showed notable resistance to nuclease degradation and prevented non-specific protein adsorption onto the nitrocellulose surface – both key considerations for paper-based biosensors (see Section 6.3).

4. RCA Detection Outputs

4.1. Overview of Detection Methods

Several different approaches can be used to detect RCA reaction products, some of which, some of which are independent of the specific RP sequence, and others which require encoding a specific sequence into the CT to generate an antisense sequence in the RP that is used specifically as part of the detection system. In general, the detection methods are independent of the input methods outlined in Section 2, though as noted below, there are very specific requirements for the design of CTs to allow compatibility with some exponential RCA methods such as H-RCA.

Detection of RP can be divided into four broad categories: 1) detection of RCA reaction by-products (i.e., protons, inorganic phosphate, labelled dNTPs); 2) intercalation or adsorption of signalling moieties into or onto the RP; 3) hybridization of DNA carrying a detection moiety to the intact or monomerized RP or; 4) production of a G-quadruplex or DNAzyme output (PMD or RCD). The first two methods are compatible with any output sequence, while the latter two methods require specific CT sequences to generate outputs that allow signal generation. These outputs can generally be used to produce colorimetric, fluorescent, or electrochemical outputs, as shown in Figure 2.9. We have chosen to focus on these outputs owing to their compatibility with POC devices, and in particular due to the availability of simple and portable readers to meet the ASSURED criteria and allow use in low-resource settings.[204–206]

We note that in addition to these three signalling methods, there are several other sensitive instrument-based detection methods for direct detection of RPs.[73,74,207] These include methods such as surface plasmon resonance (SPR) to measure changes in optical mass of growing RPs[141,208–210], surface-enhanced Raman spectroscopy (SERS) to measure vibrational bands within RPs, [211–213]and detection of RP mass using quartz crystal microbalance (QCM) measurements.[141,214,215] However, such methods are not currently possible using simple and portable instrumentation, and will not be covered here as they are not compatible with the ASSURED criteria.

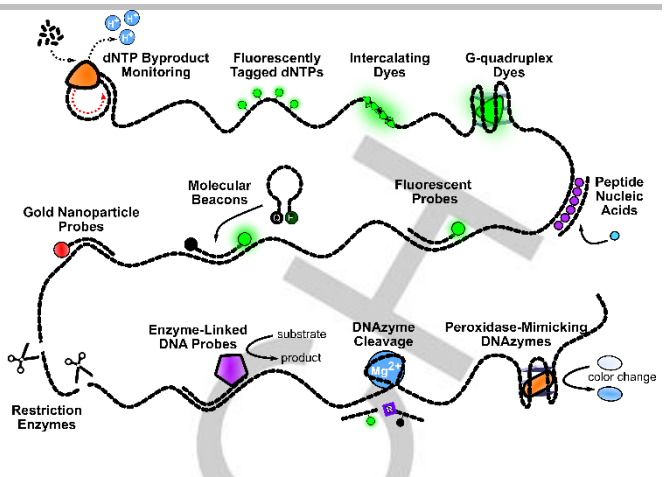

Figure 2.9. Examples of methods of detection and signal readouts employed for RCA detection.

4.2. Generic Detection Methods with Unstructured RPs

4.2.1 Monitoring RCA by-products

The simplest strategy for the detection of RP involves monitoring the by-products of amplification. In addition to the concatenated DNA strand, the RCA reaction also produces a proton (H^+) and pyrophosphate (PPi) for each dNTP added to the RCA product,[216] which can be probed to indirectly assess RP generation. Detection of RCA-mediated pH changes can be achieved by using pH indicator dyes[217], and pH paper[187], for colorimetric detection. To date, no RCA examples utilizing fluorescent pH indicator dyes have been reported. Likewise, though pH meters are common in electrochemistry, no method has been reported for RCA by-product monitoring. Accounting for the variability in pH of real samples poses a challenge to these styles of assay, especially in POC scenarios. While monitoring of pH is simple and cost-effective, it should be noted that indicator dyes are sensitive over a relatively narrow pH range, requiring careful control of initial solution pH. Solutions with low buffer capacity are generally required to achieve adequate changes in pH, which can require significant sample processing prior to RCA to obtain good sensitivity.[218,219]

The detection of PPi is typically achieved by monitoring the chelation of PPi with Mg^{2+} in the reaction buffer, which depletes the amount of free Mg^{2+} and causes a color change.[220] The hydroxy napthol blue (HNB) metal indicator dye from turns from violet (Mg-HNB) to sky blue (free HNB) as the concentration of free Mg^{2+} decreases. It was reported however, that the violet-to-blue color change may not be easily observed by eye, requiring a plate reader. Fluorometric monitoring of PPi as an RCA by-product has been reported, where a terpyridine-Zn(II) complex ($ZnCl_2L$) specifically binds to the PPi by-product and triggers fluorescence.[91,221] In this case the $ZnCl_2L$ is fluorogenic, and will only fluoresce when bound to PPi, avoiding the need for a washing step to remove unbound reagent.

4.2.2 Incorporation of Labelled dNTPs

An alternative method to monitor RCA reaction products is to incorporate labelled dNTPs directly into the reagent pool used to generate the RCA product. This is most commonly done using fluorescently-tagged dNTPs, where either the consumption of free dNTPs or generation of the fluorescent RP can be monitored.[196,222–224] While the detection of labelled dNTPs is highly specific, the used of labelled dNTPs can cause a reduction in the rate of RP production as these species have a lower rate of incorporation. Additionally,

unincorporated nucleotides must be removed using a washing step to eliminate background fluorescence. A significant drawback of using labelled dNTPs is the assay cost, as large numbers of relatively expensive labelled dNTPs must be incorporated into the RP to provide good detection limits. To this issue, Linck *et al.* reported that a novel dye was able to reduce costs by one-sixth relative to a Cy3-labelled dUTP.[222] The authors noted that direct addition of the dNTPs into the RP also avoided the need for subsequent processing steps, as the signal is generated during the polymerization reaction rather than during a subsequent reagent addition step.

4.2.3 Intercalating Species

As RCA generates a substantial amount of DNA, fluorescent DNA intercalating dyes offer a general method to detect RP without the need to encode specific outputs into the CT. The dyes are often fluorogenic cyanine or rhodamine derivatives and undergo conformational changes upon binding to single- or double-stranded DNA sequences, resulting in large increases in their quantum yield (up to 1000-fold), and hence their high emission intensity.[225] The background emission from such dyes is typically very low, avoiding the need for a washing step to remove unbound dye. Intercalating dyes are also able to monitor RP formation in real-time, which make assays based on dynamic signal changes possible. Taken together, this makes intercalating dyes well suited for POC applications using RCA. It is important to note that these dyes can also bind directly to the CT, and hence can potentially affect the thermodynamics and kinetics of the polymerase reaction,[226] and can produce high background signals that can impact detection of low levels of RP.

A large number of studies have utilized intercalating dyes for both solution and solid-phase assays (see sections 5 and 6), with typical dyes including SYBR Green I, SYBR Green II, Eva Green, SYBR Gold, and QuantiFluor.[101,113,116,119,125,132,143,181,199,227–229] These dyes offer a wide range of properties, including various excitation/emission wavelengths, selectivity for certain DNA sequences over others, different affinities for DNA relative to RNA, or different affinities for single- or double-stranded DNA. Hence, it may be necessary to evaluate several dyes to optimize a given RCA based assay.

4.3. Detection using Selective Hybridization or Adsorption of Signalling Moieties

While the examples above could utilize any RP sequence and hence did not require any encoding of outputs into the CT, such methods can suffer from background signals if there are endogenous NAs that can bind to intercalating dyes or affect detection of reaction by-products. To increase detection selectivity it is possible to encode specific sequences into the CT so that the multiple repeats of the antisense sequence appear in the RP. Among the most common methods for detection of RCA products is the hybridization of specific NA sequences to complementary sequences on the RP, which can produce a variety of detection outputs. A summary of these methods is provided below.

4.3.1 Hybridization of Peptide Nucleic Acids

For colorimetric outputs, a typical approach is to hybridize peptide nucleic acids (PNA) to the RP, followed by aggregation of specific dyes into the PNA-DNA complex. DisC2 (3,3'-diethylthiadicarbo-cyanine) is a common dye that aggregates to the PNA-DNA duplex,[230,231] causing a blue-to-purple color change. This method can reduce background signal generation as PNA is not native to biological samples and is not vulnerable to nucleases,[232] though the color change can be difficult to determine by eye. This assay can also be relatively slow at room temperature, and thus may require a heating step to increase the rate of the color change.[120]

4.3.2 Hybridization of AuNP-Labelled DNA

Complementary DNA sequences directly labelled with reporter molecules can also be used to bind to the repeating units in the RP. For colorimetric detection, the most common reporter is gold nanoparticles (AuNPs),[98,115,233] which have found widespread use for colorimetric biosensing owing to their distinctive red color and large molar absorptivities relative to other organic dyes.[234,235] The high absorptivity is due to the presence of localized surface plasmon resonance (LSPR) in the AuNP, which causes absorbance of light that is in resonance with the surface plasmon. The wavelength absorbed is highly dependent on nanoparticle size, shape, and immediate environment,[234] making AuNPs highly tuneable for biosensing applications.[236] AuNPs are also easily modified with thiolated DNA through the well-known sulfur-gold interaction,[237,238] allowing AuNPs to be modified with specific DNA sequences (AuNP-DNA) that can hybridize to repeating segments of RPs. It is important to note that AuNPs are relatively large (diameter of 5 – 20 nm or more) and carry multiple DNA strands per particle, and hence can bind across multiple regions of RPs, or to multiple RPs, which can increase overall binding affinity but may also promote aggregation. Examples of assays using AuNPs will be covered in Sections 5 (solution assays) and 6 (solid-phase assays).

4.3.3 Hybridization of DNA Labelled with Fluorophores or Redox Probes

DNA sequences can also be modified with small molecules, and unlike AuNPs, the hybridization sequences typically contain one signalling moiety per strand. A common detection approach involves the hybridization of DNA with covalently bound fluorescent probes (F-DNA) to the RP.[136,239–246] Under optimized conditions, this method can be applied successfully for single molecule detection using RCA.[85–87] Although this method normally requires a washing step to remove unbound F-DNA, it is possible to implement methods such as dipstick-based strategies to directly separate bound and unbound probes.[239] Unlike intercalating dyes, hybridization of F-DNA is selective for the output sequence in the RP, thus minimizing interactions with background NAs. Most commonly, F-DNA is a DNA strand modified with a fluorescent linker such as a fluorescein or cyanine derivative. However, less common fluorophores such as quantum dots can also be used.[245]

For electrochemical detection, hybridization probes are modified with electrochemically active reporter molecules. Various reporter labels can be attached to single stranded hybridization probes, including those that otherwise would have no affinity for DNA. These can include methylene blue,[281] ferrocene,[125] AuNPs,[125] or quantum dots.[137] In these cases, the mediator binds to RP that is tethered to an electrode surface. Gold nanoparticles themselves can play a large role in signal amplification because they can assist in electron transfer along the long surface area of bound RP.[141,210,247] The presence of the redox mediator along the RP allows for generation of a current based on oxidation or reduction of mediators that are in close proximity to the electrode surface. As with fluorescently-labelled hybridization probes, it is necessary to employ a washing step to remove unbound probes that could contribute to background current.

4.3.4 Hybridization of Molecular Beacons

An interesting method to overcome the need for a washing step is the use of molecular beacons (MBs) as hybridization probes. These

single-stranded DNA sequences form a hairpin loop structure with the termini modified with a fluorophore-quencher pair, a conformation that quenches the fluorophore.[248] Upon hybridizing to the RP, the MB adopts an extended conformation that separates the fluorophore and quencher ends, resulting in a 15- to 20-fold increase in fluorescence emission intensity. Given the ability to avoid a washing step and the selective binding to the RP, multiple groups have utilized this approach for sensitive detection of RCA products generated from both FNA initiated and nucleic acid initiated RCA.[110,111,135,249–253] Careful design of the CT is required to maximize signal generation with MBs as intermolecular quenching of neighboring fluorophores present in the concatemeric monolith can occur when quencher arms are not hybridized to the RP.[254] It has been observed that RPs that fully bind to the Q-labelled arm, but not the F-labelled arm, led to the best signal contrast. In addition, it is necessary to protect the 3' end of the MB using species such as 2'-O-Me-RNA to prevent exonucleolytic digestion of the MB by the phi29 DP.

An advantage of MBs (and also hybridization of F-DNA species) is the ability to use fluorophores with different excitation/emission wavelengths bound to different DNA sequences to allow one-pot multiplexed detection of RPs generated by two distinct targets initiating RCA with distinct CTs, or to incorporate a control CT as an internal reference for normalizing variability in assay conditions.[254]

4.3.5 Hybridization of DNA-modified Enzymes

To improve signalling levels, it is possible to bind an enzyme to a DNA sequence that hybridizes to the RP, which provides a second level of amplification and can dramatically improve detection limits. The attachment of the enzyme is typically done by first binding biotinylated DNA to the RP, followed by the addition of streptavidin-modified recombinant enzymes. This approach has been widely used for colorimetric detection, using enzymes such as glucose oxidase (GOx) to produce pH changes upon formation of gluconic acid,[184] which can be detected using pH indicator dyes. Avoiding buffer capacity issues with monitoring pH changes, horseradish peroxidase (HRP) can reduce chromogenic substrates such as 3,3',5,5'-tetramethylbenzidine (TMB)[255–258] in the presence of peroxide to generate colorimetric or electrochemical outputs for RCA-based assays. Importantly, the RCA reaction must reach completion before colorimetric detection can occur as the peroxide can denature the DP.

Redox active enzymes can also be hybridized to RPs to generate RCA-linked electrochemical assays. A commonly used enzyme is alkaline phosphatase (ALP),[96,259] which is used to convert ascorbic acid 2-phosphate into ascorbic acid, subsequently reducing silver ions which are deposited on the electrode and monitored by linear sweep voltammetry. Alternatively, streptavidin-tagged GOx can be added to a biotinylated probe on an immobilized RP for subsequent redox monitoring of pH changes associated with the oxidation of glucose,[260,261] though these methods suffer similar drawbacks to other pH based detection strategies such as the need for careful control of buffer capacity and initial pH. It is also possible to hybridize DNA carrying an invertase enzyme, which is used sucrose into fructose and glucose.[193,262–264] The latter product can be detected directly using a personal glucose meter (PGM), which can allow for operation in complex biological media (see Section 6).

4.3.6 Dequenching of Hybridized Sequences using Nicking Enzymes

Alternatively, nicking enzymes can be used to generate a fluorescence signal through site-directed cleavage of a hybridized DNA strand carrying a fluorophore quencher pair. The DNA can be hybridized to repeating units of the RP with a nicking site placed between the fluorophore and quencher with subsequent nicking causing release of the F-DNA from the quencher (Q-DNA) and a corresponding increase in fluorescence intensity. This approach may be more sensitive than traditional MBs as the nicking enzyme can cleave multiple probes per monomeric unit, whereas MBs only produce one signal once per RP monomer. The released cleavage products (F-DNA or Q-DNA) can also be used as a secondary primer to provide an exponential RCA output due to their inherent complementarity to the CT.[252] Similarly, the use of AuNP as an alternative quencher has also been explored.[265]

4.3.7 Nanoparticle Adsorption to RPs

Adapting the CT to produce long stretches of either adenine or thymine bases in the RP can allow for signalling based on nanoparticle adsorption to the RP, which is typically detected using an electrochemical method that takes advantage of the conductive nature of metallic nanoparticles.[266] Given that many nanoparticles can adsorb to a RP, these moieties can play a large role in signal amplification because they can assist in electron transfer along the surface of bound RP.[141,210,247] The two most common systems involve the adsorption of preformed AuNPs to polyadenosine DNA sequences in the RP[267] and production of copper nanoparticles (CuNP) along a RP via reduction of Cu^{2+} onto polythymine-rich RPs in the presence of ascorbate.[260] In the latter case the CuNP can either be detected by monitoring the oxidation current for subsequent production of Cu^{2+} or by monitoring the oxidation of a redox probe during the initial reduction of Cu^{2+} to form the CuNP.[280]

4.4. Detection using RPs Incorporating G-Quadruplexes

It is also possible to encode G-rich output sequences into the RP that can fold into highly structured moieties such as G-quadruplexes,[268] which are present as a specific repeating component of RPs. These guanine-rich sequences can fold into several different four-stranded topologies formed via intermolecular or intramolecular association induced by Hoogsteen interactions between guanine bases.[269] There are several G-quadruplex specific fluorescent dyes,[270–272] however RP detection has thus far been demonstrated only with Thioflavin T (ThT),[190,273–276] N-methyl mesoporphyrin IX (NMM),[117,191,277–279] and protoporphyrin IX (PPIX)[280–282] using either FNA-initiated or NA-initiated RCA. These dyes are similarly sensitive with detection limits ranging from picomolar to as low as attomolar[273] when exponential RCA is used. However, while both ThT and NMM dyes have been used for real-time monitoring of amplification signal, PPIX has not yet been used for real-time monitoring of RCA.

An advantage of detection based on dye-binding to G-quadruplexes is the specificity of the binding interaction, which can reduce nonspecific background signals from interfering with NA species. This can be an issue for general intercalating dyes that bind unstructured single- or double-stranded DNA. A disadvantage of the use of G-quadruplexes is the lower overall signal enhancement upon binding (typically 10- to 20-fold enhancements in emission intensity upon G-quadruplex binding versus up to a 1000-fold enhancement for SYBR Gold binding to DNA), which can result in higher background signal levels. For this reason, strategies using fluorescent G-quadruplex binding dyes commonly incorporate nicking enzymes for exponential RCA to generate sufficient G-quadruplex binding regions. Often these enzymes require elevated temperatures for optimal activity thus potentially limiting its utility as a POC approach.

G-quadruplex outputs can also be used to selectively intercalate redox probes. Subsequent reduction or oxidation of these probes

changes the overall chemical environment which can be readily monitored via changes in current or impedance. Common redox probes include methylene blue,[126,138,194,283–288] molybdate-[289–292] and ruthenium-based[293,294] DNA intercalating complexes. There are two common formats for the use of intercalating redox probes. In the first, the RP is immobilized on an electrode and with the intercalation of the mediator with the RP brings the mediator in close proximity of the electrode, thus increasing the measured signal. [283] Alternatively, RCA reactions can be carried out free in solution to produce RP rich in G-quadruplex subunits. Free mediator in solution intercalates with the RP, thus reducing its availability at the electrode surface and hance decreasing the current.[286]

4.5. Detection using RPs Incorporating DNAzymes

An alternative to hybridizing enzyme-DNA conjugates to RP is to produce RP that contain repeating DNAzymes units that catalyze reactions that can be detected by optical or electrochemical methods. This is commonly achieved by incorporating a peroxidase-mimicking DNAzyme (PMD) into the RP, which will contain hundreds to thousands of PMDs per RCA reaction. Reported nearly 3 decades ago,[43] the PMD is a specific G-quadruplex that can form a complex with hemin, resulting in HRP-mimicking peroxidase activity.[295] These G-quadruplex sequences enhance the natural peroxidase activity of hemin upon binding and therefore can be utilized with common optical and electrochemical peroxidase assays, making them attractive as reporter elements for biosensing.[296] Importantly, the direct formation of the PMD in the RP overcomes the need to hybridize an external enzyme and remove excess unhybridized enzyme with a washing step, making it more compatible with POC diagnostics. There are many examples of RCA-based assays that use PMDs to produce colorimetric outputs based on oxidation of 2,2'-azino-bis(3-ethylbenzothiazoline-6-sulfonic acid (ABTS),[112,131,140,151,297–301] or TMB,[98,112,114,255] which will be covered in detail in Sections 5 and 6. It must be noted, however, that as is the case for HRP-based assays, long-term peroxide stability becomes a challenge for operation in a POC setting.

PMDs can also be used for fluorescence-based sensing, based on the quenching of fluorescent quantum dot (QD) probes via a peroxidase-mediated photoinduced electron transfer system.[129,302] In this approach a PMD-containing RP is first generated by RCA followed by hybridization of a fluorescent QD-DNA probe. The proximity of the PMD to the QD causes fluorescence quenching owing to QD-to-hemin electron transfer, resulting in a decrease in signal intensity in the presence of RP.

The catalytic action of PMDs can also be monitored electrochemically by measuring the current related to the reduction of H_2O_2. This method has been extensively utilized for monitoring of RCA reactions (see Section 6) and is compatible with opaque samples that may not be amenable to colorimetric or fluorometric outputs.[303][304] It is also possible to use the PMD to produce an electrochemiluminescence signal wherein the PMD catalyses the oxidation of luminol in the presence of hydrogen peroxide generation of a luminescence output.[305]

Alternatively, RCA can be used to produce an RNA-cleaving DNAzyme as a component of the RP. When repeating RCD units are incorporated within the RP, they can be used to cleave fluorogenic DNA-RNA substrates to generate a fluorescence output.[148,189] These substrates have a specific DNA sequence that contains a single ribonucleotide cleavage site flanked by a fluorophore and quencher, which leads to low fluorescence background. The RP contains many RCDs which can cleave multiple substrates per repeat unit, producing substantial fluorescence enhancements.[148] The cleavage reaction is performed at room temperature and secondary enzymes do not need to be added following completion of the RCA reaction, making this approach more amenable to POC applications. However, it is important to stabilize the RNA-containing substrate to avoid the potential for self-cleavage which can increase the fluorescence background signal.[195]

5. FNA-Based POC Biosensors Utilizing RCA

The development of a final FNA-enabled RCA assay requires the integration of input, amplification, and detection methods in a manner that produces optimal performance in terms of selectivity, sensitivity, and limits of detection, while ideally meeting all the ASSURED criteria. In many cases, the development of a POC biosensor begins with the optimization of assay parameters using solution-based assays, and it is important to note that the emergence of simple commercially available handheld colorimetric and fluorometric readers (i.e. the Nix Pro Color Sensor™, or the ANDalyze AND1100 Fluorimeter) makes it possible to perform solution-based assays at the point-of-care. For this reason, we first consider simple solution-based RCA assays utilizing DNA aptamers or DNAzymes as MREs and producing optical outputs, and then describe how these assays are integrated into simple POC devices to produce portable sensors that better meet the ASSURED criteria. We then move on to consider heterogeneous optical assays utilizing solid supports such as beads or microwell plates. Optical assays that utilize fluidic systems based on glass, plastic or paper systems to enable multistep assays without user intervention are then discussed. We then conclude this section with a discussion of RCA-based electrochemical biosensors.

5.1 Homogeneous Optical Assays

Homogeneous assays are designed to operate without the inclusion of separation or washing steps, making them one of the simplest POC formats. These assays are generally done in solution (i.e., microwell plates or tubes) and comprise the majority of RCA-enabled sensing strategies as noted in several reviews.[306,307] Herein, we describe homogeneous assays that are amenable to use of simple optical readers, and highlight the advantages and disadvantages of such methods relative to various heterogeneous RCA-enabled assays. We consider both one-step and multi-step homogeneous assays, though in general it is best to minimize user steps to avoid the potential for user error and minimize assay time.

An early example of an RCA-based homogenous assay was reported by Di Giusto *et al.* in 2005, who described a thrombin-targeting assay that was able to fluorometrically detect thrombin in real-time within 30 minutes in a one-step, one-pot assay.[143] In this case both a linear and circular thrombin aptamer were employed for a proximity extension assay (see Section 2.2.2), with the RCA reaction product detected using SYBR Green I with a detection limit of 30 pM (Figure 2.10A). A drawback of this method is the low number of targets having two or more distinct aptamers that bind to different epitopes, and the need to circularize one of the aptamers, which could have detrimental effects on the native binding affinity of the aptamer.[113]

The majority of homogenous FNA-enabled RCA assays utilize structure-switching aptamers to generate inputs to the RCA reaction and fluorescence outputs for detection. Several variations on this approach are described below. One of the initial reports on use of

structure switching aptamers as FNAs was by Zhu et al. who developed a simple method for thrombin detection that operated by aptamer-based inhibition of a PLP reaction, with RP being detected with SYBR Green I (see Section 2.2.1).[181] Without thrombin, the aptamer is able to hybridize to the ligation strand, preventing the formation of a CT and blocking RCA by Bst DP. Thrombin causes switching of the aptamer off the ligation strand, allowing CT formation followed by linear RCA, producing a detection limit of 1 pM, or hyperbranched RCA to achieve a 2 fM detection limit in 3 hrs.

Yang *et al.* also used a structure switching approach linked to PLP inhibition for PDGF detection (see Section 2.2.1, Figure 2.5A).[125] In this approach, target binding caused a structural change in the aptamer to release the terminal ends, which permitted ligation to convert the aptamer into a CT for real-time monitoring of linear RCA with SYBR Green I. A drawback was that the assay requiredy four steps, including a heating step, and also required 3 hours to produce a detection limit of 0.3 nM of PDGF. However, the assay was also shown to be amenable to detection of PDGF in cell lysate with a comparable LOD of 0.4 nM.

Simple structure-switching systems have also been developed using colorimetric outputs. For example, Liang *et al.* combined structure-switching aptamers to control RCA with the adsorption of unfunctionalized AuNPs onto the RP to detect carcinoembryonic antigen (CEA).[139] Once again, target binding to an aptamer modulated a PLP reaction (see Section 2.2.1), with target binding permitting ligation and amplification. The final LOD was 2 pM using H-RCA, based on a red-to-blue colour transition upon AuNP adsorption to the RP (Figure 2.10B), which is a particularly good LOD for a colorimetric assay. The assay was also highly selective with 10000-fold concentrations of various interferents having no effect on the signal.

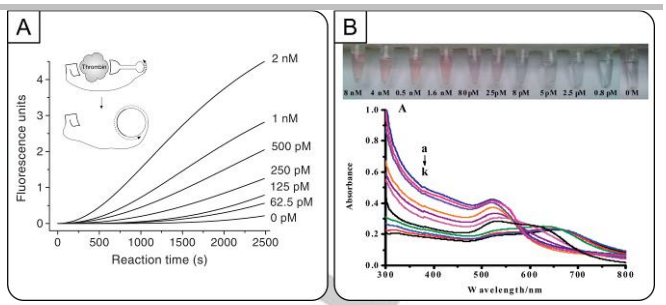

Figure 2.10. Homogeneous FNA-RCA assays with optical detection methods. (A) Fluorescence data for proximity extension of circular DNA aptamers with real-time detection of the thrombin target. (B) Visual detection of CEA based on PLP ligation, hyperbranched rolling circle amplification and AuNP aggregation. Figures adapted from references cited in text.

More complicated structure switching systems can be developed by integrating the aptamer into a tripartite system comprising the aptamer, pre-primer and CT (see Section 2.1.2, Figure 2.3A), as was demonstrated for PDGF-mediated activation of H-RCA.[116] In this case, the target removes the aptamer, which acts as a control element to prevent priming of the RCA reaction. Upon removal, phi29 DP mediated exonucleolytic digestion of a pre-primer produces a mature primer to initiate H-RCA, with the RP generation monitored in real-time by EvaGreen (Figure 2.11A, top). This method could detect 100 fM of PDGF after 15 minutes of amplification, and 1 fM of PDGF using a RCA time to 2 hours (Figure 2.11, bottom). Wang *et al.* used the same tripartite regulation method to initiate an initial catalytic hairpin assembly approach that was then coupled with exponential RCA, providing a detection limit of 0.2 pg/mL) of OTA in 90 min (Figure 2.11B).[191] In addition, a split aptamer variation was reported utilizing a similar 3'-exonuclease regulation method paired with an endonuclease-assisted feedback system (Section 2.1.2, Figure 2.3B) for the detection of ATP (LOD of 0.09 nM) (Figure 2.11C).[117] Both systems were successfully tested against samples of red wine for OTA and human serum for ATP, respectively, with the fluorogenic probe NMM binding to G-quadruplexes present in the RP.

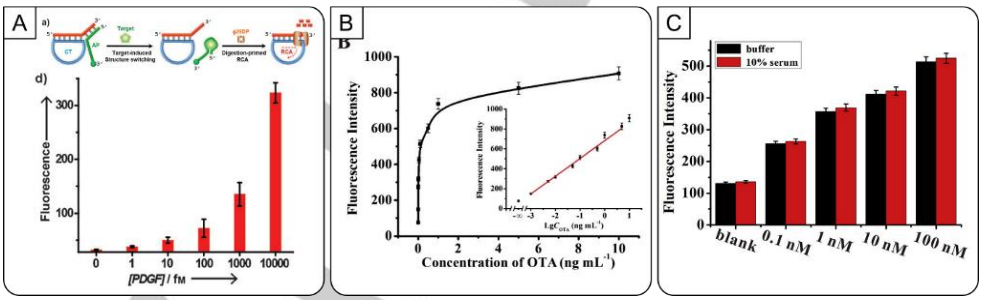

Figure 2.11. Homogeneous FNA-RCA methods utilizing tripartite structure-switching systems paired with the 3'-exonuclease activity of phi29 DP. (A) Tripartite structure-switching and DNA amplification of a DNA assembly for detection of PDGF. (B) Tripartite structure switching detection paired with catalytic hairpin assembly for the detection of PDGF. (C) A dual-aptamer approach for ATP detection based on endonuclease-fueled feedback amplification Figures adapted from references cited in text.

Recently, Liu et al. reported on a a simplified variation of the tripartite structure-switching assay system that removed the need for inverted dT protecting groups on the 3'-end of the pre-primer as phi29 digestion was not used (Section 2.1.1, Figure 2.2B).[107] This approach used a dendritic RCA method for exponential amplification and PMDs as the output, resulting in the colorimetric detection of PDGF via oxidation of TMB led with a LOD of 1.96 fM in diluted serum samples. Though very sensitive for a colorimetric assay, the method required over 3 h to perform and required addition of peroxide and

TMB following RCA, adding complexity to the assay and preventing real-time signal generation.

It is also possible to use an internal structure switching system based on aptamers that can form hairpin structures. Here, a weak hairpin is initially present, which can be extended with Klenow fragment (KF) to produce a strong hairpin, denoted as a shielded aptamer, that is unable to bind target or initiate RCA. Addition of target prior to KF opens the hairpin and prevents hairpin extension by KF, thus allowing a primer extension on the aptamer to initiate RCA (Section 2.1.2, Figure 2.3D).[119] The aptaprimer approach was used for detection of three small molecules, with linear RCA providing one-pot, three-step detection of OTA (LOD of 38.8 fM), kanamycin (LOD of 8.9 fM), or L-tyrosinamide (LOD of 47.5 pM) with a 3 hour assay time (Figure 2.12A), and were amenable to detection of these targets in spiked serum (kamaycin and L-tyrosinamide) or red wine (OTA).

Control of RCA can also be accomplished by having aptaprimers switch off a reduced graphene oxide surface (Section 2.1.1, Figure 2.2C).[110] This approach has been reported for detection of several types of targets, including thrombin (protein), ATP (small molecule), and HCV-1 DNA (NA). Here, the aptamer was modified with a primer extension, producing an aptaprimer that could initiate RCA. When bound to rGO, the aptaprimer was prevented from binding to a CT. However, release of the aptaprimer upon target binding freed the primer to bind the CT and initiate RCA, with the RP being detected by binding of a molecular beacon (Figure 2.12B). The authors reported detection limits of 10 pM for thrombin, 60 nM for ATP, and 0.8 pM for HCV-1 DNA each with a total assay time of under 3 hours with linear amplification. The thrombin-targeting assay was also shown to be amenable to detection in 50-fold diluted human serum, with a LOD of 10 pM. In a follow-up paper, Mao *et al.* further optimized the CT with stronger binding to the released aptaprimer to further drive the detection limit down and improved the LOD of the thrombin system 10-fold from 10 pM to 1 pM.[111]

An alternative method to structure-switching is to use an aptaprimer that can either be blocked from priming RCA upon binding of target (Section 2.1.1, Figure 2.2D) to produce a turn-off assay,[101] or used in combination with the inherent 3'-exonuclease activity of phi29 DP to produce a turn-on assay (Section 2.1.2, Figure 2.3C) (Figure 2.12C, top).[118] In the first case, the binding of either thrombin or PDGF to their respective aptamers resulted in a reduction in RCA product formation, leading to a detection limit of 10 nM for PDGF and 100 pM for thrombin within 1 hour.[101] By incorporating the digestion step along with CT mediated strand displacement, an activation assay was produced with detection limits of 100 pM for both PDGF and thrombin using real-time monitoring of linear RCA with SYBR Gold within 2 hours.[118] Notably however, the activation assay showed signal inhibition at higher concentrations of target (above 10 nM) independent of toehold length (Figure 2.12C, middle) which the authors ascribe to the inability of the toehold system to displace the target when the target is in large excess. With clinically relevant levels of PDGF and thrombin often falling within only one or two orders of magnitude, the assay could still be applicable at the POC. As well, the assay was optimized for detection of PDGF in human plasma or serum (Figure 2.12C, bottom). As target binding confers protection onto the aptamer from nuclease activity, this approach may be particularly well suited for nuclease-containing samples.

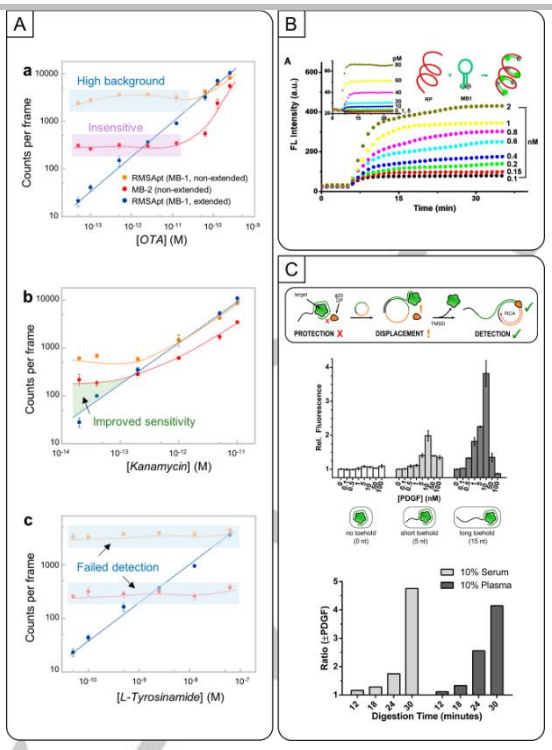

Figure 2.12. Homogeneous FNA-RCA methods where the aptamer and primer are in the same sequence. (A) Digital fluorescence quantification of small molecules using shielding aptamer-triggered RCA. (B) Real-time fluorescence detection of RP using molecular beacons with varying concentrations of thrombin. (C) A signal-on biosensing strategy for PDGF and thrombin enabled by toehold-mediated RCA. Figures adapted from references cited in text.

In addition to aptamer-based homogeneous assays, it is also possible to produce such assays under the regulation of DNAzymes. Liu et al. pioneered an approach for the detection of *E. coli* by using a DNA catenane to mechanically lock the system in place until cleaved by the RCD (Section 2.2.3, Figure 2.7D) (Figure 2.13A, top).[151] Topologically constrained nanostructures that are regulated by the use of DNAzymes can increase the specificity of the interaction between the target and FNAs. Amplification at the RNA cleavage site cannot proceed until the base is treated with PNK to remove the 2'3' cyclic phosphate, a common cleavage product for several RCDs.[308,309] While this was an individual 30-minute step in this assay, the same group has shown that the PNK and amplification steps can be combined together.[310] The authors investigated the integration of a PMD into the CT for colorimetric linear RCA (Figure 2.13A, middle) and compared it to fluorometric hyperbranched RCA (Figure 2.13A, bottom). The linear PMD approach (1000 cells per mL) underperformed compared to the H-RCA approach (10 cells per mL). The less sensitive colorimetric strategy requires six steps in three hours for detection by eye. In contrast, the fluorometric strategy is much more sensitive and requires only three steps with a total time of 2.5 hours, though quantification requires a reader.

Another example of DNAzyme-mediated RCA is the use of DFA to achieve exponential signal enhancement when using RCDs as the recognition element, as demonstrated by Liu et al. demonstrated for the real-time detection of *E. coli*. [121] Primary amplification through the cleavage of the unique tripartite system (Section 2.1.3, Figure 2.4B) allowed for the autonomous generation of primers and secondary amplification products (Section 3.2.3). The two-step isothermal amplification incorporated both cleavage and PNK treatment simultaneously within one hour. After sufficient generation of RCA

precursors, linear amplification resulted in detection limit of 10 cells per mL of *E. coli* after one hour of amplification (Figure 2.13B), or a total assay time of 2 hours. Notably, DFA improved detection limits by 1000-fold relative to the unamplified RCD, requiring just a single additional step. Though it has only been demonstrated for NA (mi-RNA) and RCD-mediated (*E. coli*) targets, the authors indicate that the assay should be amenable to many other analytes as long as generation of complex I can be regulated through a molecular recognition event.

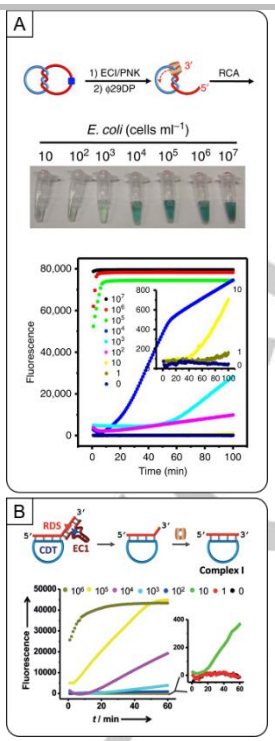

Figure 2.13. Homogeneous FNA-RCA methods incorporating RCDs. (A) Colorimetric (top) and fluorescent (bottom) detection of a catenane-RCD triggered amplification. (B) A DNAzyme Feedback Amplification (DFA) strategy for fluorescent detection of *E. Coli*. Figures adapted from references cited in text.

Table 2.1. Homogeneous solution-based methods.

Detection Method	RCA Method	MRE Type	Regulation Method	Target	LOD	# Steps	Temperature	Assay Time	Ref.
				Colorimetric Detection					
AuNP	hyperbranched	aptamer	structure-switching [PLP]	CEA	2 pM	many [P]	multiple	≥ 2 hrs	[139]
PMD	linear	DNAzyme	RCD	*E. coli* [CM]	1000 cells / mL	many [P]	multiple	≥ 2 hrs	[151]
PMD	dendritic	aptamer	structure-switching	PDGF [CM]	1.96 fM	many [P]	multiple	≥ 3 hrs	[107]
intercalating dye	linear	captamer	inhibition RCA	thrombin	15 nM	many [P]	multiple	≥ 1 hr	[145]
				Fluorometric detection					
cDNA (fluorophore)	linear	aptamer	inhibition RCA [PLP]	aflatoxin M1 [CM]	0.0194 pg/mL	many	37 °C	≥ 3 hrs	[133]
G-quad dye	enzyme-assisted	aptamer	structure-switching [PLP]	ATP [CM]	84 nM	many	multiple	≥ 8 hrs	[275]
intercalating dye	hyperbranched	aptamer	structure-switching [PLP]	ATP	1 nM	many	multiple	≥ 2 hrs	[183]
intercalating dye	hyperbranched	aptamer	structure-switching [PLP]	ATP	ATP in a single HeLa cell	many	multiple	≥ 2 hrs	[183]
cDNA (MB)	linear	aptamer	structure-switching (rGO)	ATP [CM]	60 nM	many	multiple	≥ 2 hrs	[110]
G-quad dye	enzyme-assisted	aptamer (split)	structure-switching	ATP [CM]	0.09 nM	2	37 °C	≥ 1 hr	[117]
G-quad dye	enzyme-assisted	aptamer	structure-switching [PLP]	BPA [CM]	54 aM	many	multiple	≥ 5 hrs	[280]
intercalating dye	hyperbranched	DNAzyme	RCD	*E. coli* [CM]	10 cells /mL	many [RT]	multiple	≥ 3 hrs	[151]
intercalating dye	DFA	DNAzyme	RCD	*E. coli*	10 cells / mL	2 [RT]	37 °C	≥ 2 hrs	[121]
cDNA (MB, Fr/Q)	linear	DNAzyme	DNAzyme kinase [PLP]	GTP	4 μM.	many	multiple	≥ 4 hrs	[148]
intercalating dye	linear	aptamer	structure-switching	kanamycin [CM]	8.9 fM, 1	many	multiple	≥ 3 hrs	[119]
intercalating dye	linear	aptamer	structure-switching	L-tyrosinamide [CM]	47.5 pM	many	multiple	≥ 3 hrs	[119]
cDNA (QD)	linear	aptamer	structure-switching [PLP]	lysozyme [CM]	2.6 nM	many	multiple	≥ 3 hrs	[129]
G-quad dye	strand-displacement assisted RCA	aptamer	structure-switching	MUC1 [CM]	0.5 pM	3	37 °C	≥ 2 hrs	[311]
intercalating dye	hyperbranched	aptamer	structure-switching [PLP]	OTA [CM]	1.2 fg/mL	many	multiple	≥ 4 hrs	[182]
intercalating dye	linear	aptamer	structure-switching	OTA [CM]	38.8 fM	many	multiple	≥ 3 hrs	[119]
G-quad dye	CHA-assisted	aptamer	structure-switching	OTA [CM]	0.0002 ng/mL	2	37 °C	≥ 1 hr	[191]
dNTP monitoring	linear	aptamer	structure-switching [PLP]	OTA [CM]	0.01 ng/mL	many	multiple	≥ 8 hrs	[224]

intercalating dye	linear	aptamer	inhibition RCA	PDGF	10 nm	2 [RT]	r.t.	60 min	[312]
intercalating dye	linear	aptamer	structure-switching [PLP]	PDGF [CM]	0.3 nM	many [RT]	multiple	≥ 3 hrs	[125]
intercalating dye	hyperbranched	aptamer	structure-switching	PDGF	1 fM	1 [RT]	30	≥ 2 hrs	[116]
cDNA (MB)	linear	aptamer	structure-switching [PLP]	PDGF	6.8 pM	many	multiple	≥ 3 hrs	[249]
G-quad dye	enzyme-assisted	aptamer	structure-switching [PLP]	PDGF [CM]	0.38 fM	many	multiple	≥ 8 hrs	[277]
G-quad dye	HCR-assisted	aptamer	structure-switching [PLP]	PTK7	0.3 fM	many	multiple	≥ 7 hrs	[279]
G-quad dye	HCR-assisted	aptamer	structure-switching [PLP]	PTK7	10 CCRF-CEM cells	many	multiple	≥ 7 hrs	[279]
G-quad dye	HCR-assisted	aptamer	structure-switching [PLP]	PTK7	20 HeLa cells	many	multiple	≥ 7 hrs	[279]
intercalating dye	linear	aptamer	inhibition RCA	thrombin	100 pM	2 [RT]	r.t.	30 min	[312]
intercalating dye	linear	aptamer	inhibition of PLP [PLP]	thrombin	1 pM	many	37 °C	≥ 3 hrs	[181]
intercalating dye	hyperbranched	aptamer	inhibition of PLP [PLP]	thrombin	2 fM	many	37 °C	≥ 3 hrs	[181]
cDNA (MB)	linear	aptamer	structure-switching (rGO)	thrombin [CM]	10 pM	many	multiple	≥ 2 hrs	[110]
intercalating dye	linear	aptamer	sandwich (apt 2x)	thrombin	30 pM	1 [RT]	37 °C	30 min	[143]

[a] Table Footnote. [b] … [RT] denotes that detection was done with real-time monitoring; [PLP] denotes that the assay used a padlock probe ligation reaction; [CM] denotes that the assay was tested with complex media; “many” denotes any assay that required 4 or more steps; r.t. denotes that room temperature was used.

5.2 Heterogeneous Assays

Heterogeneous assays employ some form of separation step to physically separate assay components. While this increases the assay complexity and number of steps, it gives researchers more control over the reaction buffer, which may require strict conditions for subsequent reactions including RCA. Heterogeneous solution-based assays are summarized in Table 2.1. As well, it aids in the removal of unreacted components that may adversely affect downstream steps. For example, FNA-based heterogeneous assays may employ ethanol precipitation as a means of separating NA species during the assay, though this method is intensive and less applicable at the POC. In this approach, Ali and Li used an RCD for the detection of ATP (Section 2.1.3, Figure 2.4A) where The linearly amplified output RP was hybridized with PNA probes in solution.[120] Physical separation using ethanol precipitation was used to isolate the RP and reconstitute it in a hybridization buffer designed to maximize PNA probe hybridization to RP and intercalation of the colorimetric indicator, DisC2. This method can reduce background signal generation as PNA is not native to biological samples and they are not vulnerable to nucleases,[232] though the blue-to-purple color change can be difficult to determine by eye (Figure 2.14A, top). Notably, the assay was relatively slow at room temperature, and thus required a heating step to increase the rate of the color change otherwise several minutes of incubation at room temperature was required. The assay achieved a detection limit of 100 µM of ATP in over 4 hours (Figure 2.14A, bottom).

Huang et al. demonstrated a more practical method of separation by using a membrane filter to separate unbound aptamers for gastric cancer exosome detection.[132] The authors incubated anti-MUC1 aptamers with gastric cancer exosomes allowing the aptamers to hybridize with the MUC1 cell surface protein, which is overexpressed in gastric cancers (Section 2.2.1, Figure 2.5E). A 22 nm pore size membrane then filtered the solution to separate free and bound aptamers, removing the large cell-aptamers complexes (Figure 2.14B, top). The aptamer was liberated from the cell surface by heat treatment and subsequently circularized by PLP reaction only if the unbound aptamer remains in the filtered solution. Finally, they monitored H-RCA in real-time using SYBR Green I (Figure 2.14B, bottom) for detection of as low as 4.27 x 10^4 exosomes per mL. Though filtration is faster and less labor-intensive than ethanol precipitation, the added processing steps, including heat denaturation, make this approach challenging for POC applications.

Several strategies have been suggested for the physical separation of RP from its endogenous solution, including those tethered to a bulk solid surface (i.e. microwell plates, glass slides, discussed in 6.2.2) or their particulate equivalents (i.e. agarose beads, or magnetic beads). These particulates, sometimes called beads, may be used to tether sandwich-style MREs as Tang *et al.* demonstrated in their dual-aptamer assay for PDGF detection (Section 2.2.1, Figure 2.5D).[313] The centrifugation step was key to this approach as it physically separated any avidin beads with biotin-aptamer-target complexes formed on the bead surface from solution(Figure 2.14C, left). As opposed to ethanol precipitation and membrane filtration, bead-based centrifugation can be performed quickly and with ease where equipment is available. The sandwich formation acted to tether a primer-CT duplex to the bead surface, forgoing any PLP step and allowing for the linear amplification of PMD-rich RP for colorimetric detection (Figure 2.14C, top right). Avidin beads have great utility as the target-binding stage occurred in a volume of 100 µL whereas the centrifuged beads were resuspended in only 10 µL of buffer, effectively concentrating the solution ten-fold. This pre-concentration effect is a typical advantage of bead-based assays and may be a substantial factor in achieving the reported detection limit of 7.1 fM of PDGF (Figure 2.14C, bottom right).

Several classes of particulates used in these homogeneous assays have characteristics that can be exploited to increase assay sensitivity. Gold nanoparticles, specifically, can be used as a surface for target immobilization and for their redox capabilities. Abnous *et al.* made use of these features in their their aptasensor to detect the small molecule aflatoxin M1.[314] This approach regulates the digestion of single-stranded DNA by a CRISPR-Cas12a system, a version of circular ligation regulation (Section 2.2.1). CRISPR-Cas12a regulates the availability of a ligation strand for a PLP reaction. In the presence of unbound aptamer, CRISPR-Cas12a is activated and digests the ligation strand, thus blocking RCA. Centrifugation is used in several steps, including one for the removal of unbound aptamers and padlock probes. Target-triggered amplification results in an accumulation of RP on the AuNP surface which limits its ability to reduce endogenous yellow 4-nitrophenol to the colorless 4-aminophenol, giving clear colorimetric indication of amplification. Though this approach utilized a ligation step, it achieved a detection limit of 0.05 ng/L. With sensitive detection achieved in spiked milk samples as well (0.15 ng/L), this approach rivalled several electrochemical alternatives.

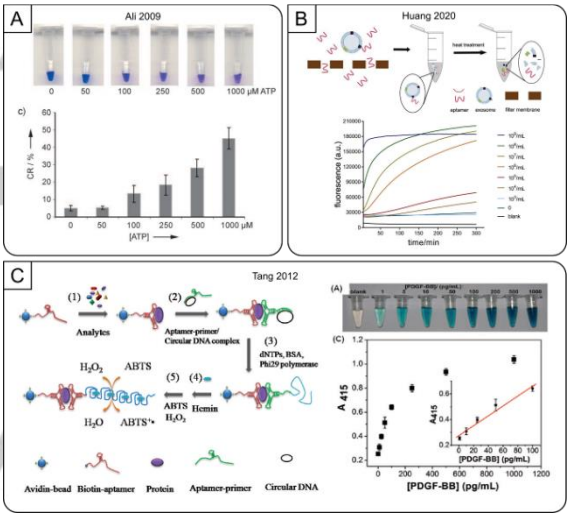

Figure 2.14. Heterogeneous FNA-RCA methods where magnetic beads are not used. (A) Colorimetric sensing by using allosteric-DNAzyme-coupled RCA and a PNA–organic dye probe. (B) Fluorescence detection of gastric cancer exosomes based on an aptamer-PLP E-RCA (C) A dual-aptamer PDGF bioassay using the colorimetric detection of PMD-rich RP. Figures adapted from references cited in text.

5.2.1 Magnetic Beads

Magnetic beads are another class of particulates used in homogeneous assays that can replace centrifugation-based bead strategies where centrifugation is not practical, as may be the case with portable POC devices. As implied, a magnetic force applied to the beads allows for simple separation of bead-bound and unbound compounds. This allows researchers to retain the separation powers of the technique while minimizing the infrastructure required to achieve it. Song *et al.* used magnetic beads for the aptameric detection of the bacteria *V. parahaemolyticus* (Figure 2.15A, top). [300] This method used a dual-aptamer approach with the addition of a biotinylated anchoring aptamer and a detecting aptamer into a target sample. Next, streptavidin-coated magnetic beads were added and used to extract the pathogenic bacteria. The detecting aptamer could be converted into a CT through a PLP step for amplification with nicking-assisted RCA.

With PMDs integrated into the RP, the addition of hemin and ABTS allowed for the colorimetric generation of a green solution in the presence of the target bacteria corresponding to a detection limit of 10 CFU/mL (Figure 2.15A, middle). Monitoring of food-borne pathogens is an ongoing need with *V. parahaemolyticus* being a common pathogen in seafood. Even more so, any colorimetric approaches could be impacted by the composition and opacity of the food product itself. This assay employed magnetic bead-based separation and colorimetrically detected the bacteria in various spiked food samples (oyster, clam, codfish, jellyfish, shrimp, milk, and squid) (Figure 2.15A, bottom). In all, the full assay could be conducted in just 1 h 40 min though it did require several steps including a 95 ˚C termination step for the PLP reaction.

MRSA cells were reliably enriched using a magnetic bead strategy in Xu *et. al*'s assay that used a dual-aptamer sandwich approach to separate the cells using a streptavidin-avidin interaction (Figure 2.15B, top). [315] Several washing steps liberated the unbound sample components, leaving MRSA cells tethered to the magnetic bead. A second aptamer was introduced, comprised of a PBP2a-specific structure switching aptamer that released a hybridized blocking sequence after binding to the target protein on the cell surface (Section 2.2.1, Figure 2.5B). PLP is only initiated when this second aptamer has MRSA cells to bind to, freeing the blocking strand to act as a ligation template and primer. Together PLP and linear amplification takes approximately 70 minutes. To improve assay sensitivity, instead of using an E-RCA the assay employed CRISPR-Cas12a enzymes whose *trans*-cleavage activity would cleave MBs accumulated on the RP. The wide linear range of this assay (10^2 to 10^6 CFU/mL, Figure 2.15B, bottom) was attributed to the combined powers of RCA and the attached CRISPR-Cas 12a, allowing for bacterial quantification in less than 3 hours. Clinically-obtained serum was spiked to assess the clinical effectiveness of the proposed microwell assay with good success.

Aside from removing assay components from a complex sample matrix, magnetic beads can be advantageous particularly for removing unreacted detection agents, such as fluorescently-tagged cDNA probes. Yao *et al.* utilized magnetic beads to remove unbound fluorescent quantum dot probes, which were then used as in indicator of OTA-triggered RP (Section 2.1.1, Figure 2.2D).[245] In this instance, the magnetic bead was tethered to the 5'-end of the aptamer such that any RP generated would stay immobilized on the magnetic bead (Figure 2.15C, top). As it was an inhibition RCA regulation approach, only 15 minutes of linear RCA were required with the QD-labelled cDNA probe requiring 30 minutes of incubation with RP, resulting in a total assay time of just over one hour. The resuspension of the beads allowed for high fluorescence with minimal background, achieving a detection limit of 0.13 ppt for OTA (Figure 2.15C, bottom), with validation in red wine samples.

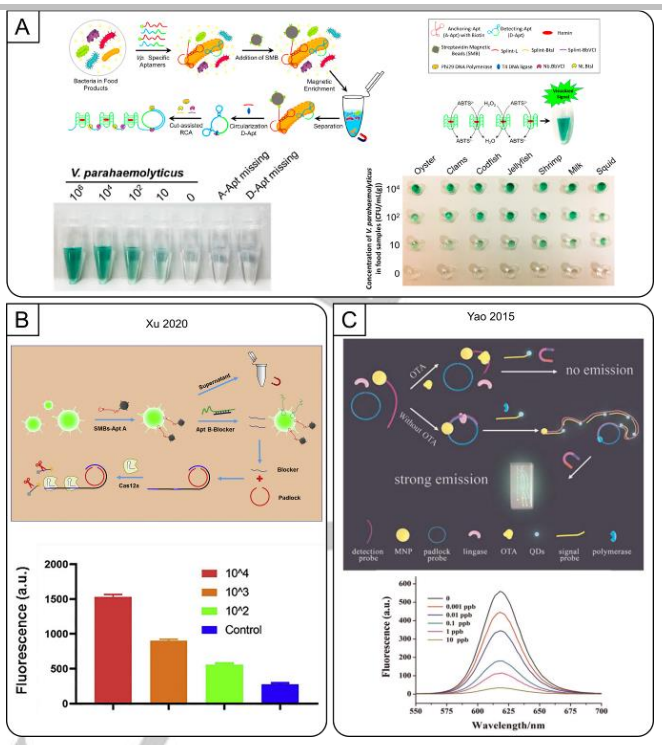

Figure 2.15. Heterogeneous FNA-RCA methods utilizing magnetic beads. (A) Visualized detection of *Vibrio parahaemolyticus* in food samples using dual-functional aptamers and E-RCA (B) Dual-functional aptamer and CRISPR-Cas12a assisted RCA for the detection of MRSA. (C) Magnetic bead inhibition RCA using quantum dot fluorescent detection of OTA. Figures adapted from references cited in text..

Background fluorescence from intercalating dyes can similarly be minimized by ensuring other NA contaminants are removed, as demonstrated in this assay monitoring real patient faecal samples in real-time using a GDH captamer (Section 2.2.2, Figure 2.6C).[113] After magnetic bead isolation of nGDH-bound captamer in the supernatant, the solution was heated to release the captamer for downstream RP generation at 30 °C (Figure 2.16A, top). Here, the separation step aided in ensuring that there would be minimal interfering NAs that the SYBR Gold could intercalate with, allowing for real-time detection of RP. The authors reported an LOD of 10 pM of GDH in human faeces in just over 1 hour using this strategy (Figure 2.16A, middle), despite employing a linear amplification. More interestingly, this group was able to demonstrate their assay's real-world applicability by testing several real-patient samples (Figure 2.16A, bottom).

Miao *et al.* used immunomagnetic beads to capture and isolate PDGF and used the catalytic power of GOx detection to boost sensitivity (Figure 2.16B, top).[184] This assay utilized an antibody and aptamer-primer sandwich complex to reduce non-specific target bonding (Section 2.2.1, Figure 2.5D). As there are few targets with aptamers for two unique epitopes to participate in the sandwich, it is very common to see antibody-aptamer (Ab/apt) sandwich interactions.[289,303,316] Exponential dendritic RP propagates from its sandwich complex anchor, and GOx-labeleld primer complexes accumulate within the branched concatemeric RP. The immunomagnetic bead was again magnetically isolated from solution and resuspended in fresh solution. Next, glucose and bromocresol purple pH indicator were added and the remaining RP-bound GOx drove a color change from purple (basic) to yellow (acidic) (Figure 2.16B, middle), generating a LOD of 0.94 pM of PDGF within 3.5 hours (Figure 2.16B, bottom). Many examples throughout this review

have demonstrated the various ways to convert a linear RCA process to exponential for the ultrasensitive detection of analyte. However, this approach combined both exponential RCA with GOx-mediated detection, making for a relatively sensitive dual-exponential approach that could be evaluated by the naked eye. The use of magnetic beads was required to remove background RP as well as to carefully control the buffer capacity in the final detection step, key for the use of the pH indicator.

Huang *et al.*'s assay increased sensitivity by capitalizing on the fluorescence quenching ability of AuNPs . Aptamer-primer binding to nucleolin completed the sandwich assay formation, allowing tethered RCA to occur upon binding to leukaemia-derived exosomes (Section 2.2.1, Figure 2.5D).[265] However, in this case the detection was based on hybridization of F-DNA probes bound to and quenched by a gold nanoparticle in the assay solution (Figure 2.16C, top). These quenched probes would preferentially bind to the target-triggered RP and be cleaved by a nicking endonuclease, separating it from the quenching AuNP and restoring fluorescence. The detection cycle can be repeated multiple times per AuNP, providing an exponential signal enhancement beyond RCA, limited only by the number of probes immobilized on the AuNP surface (~55 probes per AuNP). This room-temperature approach could detect as few as 10^2 exosomes per µL in slightly more than three hours (Figure 2.16C, bottom). A drawback of this approach was the need to perform the nicking enzyme detection step after the completion of the linear RCA reaction to avoid the possibility of the nicking enzyme cleaving the CT (which must also include the nicking site to produce the complementary sequence), as this would halt RCA entirely.

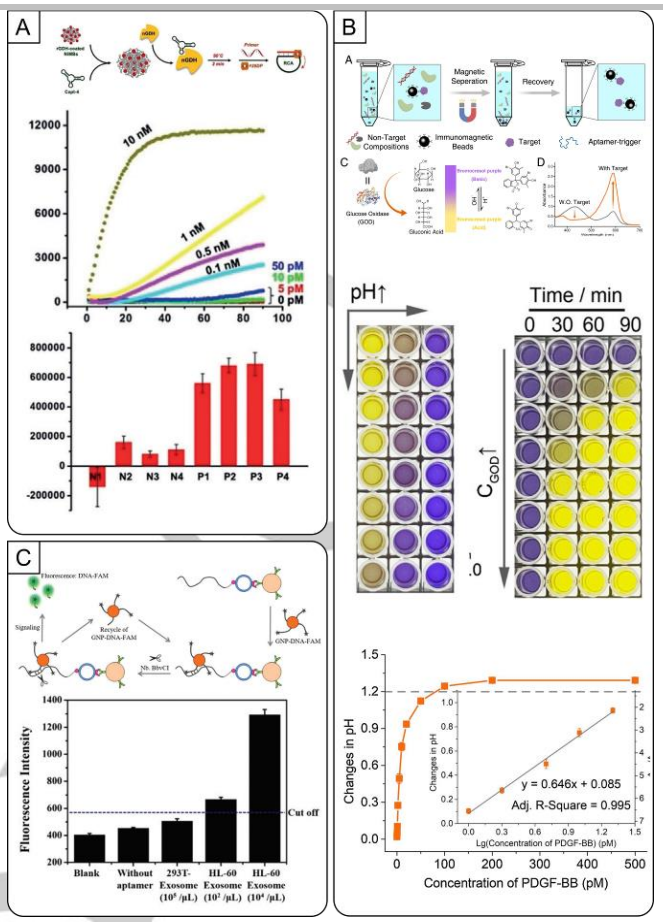

Figure 2.16. Heterogeneous FNA-RCA utilizing magnetic beads. (A) Epitope-specific detection of GDH using circular aptamers and SYBR Gold fluorescence detection of RP. (B) An immunomagnetic strategy for colorimetric pH sensing strategy with GOx for the detection of PDGF. (C) Fluorescence dequenching AuNP biosensing strategy for the detection of leukemia-derived exosomes. Figures adapted from references cited in text.

Table 2.2. Heterogeneous solution-based methods.

Separation Method	Detection Method	RCA Method	MRE Type	Regulation Method	Target	LOD	# Steps	Temperature	Assay Time	Ref.
				Colorimetric detection						
centrifugation	4-nitrophenol	linear	aptamer	structure-switching [PLP]	aflatoxin M1 [CM]	0.05 ng/L	many	multiple	≥ 7 hrs	[317]
ethanol precipitation	intercalating dye	linear	DNAzyme	RCD	ATP	100 µM	many	multiple	≥ 4 hrs	[120]
magnetic bead	PMD	enzyme-assisted	aptamer	structure-switching [PLP]	cancer cells (ramos)	81 cells	many	multiple	≥ 6 hrs	[297]
magnetic bead	PMD	enzyme-assisted	aptamer	structure-switching [PLP]	lysozyme	7.2 fM	many	multiple	≥ 6 hrs	[297]
magnetic bead	PMD	linear	aptamer	sandwich (apt x2)	OTA [CM]	1.09 ng/mL	many	multiple	≥ 5 hrs	[301]
avidin bead	PMD	linear	aptamer	sandwich (apt 2x)	PDGF [CM]	~7.1 fM (0.2pg/mL)	2	multiple	≥ 2 hrs	[313]
magnetic bead	pH dye	dendritic	aptamer	sandwich (apt/Ab)	PDGF [CM]	0.94 pM	many	37 °C	≥ 3 hrs	[184]
magnetic bead	PMD	enzyme-assisted	aptamer	sandwich (apt x2) [PLP]	*V. parahaemolyticus* [CM]	10 cfu/mL	many	multiple	≥ 1 hr	[300]
				Fluorometric detection						
magnetic bead	cDNA (MB)	enzyme-assisted	aptamer	structure-switching	17β-Estradiol (E2) [CM]	63.09 fM	many	multiple	≥ 3 hrs	[253]
magnetic bead	cDNA (MB)	linear	aptamer	structure-switching [PLP]	cocaine	0.48 nM	many	multiple	≥ 3 hrs	[135]
magnetic bead	cDNA (MB)	linear	aptamer	sandwich (apt/Ab)	EpCAM [CM]	10 BT474 cells	4	multiple	≥ 7 hrs	[250]
magnetic bead	cDNA (MB, F/Q)	enzyme-assisted	aptamer	sandwich (apt/Ab) [PLP]	exosomes [CM]	100 particles per µL exosomes	many	r.t.	≥ 3 hrs	[265]
magnetic bead	intercalating dye	linear	captamer	structure-switching (recombinant to native protein)	GDH [CM]	10 pM	many [RT]	multiple	≥ 1 hr	[113]
magnetic bead	cDNA (MB, F/Q)	linear	aptamer	sandwich (apt x2) [PLP]	MRSA [CM]	100 CFU/mL	many	multiple	≥ 2 hrs	[315]
centrifugation	intercalating dye	hyperbranched	aptamer	separation by spin-down, no switching [PLP]	MUC1 [CM]	4.27 x 10^4 exosomes / mL	many [RT]	multiple	≥ 5 hrs	[132]
magnetic bead	cDNA (QD)	linear	aptamer	structure-switching [PLP]	OTA [CM]	0.2 pg/mL	many	multiple	≥ 5 hrs	[136]
magnetic bead	cDNA (QD)	linear	aptamer	inhibition RCA	OTA [CM]	0.13 ppt	many	multiple	≥ 1 hr	[245]
magnetic bead	intercalating dye	linear	aptamer	structure-switching [PLP]	tetracycline [CM]	0.724 pg/mL	3	multiple	≥ 6 hrs	[227]
magnetic bead	intercalating dye	linear	aptamer	sandwich (apt/Ab)	thrombin	2 nM	many [RT]	multiple	≥ 2 hrs	[229]
centrifugation	cDNA (MB)	linear	aptamer	structure-switching	thrombin	1 pM	many	multiple	≥ 2 hrs	[111]

				(rGO)						
magnetic bead	intercalating dye	linear	aptamer	sandwich (apt/bead fixation)	Tip60 [CM]	220 fM	many	multiple	≥ 3 hrs	[228]

[a] Table Footnote. [b] … [RT] denotes that detection was done with real-time monitoring; [PLP] denotes that the assay used a padlock probe ligation reaction; [CM] denotes that the assay was tested with complex media; “many” denotes any assay that required 4 or more steps; r.t. denotes that room temperature was used.

6. Solid-phase Assays

POC biosensors that utilize the solid-phase in lieu of solution phase are the most likely to be practically applied for real-world applications as many aspects of solid-phase device design intend to simplify user handling steps and increase portability. In solid-phase assays, a portion of the assay components is tethered to a solid surface with the rest free in solution. We focus on solid-phase most often used with POC testing, including the surface of beads (as discussed in S5), glass slides, microwell plates, microfluidic channels, or on paper. With proper care and optimization, FNA-based biosensors that utilize RCA can be integrated into these formats to create powerful, portable devices with an integrated amplification system primed for ultrasensitive detection. Individual POC applications may have unique characteristics and demands that make certain strategies more practical than others. For instance, paper-based biosensing offers a host of advantages compared to using glass or plastic surfaces. Likewise, lateral flow devices allow for simple on-device separations or timed reactions. As such, it is imperative that the assay requirements are well understood such that the best combinations can be selected. In this section, we will focus on these solid-phase mediums that can be detected optically, and the considerations for different surface formats are discussed. A summary of solid-phase examples can be found for colorimetric-based methods in Table 2.3 and fluorometric-based methods in Table 2.4.

6.1 Microwell plates and glass slides

Bulk solid immobilization differs from bead immobilization in many ways, and each offers its own advantages and disadvantages compared to their particulate counterparts. While a bulk solid and a particulate solid may have the same volume, their effective surface area differs greatly. The strategies for washing these two different solid surfaces differ, as one is dispersed within solution and the other is submerged within. Commonly these assays will incorporate multiple steps including washing steps, and the use of optical instrumentation to allow for high-throughput analysis. High-throughput analysis is not necessarily applicable at the POC directly, but surely these approaches can simplify, expedite analysis, and decrease costs in those scenarios where basic optical instruments can be maintained. Specifically, microwell plate-based analysis is highly attractive for real-time analysis.

Cheng and co-workers utilized AuNP-DNA to hybridize to RP immobilized on glass slides, further improved by their application of silver enhancement (Figure 2.17A, top).[115] This scanometric method did not require sophisticated instrumentation but did require washing steps to remove unbound AuNPs that contribute to background signal. The authors covalently immobilized an aptamer-primer and CT on a glass slide, competitively binding with either the target or the CT (Section 2.1.1). Any unbound VEGF or displaced CT was removed from solution with a washing step and phi29 DP was added to initiate RCA. Where VEGF had bound to aptamer, no RCA was generated, creating an inhibitory assay. Next, AuNP-DNA was allowed to hybridize with the RP and was followed by a silver enhancement step to further improve the visibility of the detection probe, which could be visualized with a simple flatbed scanner and quantified. Despite several washing steps, this four-step isothermal (37 ˚C) approach was able to achieve an ultralow detection limit of 10 fM of VEGF in just over 3 hours (Figure 2.17A, bottom).

Wang *et al.* exploited AuNP's peroxidase activity to develop an ultrasensitive sensor for thrombin detection.[146] Here, the authors used an inhibition RCA regulation method with a thrombin captamer such that target binding prevents RCA (Section 2.2.1, Figure 2.6D) (Figure 2.17B, left). Hydrogen peroxide reduced gold (III) to form well-dispersed AuNPs that are a characteristic red color indicating an absence of thrombin. Conversely, target-triggered RCA generated PMD-rich RP which competes to reduce hydrogen peroxide into water and oxygen gas. A decrease in available hydrogen peroxide slows the kinetics of AuNP growth and results in AuNPs with poor morphology and a tendency to aggregate, leaving a characteristic blue color in solution. This ultrasensitive approach was able to achieve a detection limit of 10 aM for thrombin in just over 4 hours (Figure 2.17B, right), which is particularly impressive for a colorimetric assay. The PMD strategy is the most widely used colorimetric approach for FNA-linked RCA assays, and typically achieves detection limits in the femto- to picomolar ranges. Here, the same modifications of CT are required but utilizing gold as a redox agent has proved to be very effective relative to the commonly used TMB or ABTS alternatives.

Zhan *et al.* demonstrated an example of colorimetric bacterial detection in food samples using microwell plate detection of *L. monocytogenes* (Figure 2.17C, left).[256] The authors state their intention to develop a test to compete with the standard ELISA assay, as ELISA been accepted as the gold-standard for antibody-based biosensors, noting their assay's competitive LOD when compared to similar antibody-based tests. This device (and other sandwich-like RCA assays) required several steps and a comparable assay time (over 5 hours) indicating that there is high demand for these tools despite the technical skill required. Structure-switching aptamers were immobilized on the surface, primed to release the aptameric sequence through target binding to *L. monocytogenes* (Section 2.1.1), leaving an exposed primer for RCA. Biotinylated DNA and streptavidin-tagged HRP were added to the wells for hybridization to the surface-tethered RP. The HRP converted TMB from colorless to yellow in a target-dependent manner leading to the quantification of *L. monocytogenes* with a detection limit of 460 CFU/mL. This isothermal (37˚C) assay successfully detected target in spiked fresh lettuce samples, showing the approach's applicability for food-based detection (Figure 2.17C, right).

In situ RCA analysis allowed Gao *et al.*to distinguish between six cancer cell lines by independently monitoring three different plasma membrane protein (PMP) targets: MUC1, EpCAM, and HER2 (Figure 2.17D, top).[252] Here, the cells were fixed on glass slides to allow for subsequent washing steps to remove unbound probes. Once immobilized, aptamer-primer sequences bound available PMPs and the primer end was free to initiate RCA (Section 2.2.1). Nicking enzymes nicked bound MB probes, restoring fluorescence for quantification of each target. The authors report they were able to detect as low as 25 copies per cell (or 166 aM) of PMPs based on an analysis of 100 cells. Further, the authors were able to distinguish and identify cell types by running the assay in parallel with different aptamer probes for PMP profiling (Figure 2.17D, bottom), providing a useful multiplexing approach. An important caveat here is that the RCA reaction and amplification must occur consecutively, limiting the ability for real-time RP monitoring. Further, a temperature of 37 °C for 60 min was required to allow optimal function of the nicking enzyme, a common observance for enzyme-assisted amplification strategies

Most FNA-based optical detection platforms using RCA focus on the monitoring of wavelengths in the visible spectrum, either via color

or fluorescence. Lv *et al.* showcased a portable smart-phone based infrared-based thermal assay for the sensitive detection of PSA using CuxS, a heat-active nanocrystal, tethered to a DNA strand (CuxS-DNA) as the hybridization probe.[318] For the assay, an antibody-aptamer sandwich complex was used to perform PLP (Section 2.2.1, Figure 2.5D) on a microwell plate in several steps. Linear RCA was generated on the microwell surface and CuxS-DNA was hybridized to the RP (Figure 2.17E, left). Heat from an IR laser was absorbed by CuxS, increasing the solution temperature and with temperature changes monitored using a smartphone with an infrared thermal imager equipped. The authors reporting a detection limit of 0.2 ng/mL of PSA in just over 5 hours (Figure 2.17E, right) and could potentially be used as an optical detection strategy in otherwise optically challenging mixtures. With the thermal monitoring being conducted at 20˚C, we suspect careful calibration of the assay would be required in different environments. Notably, beyond incorporating a smartphone for signal detection, it can also be used for data transmission for interpretation by highly qualified personnel that may not otherwise be present at the POC.[319]

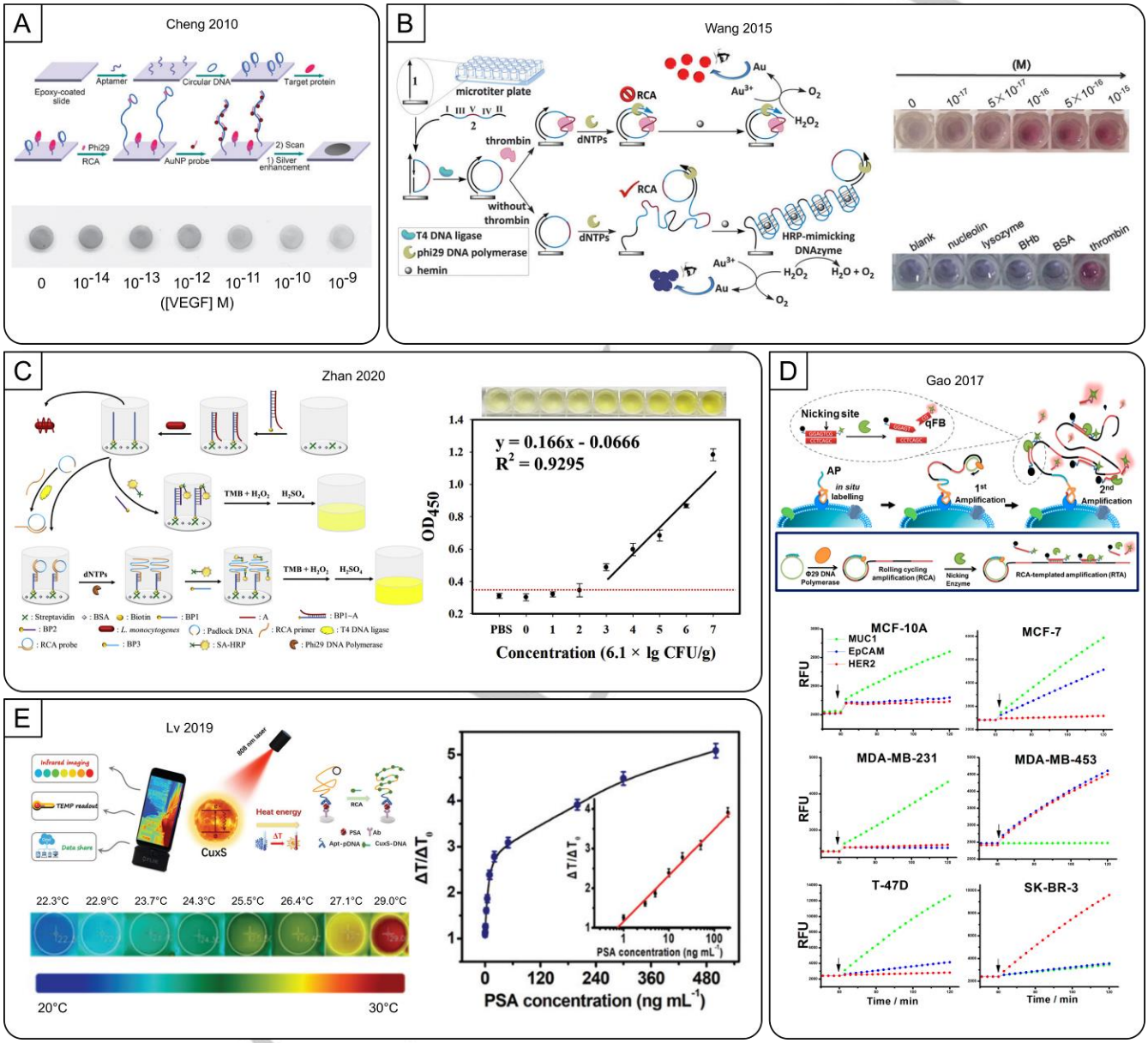

Figure 2.17. Microwell plate and glass slide-based FNA-RCA assays with optical detection methods. (A) An aptamer-initiated RCA method for the scanometric detection of VEGF. (B) An inhibitory aptasensor using HRP-mimicking DNAzymes for the reduction of AuNPs and the visual detection of thrombin. (C) Foodborne pathogen RCA-linked aptasensor using colorimetric detection of catalytic HRP action. (D) Quantitation of plasma membrane proteins using an in situ aptasensing approach with fluorometric RP detection. (E) A portable smart-phone infrared-based thermal aptamer-RCA assay for the detection of PSA. Figures adapted from references cited in text.

6.2 Microfluidic Devices

Microfluidic devices operate miniaturized assays that utilize extra low volumes, manipulating liquids in apparatus' on a nanometer to

micrometer scale.[320] Microfluidic devices often prioritize the all-in-one aspect of their design, in that all aspects of the assay proceed without user intervention. Analysis of small volumes in turn requires less reagents, solvents, and assay time, making them an obvious choice for POC designs. Microfluidic devices use comparatively less volume than conventional patient sampling, which may be attractive for invasive and/or frequent sampling measures, such as blood drawing. However, with such small volumes, detection of trace analytes can be a challenge, necessitating on-board amplification strategies. RCA can be paired with microfluidic devices to enhance target signal despite the relative low abundance of target in these small volumes. Another key feature of microfluidic approaches is that the fluidic system can automate sequential steps and direct flow through from one region to another, mimicking separation steps. With such small sample volumes on-board heating elements can be incorporated to rapidly heat solutions to regulate temperature-sensitive reactions or facilitate dissociation of key assay components. The caveat is that this necessitates the use of a power source for the on-board pumps or heaters, complicating its use at the POC.

Feng et al. incorporated a unique open-space microchip for integrating cell culturing with the detection of VEGF that took advantage of fluid flow on a solid surface.[321] In this design, the chip was segmented in half by a connecting channel containing an interfacial tension valve that prevented the flow of reagents from one end to the other, specifically enabling sequential reactions. On one end of the chip was the cell culture chamber, and on the other end of the interfacial tension valve was a capture aptamer immobilized on the microchip surface (Figure 2.18A, top) By connecting the two reservoirs, the VEGF excreted into the extracellular matrix flowed to the capture zone and was immobilized (Figure 2.18A, bottom),. The channel was again severed and a signalling aptamer was added to the capture zone to form a sandwich for PLP generation (Section 2.2.1, Figure 2.5D). The authors were able to detect as low as 10 pg per mL of VEGF, requiring only 10 µL of solution and just under 2 hours using fluorescently labelled cDNA. Further, as the chip had on-board cell culturing, inducing a hypoxic cellular microenvironment was confirmed by the measured increased secretion of VEGF into the extracellular matrix.

Microchip devices are designed from the inception with portability in mind, making it logical to pursue detection strategies that can be detected by eye without bulky instrumentation. Integrated devices are well-suited for on-site detection for this reason. The microchip device developed by Lin *et al.* for thrombin detection, a model analyte for protein biomarkers, anticipated the need to dilute their real-blood samples to minimize matrix interferences by incorporating RCA.[140] The device itself was produced using soft-lithography technology to design the µm-wide channels . Blocking of the microchannel surface with fetal bovine serum was necessary to prevent the absorption of the protein matrix as unblocked channels lead to high recoveries despite the samples being diluted a thousand-fold. The assay is triggered by aptamer-target binding using dual aptamers (Section 2.2.1, Figure 2.5D) resulting in RP immobilization within the microchip (Figure 2.18B, top). Colorimetric detection is enabled through the accumulation of PMD-rich RP and the redox conversion of TMB to its colorimetric form (Figure 2.18B, middle). In as little as 45 minutes, this colorimetric device was able to detect thrombin with an LOD of 0.083 pg/mL with only 15 minutes of amplification (Figure 2.18B, bottom). Even more impressively, this was achieved with as little as 25 µL of samples or reagents, as they demonstrated in their assessment of real human serum samples.

3-D printed RCA devices can be tuned for POC testing, as demonstrated by an on-site chip for mercury detection developed by Lim and co-workers (Figure 2.18C, top).[298] This turn-off assay demonstrated sensitivity for inorganic mercury through generation of PMD-containing RPs by eye and by portable spectrophotometer. Though there is no aptamer for mercuric ions, they are capable of binding between two thymine residues to stabilize T-T mismatches, as such a twelve nucleotide polyT primer was used for mercuric ion capture. In this inhibition RCA strategy (Section 2.1.1, Figure 2.2D), unbound aptamer could be linearly amplified and rapidly heat denatured by an on-board Peltier heating module. Heating narrow channels and low volumes can be a rapid and energy efficient task. Further, pairing this device with a temperature control module minimizes user error as the temperatures can be better regulated. Here, a fluid pump was required to transfer the RP to a detection reservoir (Figure 2.18C, top), where the RP-PMD sequences reduced ABTS for colorimetric detection by a portable colorimetric reader (Figure 2.18C, middle). This 30-minute assay demonstrated an LOD of 3.6 µg/L in spiked tap water samples, comparable to conventional ICP/MS analysis (Figure 2.18C, bottom). Further, as this microfluidic device is printed rapidly on commercially available 3D printers, it highlights the strengths of 3D printing for accessible POC assays. As well, the same authors recently reported a similar on-site chip for mercury detection without the need for a fluid pump, with fluid transfer being achieved with a commercial 8-well multichannel pipette (LOD of 3.4 µg/L and 4.1 µg/L in simple, and environmental matrices, respectively).[299]

He *et al.* integrated capillary electrophoresis into a microfluidic chip for the simultaneous detection of kanamycin, AFM1, and E2 in milk samples.[322] Requiring a total assay time of just over 1 hour using low temperatures ($\leq$ 30˚C), the authors were able to achieve multiplexed detection limits of 10 pg/mL for kanamycin, 0.95 pg/mL for AFM1, and 6.8 pg/mL for E2, and were able to do so in spiked milk samples as well. The very short turnaround time and ability to detect multiple targets in tandem offers tremendous advantage despite the trade-off of requiring magnetic bead washing steps. The authors utilized the tripartite 3'-exonuclease system (Section 2.1.1, Figure 2.3A), immobilizing a mixture of three unique tripartite systems (one for each target) onto magnetic beads (Au-Fe_3O_4) to create the probes (Figure 2.18D, left). The sample was incubated with magnetic probes and phi29 DP and incubated at 30˚C for 50 minutes, when the RP-labelled magnetic beads were collected and hybridized with unfunctionalized cDNA at room temperature. The recovered supernatant was flowed through a microfluidic device for on-chip capillary electrophoresis using an intercalating dye (Figure 2.18D, right). The remaining unhybridized cDNA probes were inversely proportional to target concentration and could be size separated and quantified after just 3 minutes. For a future iteration, it may be beneficial to integrate all steps into a microfluidic chip, however the multiplexing here provides a clear advantage.

In another example, He et al. developed a ratiometric microfluidic chip that could quantify kanamycin in milk and fish samples.[323] Here, the authors used a structure-switching aptamer hybridized to an RCA primer, with the aptamer component tethered to a gold stir bar (Section 2.1.1, Figure 2.2A) (Figure 2.18E, top). With target addition triggering structure-switching and the subsequent release of the primer, the authors could remove the stir bar to isolate only the liberated primers. Addition of a CT triggered linear RCA by Bst DP and labelled with SYBR Gold, finally separated by on-chip capillary electrophoresis (Figure 2.18E, middle). By intentionally keeping the amplification time short at 30 minutes, the authors could track the ratio of RP to CT for quantification of kanamycin. As more CTs were

activated for RP generation, the proportion of RP-bound CTs to free CTs increased and this ratiometric relationship could be used to quantify the small molecule target. In just over one hour, they could detect as low as 0.3 pg per mL (Figure 2.18E, bottom) with validation in milk and fish samples.

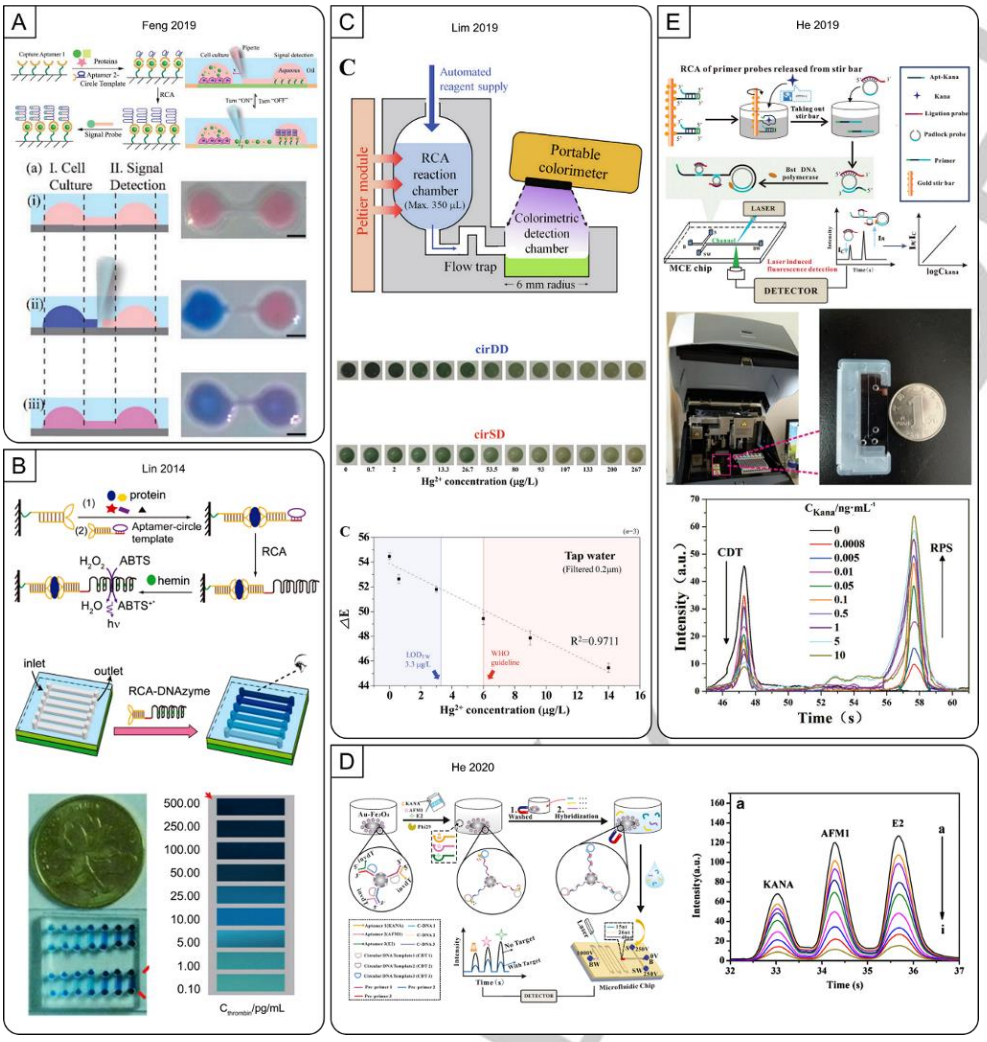

Figure 2.18. Microfluidic FNA-RCA devices with optical detection methods. (A) A cell culturing microfluidic chip for colorimetric detection of VEGF via RCA (B) A portable thrombin-detecting microchip for visual detection of RCA-generated hemin/G-quadruplexes. (C) A portable pumpless 3D-printed multiarray chip for on-site colorimetric detection of Hg^{2+}. (D) A microfluidic aptasensor for simultaneous detection of kanamycin, aflatoxin M1, and 17β-estradiol based on magnetic tripartite DNA assembly nanostructure probes (E) A ratiometric aptasensor for kanamycin using stir-bar assisted sorptive extraction and RCA. Figures adapted from references cited in text.

Table 2.3. Colorimetric-based solid-phase methods.

Surface Type	Detection Method	RCA Method	MRE Type	Regulation Method	Target	LOD	# Steps	Temperature	Assay Time	Ref.
Microchip	PMD	linear	aptamer	inhibition RCA	Hg^{2+} [CM]	3.3 µg/L	many	multiple	≥ 1 hr	[298]
Microchip	PMD	linear	aptamer	inhibition RCA	Hg^{2+} [CM]	3.4 µg/L	many	multiple	≥ 1 hr	[299]
microwell plate	cDNA (enzyme)	linear	aptamer	structure-switching	Hg^{2+} [CM]	1.6 nM	many	37 °C	≥ 5 hrs	[257]
microwell plate	cDNA (enzyme)	linear	aptamer	structure-switching	*L. monocytogenes* [CM]	460 CFU/mL	many	37 °C	≥ 4 hrs	[256]
glass slide	PMD	linear	aptamer	cell fixation	MCF-7 [CM]	10 cells/mL	many	multiple	≥ 2 hrs	[131]
microwell plate	cDNA (enzyme)	linear	aptamer	sandwich (apt/Ab) [PLP]	PDGF [CM]	3.1 pM	many	37 °C	≥ 5 hrs	[324]
microwell plate	cDNA (enzyme)	thrombin-assisted	aptamer	sandwich (apt/Ab) [PLP]	PDGF [CM]	31 pM	many	37 °C	≥ 5 hrs	[325]
Microchip	PMD	linear	aptamer	sandwich (apt 2x)	thrombin [CM]	0.083 pg/mL.	many [RT]	multiple	45 min	[140]
microwell plate	PMD	linear	captamer	inhibition RCA	thrombin	10 aM	many	multiple	≥ 3 hrs	[146]
glass slide	cDNA (AuNP)	linear	aptamer	inhibition RCA	VEGF [CM]	10 fM	many	37 °C	≥ 3 hrs	[115]

[a] Table Footnote. [b] … [RT] denotes that detection was done with real-time monitoring; [PLP] denotes that the assay used a padlock probe ligation reaction; [CM] denotes that the assay was tested with complex media; “many” denotes any assay that required 4 or more steps; r.t. denotes that room temperature was used.

Table 2.4. Fluorometric-based solid-phase methods.

Surface Type	Detection Method	RCA Method	MRE Type	Regulation Method	Target	LOD	# Steps	Temperature	Assay Time	Ref.
Microchip	intercalating dye	linear	aptamer	structure-switching	17β-Estradiol (E2) [CM]	6.8 pg/mL	many	multiple	≥ 1 hr	[322]
Microchip	intercalating dye	linear	aptamer	structure-switching	aflatoxin M1 [CM]	0.95 pg/mL	many	multiple	≥ 1 hr	[322]
glass slide	cDNA (fluorophore)	linear	DNAzyme	ligase [PLP]	ATP	10 μM	many	multiple	≥ 3 hrs	[147]
microwell plate	cDNA (fluorophore)	linear	aptamer	sandwich (apt/Ab)	cTnI [CM]	14.40 pg/mL	many	multiple	≥ 8 hrs	[326]
Microchip	cDNA (fluorophore)	linear	aptamer	sandwich (apt/dend) [PLP]	E. coli	100 cells/mL	many	multiple	≥ 5 hrs	[130]
Microchip	cDNA (fluorophore)	linear	aptamer	sandwich (MRE to capture, FNA to detect) [PLP]	E. coli [CM]	80 cells/mL	many	multiple	≥ 3 hrs	[246]
glass slide	cDNA (MB)	nicking-assisted	aptamer	cell fixation [PLP]	EpCAM	100 cells	many [RT]	37	≥ 2 hrs	[252]
glass slide	cDNA (MB)	nicking-assisted	aptamer	cell fixation [PLP]	HER2	10 cells	many [RT]	37	≥ 2 hrs	[252]
Microchip	cDNA (fluorophore)	linear	aptamer	sandwich (apt/Ab)	IL-8 [CM]	0.84 pM	many	37	30 min	[327]
Microchip	intercalating dye	linear	aptamer	structure-switching	kanamycin [CM]	10 pg /mL	many	multiple	≥ 2 hrs	[323]
Microchip	intercalating dye	linear	aptamer	structure-switching	kanamycin [CM]	0.32 pg/mL	many	multiple	≥ 1 hr	[322]
Microchip	cDNA (MB)	linear	aptamer	sandwich (apt x2)	MMP [CM]	31.25 ng/mL	many	multiple	30 min	[251]
glass slide	cDNA (MB)	nicking-assisted	aptamer	cell fixation [PLP]	MUC1	10 cells	many [RT]	37	≥ 2 hrs	[252]
glass slide	intercalating dye	linear	aptamer	structure-switching [PLP]	PDGF	8 nM	many	multiple	≥ 4 hrs	[125]
microwell plate	cDNA (CuxS) (thermal)	linear	aptamer	sandwich (apt/Ab) [PLP]	PSA	0.2 ng/mL	many	multiple	≥ 5 hrs	[318]
Microchip	cDNA (fluorophore)	linear	aptamer	sandwich (apt x2) [PLP]	VEGF [CM]	10 pg/mL	many	multiple	≥ 1 hr	[328]

[a] Table Footnote. [b] … [RT] denotes that detection was done with real-time monitoring; [PLP] denotes that the assay used a padlock probe ligation reaction; [CM] denotes that the assay was tested with complex media; “many” denotes any assay that required 4 or more steps; r.t. denotes that room temperature was used.

6.3 Paper-based Biosensors

Cellulose-based surfaces are an ultra-low cost option for point of care assays, capitalizing on the natural wicking properties of the paper surface to manipulate liquids. Few modern substrates can be so inexpensive so as to accommodate low-resource areas and to justify their use over the superior technology offered in a lab setting, and paper is simultaneous widely available and cheap . Likewise, the inherent wicking properties of paper to transport material from one location to another without the need for any on-board fluid pumps as is the case with microfluidic-based strategies. A summary of the paper-based methods discussed herein can be found in Table 2.5.

Kim and co-workers elegantly exploited the immobility of RP in a colorimetric dot blot assay for the sensitive detection of mercuric (Hg^{2+}) ions (Figure 2.19A, left).[233] The authors applied an inhibition RCA method using a polyT DNA sequence for mercury capture or as a primer for RCA (Section 2.2.1, Figure 2.2D). After incubation with Hg^{2+}, AuNP-labelled DNA and the reagents to initiate RCA were added. The 30-minute RCA reaction was heat inactivated and the solution was spotted into a nitrocellulose membrane and dried for 20 minutes. Typically, the amplicons generated by RCA are so large that transporting them across a membrane can be challenging (see Section 2.3.3 on RCA as MRE) whereas AuNP-labelled DNA is much smaller, readily wicking across a test strip. In the absence of RP the small AuNP-labelled DNA migrated and dried in a wide spot with elevated concentration in a concentric ring on the outer edge of the spot (Figure 2.19A, top right). When RP was generated the red color of the AuNPs was localized in the center of the droplet owing to the inability of the large RP to migrate. At just 2 hours, this simple three-step assay allowed for the detection of as low as 21.8 nM of Hg^{2+} in real samples (Figure 2.19A, bottom right), better than the 30 nM allowable limit for mercuric ions in drinking water as outlined by the WHO. Though only the detection step was done on paper, with the recognition and amplification steps conducted in solution, the utility of paper for integrated separation steps is evident as simply spotting the solution on the nitrocellulose surface was sufficient.

Recently we generated a simple isothermal RCA-linked FNAB on a cellulose surface without the need for any blocking steps or immobilization of DNA materials (Section 2.1.1, Figure 2.2D) (Figure 2.19B, left).[101] Similar performance between both SYBR Gold and QuantiFluor dyes was observed in solution, however QuantiFluor alone was found to be compatible with cellulose, maintaining low background fluorescence. We exploited this finding to generate a simple pullulan-coated paper-based RCA assay for the real-time detection of thrombin (the benefits of pullulan-encapsulated reagents are discussed below). Thrombin was incubated with its aptamer for 15 minutes followed by spotting onto cellulose paper containing pullulan-encapsulated RCA reagents for a 15-minute RCA reaction at room temperature. The presence of thrombin prevented the aptamer from being used as a primer to initiate RCA. With this strategy, rapid real-time detection of picomolar levels of thrombin was achieved within just a two-step 30-minute assay both in solution (100 pM) and on paper (250 pM) without the need for any heating, expensive labelling, surface treatment or blocking steps (Figure 2.19B, right). Here, we demonstrated that in contrast to QuantiFluor, certain dyes such as SYBR Gold, can produce significant background fluorescence upon binding to cellulose, making them unsuitable for paper-based sensor platforms.

RCA-based FNABs have multiple reagents that need to be stabilized to ensure their accuracy over time, an important consideration when considering the long-term storage options for real-world use. This may be especially true in low-resource and remote environments at room temperature. The utility and durability of papers such as cellulose and nitrocellulose has made them an attractive platform for a variety of POC biosensors.[48,53,329] Our laboratory has worked to expand the applicability of many of our recent biosensors through the use printable pullulan bioink as well as pullulan tablets for storage and application of labile enzymes and substrates.[330–332] Pullulan, a naturally produced polysaccharide can be used as a simple and inexpensive material for the encapsulation of otherwise labile reagents (Figure 2.19C, top). Pullulan tablets retain high assay activity for weeks with room temperature storage thanks to the entrapment and immobilization of reagents in a water soluble oxygen impermeable environment.[330–332] Challenging assays in particular may benefit from use of pullulan by simplifying the assay procedure and stabilizing sensitive reagents (Figure 2.19C, middle).[219,332,333] At approximately 1 USD per 100 tablets, this method is low cost and well-suited for use in the developing world. Recently, our lab showcased the ability to immobilize a primer on a nitrocellulose surface and initiate RCA (Figure 2.19C, bottom), much like what has been well-established on magnetic beads or microwell plates. As mentioned in S4, improved RCA efficiency was observed owing to a molecular crowding effect causing an increase in local concentrations of RCA reagents.[98] The same report demonstrated detection of surface-generated RP using a variety of methods including the incorporation of radiolabelled dNTPs, cDNA tagged to gold nanoparticles, the incorporation of PMDs, and the addition of fluorescently tagged cDNA. Several of the recent paper-based assays that utilized RCA have been simplified[98,101,112,310,334] or long-term stabilized[98,112] through the use of pullulan encapsulation.

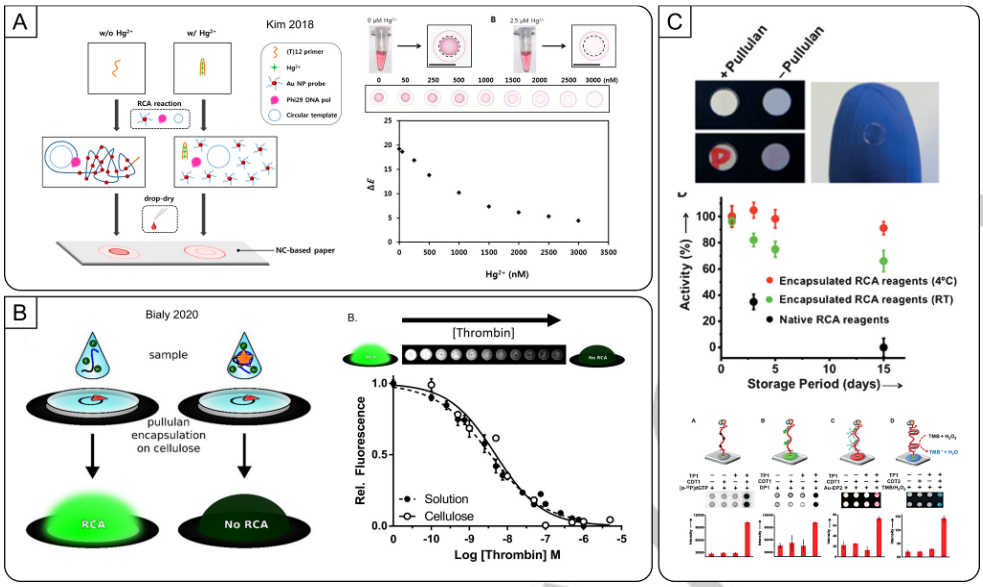

Figure 2.19. Paper-based devices with optical detection methods. (A) Hg^{2+} colorimetric dot blot assay utilizing AuNP aggregation with FNA-triggered RP. (B) A simple isothermal RCA-linked FNAB for the fluorometric detection of thrombin. (C) A structure switching aptasensor using pullulan encapsulated RCA-components. Figures adapted from references cited in text.

G-quadruplex DNAzyme functionality can be incorporated into paper-based assays, especially in FNA-RCA based assays that can act to amplify the colorimetric method's signal with amplification. Li and colleagues reported a paper-based assay[114] that utilized a captamer (Section 2.2.2, Figure 2.6B) for colorimetric detection via the peroxidase-mimicking DNAzyme PW17.[43,335–339] In solution, the captamer was bound to an rGO surface and was released upon binding to the PDGF target. Rational NA design was paramount in this assay, not only because the CT acted as an aptamer and template for PW17 generation, but also because the CT showed remarkable resistance to nuclease degradation from cell lysates, an important consideration for POC applications. Once this sample was introduced on paper, RCA was initiated by binding of the captamer to a primer encapsulated within a pullulan-coated paper surface. As the CT also contained the antisense strand for PW17, the RP was capable of converting TMB to colored TMB^+ for colorimetric detection with a limit of 10 pM for the protein target.

Lateral flow devices (LFDs) are an excellent example of utilizing the inherent wicking properties of paper for integrating sequential steps. Key materials can be immobilized on different sections of the paper and a solution can be wicked across it in a sequential manner. LFDs can be used to incorporate separation of unbound AuNP-DNA without a dedicated washing step. LFDs are a popular test format familiar both to regulatory bodies and the general public due to the popularity of the at-home pregnancy test. This is in part due to their overall simplicity for the end-user, including their operational simplicity. It should be noted that despite the popularity of AuNP-based lateral flow assays, the bulky size of RP can make it difficult for them to move along the LFD membrane. While there are now several examples of NA-based lateral flow detection with RCA,[340,341] the space remains open for FNA-based contributions.

Nonetheless, there are several FNA-based examples that incorporate natural wicking and paper origami for sequestering reagents and assay timing. Hui *et al.* reported one such paper-based assay utilizing peroxidase-mimicking DNAzymes for colorimetric detection of both NA and non-NA bacterial markers.[112] This pullulan-coated device used a bridged paper design to control sample flow (Figure 2.20A, top). This assay was the first aptamer-regulated ITA assay to be accomplished on a paper device. In the first region, the presence of target liberates an aptamer from an rGO surface adsorbed onto nitrocellulose to perform structure-switching primer release (Section 2.1.1, Figure 2.2C). The rGO surface acted both as a regulator of primer release, and also protected the aptamer sequences from degradation in the tested clinically relevant matrices. Bridging the paper allowed for the controlled flow of free aptamer to an amplification region where the aptamer could act as a primer for RCA initiation. This bridge used the inherent filtering properties of paper as the sample flowed from sample zone to detection zone, an important advantage in assays with complex matrices. It also prevented unclear colorimetric readout in the detection zone by preventing mixing with coloured matrices like stool. Colorimetric sensing showed similar sensitivity to unamplified fluorescent detection for both ATP and GDH, allowing colorimetric detection of the pathogen by eye. For both fluorescent and colorimetric detection, the LODs for the ATP sensor the GDH sensors were 10 µM and 3 nM, respectively (Figure 2.20A, middle). In this case, amplification was essential for equipment-free detection, but can also be performed more quickly where the equipment is available by omitting the amplification step. The robustness of each test was verified by using spiked human blood samples (ATP)_and spiked stool samples (GDH) (Figure 2.20A, bottom). Where many of the sensors described in this review used either ABTS or TMD as the colorimetric reagent, the authors observed that combining ABTS and TMB together provided the best balance of rapid color change and maintaining color intensity. This is an important consideration for prolonging the measurement window for accurate analyte quantification. At the POC, personnel may not be immediately available to record the colorimetric readout within a narrow 1-minute range, with any delay possibly causing invalidation of

the assay. By stabilizing the color change for a longer time period, the assay becomes functionally more robust for the end-user.

Another advantage to paper-based devices is that creative uses of origami can be incorporated for biosensing. Sun *et al.* demonstrated as much in their origami paper-based sensor for E. coli detection.[310] Here, the authors created a four-panel origami sensor (Figure 2.20B, left). Panel A was an absorbent pad, and panel B contained the dried buffer for cell lysis of E. coli. Panel C contains nanoflowers functionalized with E. coli-specific RCD. A pullulan solution containing RCA reagents is printed onto panel D. First, cell lysis of E. coli occurs on panel B and then panels B, C, and D are folded together. The free bacterial intracellular matrix is able to flow vertically through the cellulose onto panel C where target-dependent cleavage of the substrate strand is achieved (Section 2.1.3, Figure 2.4A). Through the same vertical capillary flow, the cleaved DNA fragment is captured in panel D where it is used as the primer for subsequent linear RCA. As the CT contains the sequence for PMD formation, the resultant RP can be combined with TMB, hemin, and hydrogen peroxide to generate a colorimetric signal proportional to the E. coli concentration. With this approach, the authors achieved a detection limit of 100 CFU per mL within only 35 minutes (Figure 2.20B, right), and was validated in juice and milk samples. Impressively, the cell lysis step required only 3 minutes though washing steps were required prior to initiating the cleavage reaction. Though the cleaved substrate strand required PNK treatment, the authors simply added the PNK into the pullulan mixture thus no additional step was required. Likewise, after approximately 30 minutes of cleavage, PNK treatment, and linear RCA, fresh hydrogen peroxide and TMB was added to panel D and colorimetric results were recorded within 1 minute by a digital camera. Here, several reactions were integrated into a single origami paper strip with separation of reagents occurring by the inherent wicking properties of the paper surface. Though rapid, it is important to note that the PMD reaction is time sensitive and quantification efficiency can be adversely impacted by measuring the colorimetric result after 5 or 30 minutes instead of the 1 minute recommended by the author.

In another example utilizing nanoflowers, Liu et al. created a paper device for the detection of toxin B, a *C. difficile* biomarker.[334] The paper device consisted of a sensing zone separated by a disconnected bridge to a detection region (Figure 2.20C, left). The sensing zone had NFs containing repeat sequences of hybridized aptamer-primer complexes (Section 2.1.1, Figure 2.2A). The detection and control zones each contained pullulan-encapsulated RCA reagents, though the control zone alone featured a control primer. Upon addition of target to the sensing zone, liberated primers were wicked with the buffer to the detection zone using a connecting paper bridge. This dissolved the pullulan and triggered linear RCA in the test zone proportional to toxin B, and in the control zone independent of toxin B concentration. This colorimetric PMD approach provided a detection limit of 600 pM with an RCA time of 15 minutes and a total assay time of 40 minutes (Figure 2.20C, right). Increasing the RCA time to 30 minutes improved the detection limit ten-fold to 60 pM, and validated in spiked stool samples. As with other PMD-based colorimetric detection methods, fresh TMB and hydrogen peroxide was added and the colorimetric result was recorded within 1 minute.

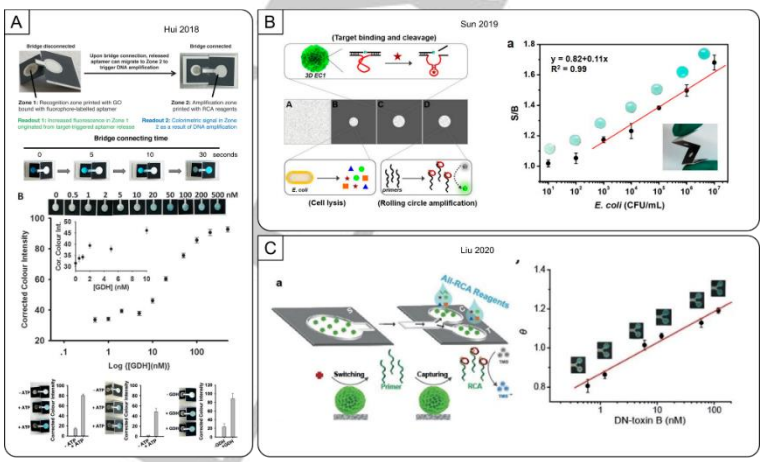

Figure 2.20. Paper-based devices with optical detection methods. (A) A bridging paper-based device for colorimetric ATP and GDH detection. (B) An origami paper-based RCD-sensor for *E. coli* detection. (C) An aptamer-containing nanoflower device for the colorimetric detection *C. difficile*. Figures adapted from references cited in text.

Table 2.5. Paper-based methods.

Surface Type	Detection Method	RCA Method	MRE Type	Regulation Method	Target	LOD	# Steps	Temperature	Assay Time	Ref.
				Colorimetric						
nitrocellulose	PMD	linear	aptamer	structure-switching (GO)	ATP [CM]	10 µM	3	r.t.	≥ 1 hrs	[112]
cellulose	PMD	linear	DNAzyme	RCD	*E. coli* [CM]	1000 cells / mL	many	r.t.	35 min	[342]
nitrocellulose	PMD	linear	aptamer	structure-switching (GO)	GDH [CM]	3 nM	3	r.t.	≥ 1 hrs	[112]
nitrocellulose	cDNA (AuNP)	linear	aptamer	structure-switching	Hg^{2+} [CM]	22.4 nM	3	multiple	≥ 1 hrs	[233]
nitrocellulose	PMD	linear	captamer	structure-switching (GO)	PDGF [CM]	100 pM	many	multiple	≥ 1 hrs	[114]
nitrocellulose	PMD	linear	aptamer	structure-switching	toxin B [CM]	60 pM	many	r.t.	50 min	[334]
				Fluorometric						
cellulose	intercalating dye	linear	aptamer	inhibition RCA	PDGF	6.8 nM	2 [RT]	r.t.	45 min	[312]
cellulose	intercalating dye	linear	aptamer	inhibition RCA	thrombin	240 pM	2 [RT]	r.t.	30 min	[312]

[a] Table Footnote. [b] … [RT] denotes that detection was done with real-time monitoring; [PLP] denotes that the assay used a padlock probe ligation reaction; [CM] denotes that the assay was tested with complex media; “many” denotes any assay that required 4 or more steps; r.t. denotes that room temperature was used.

6.4 Electrochemical Biosensors

Electrochemical methods rely on consumption or accumulation of electroactive species at the surface of an electrode, which are typically monitored as changes in either current, voltage, or impedance, allowing rapid detection of a target species. Though NAs are generally not useful electrochemically in solution at moderate voltages, the electrochemical analysis of NAs has long capitalized on their inherent electrochemical properties,[343,344] including those that form G-quadruplexes and PMDs.[345] Electrochemical detection of RCA-generated DNA is possible using several techniques,[96,346] as electrochemically active species (often denoted as mediators) can be accumulated at electrode surfaces through adsorption or intercalation with DNA, hybridization of labelled DNA species, or generation of electroactive DNAzymes. In many cases, the polymeric RP is generated directly at the electrode surface where it can act as a scaffold to attract redox probes for electrochemical RP detection.[347–349] Electrochemical assays are most often solid-phase assays due to the nature of the chemical interactions at the electrode, a solid surface. However, it is important to note that electron transfer rates drop exponentially with distance of the redox mediator from the electrode surface.[350] Thus it is important to ensure that such species bind in close proximity to the electrode surface (within a few nanometers), making it important to avoid generation of very large reaction products that extend far from the electrode surface.[351] The sensitivity of the electrode also warrants coating the surface with blocking agents to prevent nonspecific interactions with an assay's components, with washing steps being a common strategy for maintaining low background signals.

The balance between assay complexity and sensitivity is particularly delicate for electrochemical POC assays because instrumentation cannot be avoided. However with care, electrochemical assays can also be some of the most sensitive detection methods that can be paired with ASSURED criteria. Numerous FNA-based RCA electrochemical biosensors have been developed for sensitive target detection in real samples, including for human serum,[96,106,266,286,287,289,316,347,349,352–357] plasma,[304] blood,[291,348] urine,[358] beverages,[138,303,359,360] foodstuffs,[128,283] and environmental samples.[194,361] Below, we highlight electrochemical methods of RCA detection that are best suited for POC testing in low-resource settings. As well, these methods are summarized in Table 2.6.

6.4.1 Sandwich assays

With the many advantages of aptamers and popularity of sandwich-type detection (such as ELISAs, the gold standard in clinical diagnostics for detecting and quantifying protein biomarkers), a large portion of the current generation of FNA with RCA biosensors use dual antibody/aptamer interactions (Section 2.2.1, Figure 2.5D) to detect their target,[184,213,362,363,229,250,255,265,318,325–327] including in electrochemical sensors.[96,283,289,291,303,304,316,349,359,364] A sandwich-assay utilizing a PDGF aptamer and RCA was demonstrated as early as 2007 by Zhou *et al.* using alkaline phosphatase (ALP).[96] Here, an anti-PDGF capture antibody and aptamer formed a sandwich complex with PDGF on a gold electrode surface for subsequent PLP ligation and RCA (Figure 2.21A, top). Biotinylated cDNA probes and streptavidin-tagged ALP were complexed and used to convert ascorbic acid 2-phosphate into ascorbic acid to reduce silver ions deposited on the electrode and monitored by linear sweep voltammetry. As with ELISA, this approach was long (over 5 hours) and required several washing steps and reactants necessitating the immobilization of RP on an electrode. However, this isothermal (37˚C) method achieved a detection limit of 30 fM for PDGF, which was a 100-fold improvement over the RCA-free method tested (Figure 2.21A, bottom).

Rather than incorporating enzymes to generate electroactive species, Zhu *et al.* showed that copper nanoparticles (CuNPs) could be formed along electrode-bound RP to detect PSA.[349] Interestingly, this electrochemical method was largely predated by fluorometric methods of probing CuNPs, though fluorometric methods were by far less stable, limiting their application for long-term monitoring. Then, the polythymine RP generated in the presence of PSA was used as a template to grow copper nanoparticles from Cu^{2+} ions and ascorbate over 30 minutes. Nitric acid addition dissolves these RP-immobilized CuNPs and the resultant Cu^{2+} ions detected using cyclic voltammetry. One concern with the use of nitric acid is its storage in POC settings. The authors reported an LOD of 0.02 fg/mL for PSA, including in clinical human serum samples. At just over a 5 hour reaction time, the majority of the assay time was spent forming the sandwich and ligating the CT (3.5 hrs). These long assay times are typical of ELISAs as well.

Shen *et al.* utilized a sandwich-assay for the detection of the breast cancer cell MCF-7 with an impressive LOD of 1 cell per mL, and was used for detection in whole blood samples.[291] Magnetic beads coated with capture antibodies for EpCAM were used to capture MCF-7 and act as an anchoring point for subsequent addition of a signalling aptamer-primer strand (Figure 2.21B, top). Incorporating a PLP ligation step followed by RCA, this assay used molybdate ($PMo_{12}O_4^{3-}$) to generate a quantitative electrochemical current. This $\geq$ 5 hour approach had a recovery range of 50-77% in spiking experiments of whole blood with no pretreatment, perhaps demonstrating why this electrochemical assay was chosen for the optically challenging matrix (Figure 2.21B, bottom). The challenge with any sandwich assay is that the capture and signalling probes must bind to different epitopes of the target, or the target must be a polymer (dimer, trimer, etc.) to facilitate multiple binding sites.

A dual-aptamer sandwich assay was demonstrated for the electrochemical detection of thrombin by Fan *et al.* and detected by monitoring the accumulation of AuNPs along the RP (Figure 2.21C).[266] First, the capture aptamer was immobilized on the glass electrode by the incorporation of a polyA chain at its end, avoiding otherwise expensive or time-consuming surface functionalization. AuNPs have been shown to have a strong binding affinity for polyadenosine DNA sequences,[267] and the authors also designed the CT to generate a polyadenosine-rich RP which provided an anchor for AuNP adsorption onto the RP.[365,366] Subsequent electrocatalytic reduction of H_2O_2 by the bound AuNPs was monitored using cyclic voltammetry to detect thrombin. As this method utilizes the high affinity for polyadenosine to facilitate AuNP binding, RP modification was relatively straightforward and the authors reported a detection limit of 35 fM, with demonstrated functionality in spiked human serum.

Split aptamers can be used when multiple aptamers targeting different epitopes are unavailable or if the use of antibodies is not preferred. Shen *et al.* used a split aptamer for the detection of cocaine on a gold electrode (Figure 2.21D).[358] In separate parts, the split aptamer for cocaine is not effective for target binding, however this can be an advantageous feature for sandwich formation. Where sandwich assays typically separate the capture and signalling steps, the split aptamer offered the advantage of combining both steps simultaneously as cocaine capture could only occur when both split aptamers were present. As the authors had incorporated a biotin onto the signalling split aptamer, they added streptavidin and biotinylated primer-CT

duplexes to the sandwich. A complex containing biotinylated cDNA and streptavidin-tagged alkaline phosphatase annealed to the RP, where the addition of the redox reactive alpha-naphthyl phosphate into solution ultimately led to the detection of as low as 1.3 nM of cocaine in buffer and spiked urine samples. This isothermal (37˚C) approach was completed in under 4 hours despite utilizing some more laborious methods for tethering and detecting RCA (anchoring of the primer, hybridization of an enzyme).

In certain instances, unorthodox MREs can be incorporated into the assay. Hashkavayi *et al.* detected EpCAM-positive cells using an EpCAM aptamer as the capture probe and an RCA primer tethered to cholesterol as the signalling probe (Figure 2.21E, left).[367] As cholesterol is known to interact with binding sites facilitated by membrane proteins, cholesterol could interact with the target cell surface, thus avoiding the need for a secondary aptamer or antibody. After sandwich formation, RCA occurred on the cholesterol-tethered primer, generating multiple PMD units. The PMD-mediated redox reaction of TMB was used to quantify EpCAM positive HT29 cancer cells with a detection limit of 1 cell per mL in solution and in human serum (Figure 2.21E, right).

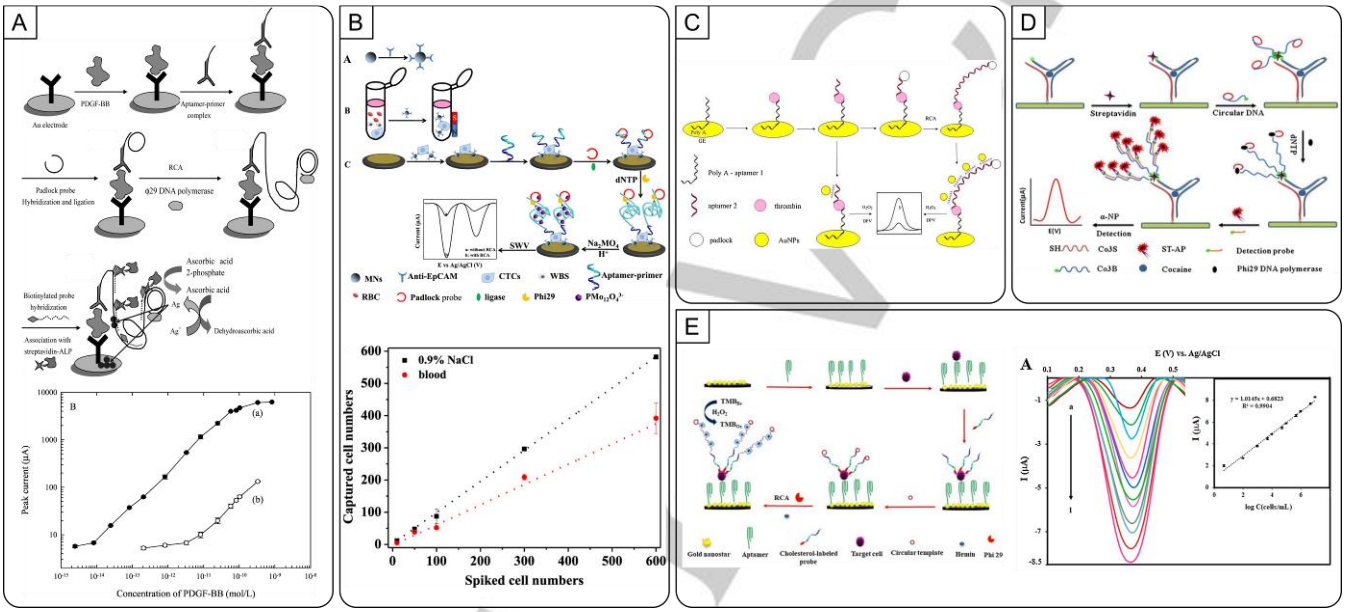

Figure 2.21. Electrochemical sandwich FNA-RCA assays. (A) Anti-PDGF antibody-aptamer sandwich approach for ALP-enabled detection of RP. (B) CuNP-reported RCA for ultrasensitive electrochemical detection of PSA. (C) Label-free detection of thrombin using dual-aptamer sandwich MRE and AuNP growth. (D)Split-aptamer-RCA assay for cocaine detection utilizing ALP cDNA. (E) EpCAM-positive tumor cell detection using a dual signal amplification strategy. Figures adapted from references cited in text.

6.4.2 Sandwich-free aptamer-based assays

Moving away from sandwich assays, structure-switching aptamers are still compatible alternatives for electrochemical sensors. In a seminal example in 2010, Wu *et al.* applied a structure-switching aptamer approach for the detection of PDGF where the structure-switching system was combined in one DNA strand such that PDGF-binding led to a conformation switch exposing a region complementary to a ligation probe (Figure 2.22A).[126] The authors utilized a competitive hybridization approach such that upon undergoing this conformation switch, phi29 DP could elongate the aptamer to form a hairpin, blocking the binding site for the ligation probe. Without this binding site, PLP and RP generation proceed. In the absence of PDGF, the hairpin is not formed and the ligation strand instead hybridizes with the aptamer strand, preventing CT formation. PDGF-triggered RP was subsequently captured on a gold electrode and methylene blue was added to enhance the electrochemical signal. This approach had a detection limit of 63 pM.

Guo et al. showcased a structure-switching aptamer assay for the detection of ATP by monitoring the PPi by-product generated during RCA (Section 2.2.1, Figure 2.5B).[368] Here, the ATP aptamer is hybridized to a cDNA which is tethered to a magnetic bead. ATP induces cDNA release and the aptamer forms a complex with ATP (Figure 2.22B). *E. coli* DNA ligase is used with a primer strand to convert the aptamer into a suitable CT for RCA. Amplification byproduct PPi can be converted into ATP by adenosine 5'-phosphosulfate (APS) and ATP sulfurylase, feeding back into the system and triggering the release of more cDNA. Afterwards, a detection DNA probe hybridized to a cadmium sulphate nanoparticle is added to bind to the liberated cDNA. Addition of nitric acid breaks down the nanoparticles, and generates a detectable electrochemical signal providing a detection limit of 100 pM of ATP and could accurately be used for the estimation of ATP in Ramos cells.

Alternatively, one can simply regulate surface-tethered RCA via an inhibition mechanism as shown by Huang *et al.* for the detection of OTA.[138] Here, a gold electrode was functionalized with capture strands complementary to an RP (Figure 2.22C). In solution, an OTA aptamer was hybridized to an unligated CT such that subsequent PLP and RCA steps could ligate the CT and permit RCA. However, with OTA present, the ligation failed. In this way, RP was only generated, and tethered onto the electrode surface only occurred in the absence of OTA. Methylene blue was added to intercalate with the RP and enhance the change in surface current. The authors reported a detection limit of 0.065 pg/mL of OTA in just over 2 hours, including successful detection in spiked wine samples as well.

Taghdisi *et al.* offered an interesting approach to converting an inhibition RCA regulation approach into a turn-on assay by using the aptamer sequence as the CT template (Section 2.2.1) (Figure 2.22D).[369] Here, a gold electrode is tethered to a ligation strand

hybridized to an anti-OTA aptamer at its terminal ends such that the aptamer can become the CT using DNA ligase. However, in the presence of OTA, the aptamer is liberated from the gold surface, and no CT can be generated. Here, a ferrocyanide redox agent ($Fe(CN)_6^{3-}$) is unable to interact with the gold electrode inhibiting the redox reaction. This leaves the redox agent is to interact with the gold surface and reduction into $Fe(CN)_6^{4-}$. With this 4-hour method, the authors reported a detection limit of 5 pM working in clean buffer and in spiked grape juice samples. A similar example was reported for ATP as well.[370]

The electrochemical response generated by PMDs can be further enhanced by the incorporation of additional redox active probes. Qing *et al.* incorporated both H_2O_2 and NADH as redox reporters into their Pb^{2+} biosensor which generated PMD-rich RP in the presence of the heavy metal ion.[361] Addition of NADH allowed the acceleration of electron transfer to the electrode surface, and the PMDs act as both a hemin mediated H_2O_2 peroxidase and a NADH oxidase. This bienzyme-type approach nearly doubled the assay response relative to using only H_2O_2 and allowed for monitoring of RP using differential pulse voltammetry pushing the LOD below any other previously reported method at 3.3 fM.

Real-time monitoring of RCA is relatively straightforward in optical devices, however it occurs rarely in electrochemical applications. Lin *et al.* showcased a method for the real-time electrochemical monitoring of RCA on an electrode for the detection of PDGF with a detection limit of 8.8 pM of PDGF (Figure 2.22E, top).[371] The regulation method was very similar to the seminal paper for real-time protein monitoring by FNA-RCA by the Ellington group (Section 2.2.1, Figure 2.5A).[125] Briefly, binding of PDGF to the aptamer causes a conformational switch, allowing the aptamer to be converted into a CT through a PLP step. With primers immobilized on sensory surface consisting of an extended-gate field-effect transistor (EGFET) surface with a standard complementary metal oxide semiconductor (CMOS) sensor, a format devoid of complex wiring and amenable to mass-manufacturing. PDGF-triggered RP is bound to and detected by this surface due to the changes in surface charge in real-time as RP is generated (Figure 2.22E, bottom), with the assay yielding a LOD of 8.8 pM.

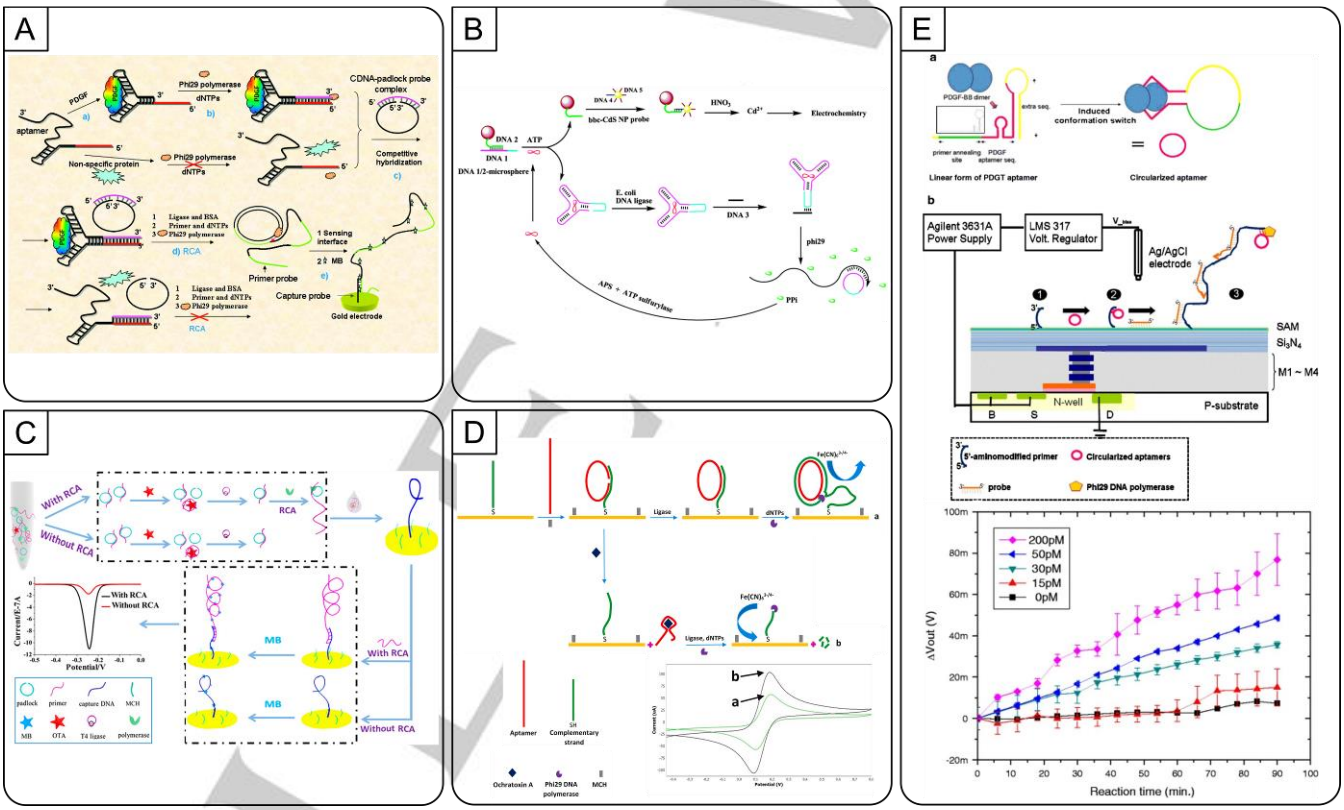

Figure 2.22. Sandwich-free aptamer-based FNA-RCA assays that use electrochemical detection. (A) Structure-switching anti-PDGF aptasensor for electrochemical detection. (B) An ATP detection and regeneration FNA-RCA assay for electrochemical detection of RP-tethered CdS NPs (C) Inhibition-RCA aptasensor for the electrochemical detection of OTA. (D) OTA aptasensor using strand-displacement polymerase reaction. (E) PDGF-triggered and immobilization-free detection on extended-gate field-effect transistor (EGFET)-modified sensor.

6.4.3 RNA-cleaving DNAzymes as MREs

Where sandwich assays require the gradual addition of binding agents onto a surface, RCDs catalytically remove protective barriers. For example, Tang *et al.* used cadmium sulfide QD-DNA probes with an RCD for the detection of lead (II).[149] The lead (II) RCD is often used as a model DNAzyme system. The magnetic beads hosted a Pb^{2+} DNAzyme sequence that cleaved its hybridized strand, allowing multiple cleavage events per bound DNAzyme (Figure 2.23A). Depletion of *trans*-substrate concentration in solution leaves a binding region for an unligated CT to hybridize to the RCD (Section 2.2.3, Figure 2.7C). After a PLP and RCA step, QD-tagged cDNA were added and the unbound washed away. Next, the remaining QDs were dissolved using nitric acid, releasing cadmium ions into solution for voltametric detection of lead (II) in buffer as well as in spiked water samples. This approach achieved a detection limit of 7.8 pM of lead

(II) and did not need multiple aptamers nor careful design of a split aptamer to be developed.

Tang *et al.* demonstrated that GOx-modified hybridization probes could be used for the detection of lead (II) by monitoring RP generation using a simple pH meter to electrochemically detect the enzymatic conversion of glucose into gluconic acid through change in solution acidity (Figure 2.23B, top).[261] Free GOx-DNA probes were washed away during magnetic bead separation and washing to properly probe for the immobilization of GOx probes along the RP. Similarly with other pH-monitoring methods, this approach required magnetic separation of RP and was resuspended in a low-capacity buffer for pH monitoring. This portable potentiometric Pb^{2+} assay's LOD was 0.91 nM, operating at room temperature and with spiked water samples. This approach had a sigmoidal response across three orders of magnitude highlighting the sensitivity of the RCD. The authors also determined assay efficacy after 5 months of reagent storage at 4˚C with the assay retaining 90% activity. The authors verified the performance of the portable reader by comparing signal generation relative to an ICP-MS system with good agreement (Figure 2.23B, bottom). With the growing availability of portable readers, their integration into electrochemical strategies can significantly improve its application at the POC.

Cai *et al*. designed an electrochemical device that used a modified micropipette tip to aid in their detection of Pb^{2+} (Figure 2.23C).[194] They used a wax-sealed carbon fiber microelectrode (CFME) to sample the solution and probe the changing redox environment instigated by target-recognition and RCA. Dual-DNAzyme feedback amplification was pioneered in this work, using two RCA amplifications simultaneously. This method differentiates itself from DFA by incorporating a second CT to participate in tandem RCA amplification. Both CTs contain an antisense G-quadruplex region. However, the CT1 contains the sequence for the 8-17 DNAzyme (Pb^{2+} DNAzyme), and CT2 contains the antisense sequence for the GR-5DNAzyme (another Pb^{2+} DNAzyme). A third substrate as a pre-primer, was prevented in participating in RCA through protection from polymerase on the 3' end. This pre-primer can bind to either CT because it contains a G-quadruplex, but only CT1 houses an active Pb^{2+} DNAzyme that can cleave the substrate upon Pb^{2+} binding. Cleavage by CT1 and PNK treatment leaves the liberated primer to be extended complementary to CT2, producing RP containing alternating units of GR-5DNAzyme and G-quadruplex regions. This careful design allows for feedback between these two tandem amplifications, not only producing many DNAzymes but also many G-quadruplex structures. Changes in diffusion were observed with the accumulation of RP and increasing intercalation of free methylene blue in solution with the G-quadruplex-rich RP. This method is completely immobilization-free, which is relatively rare for electrochemical assays especially. Local river samples were analyzed using both this electrochemical device and atomic absorption spectrometry, finding good agreement between the two methods for free Pb^{2+} in the river water. The CFME showed good electrochemical performance and had a renewable electrode surface for multiple uses.

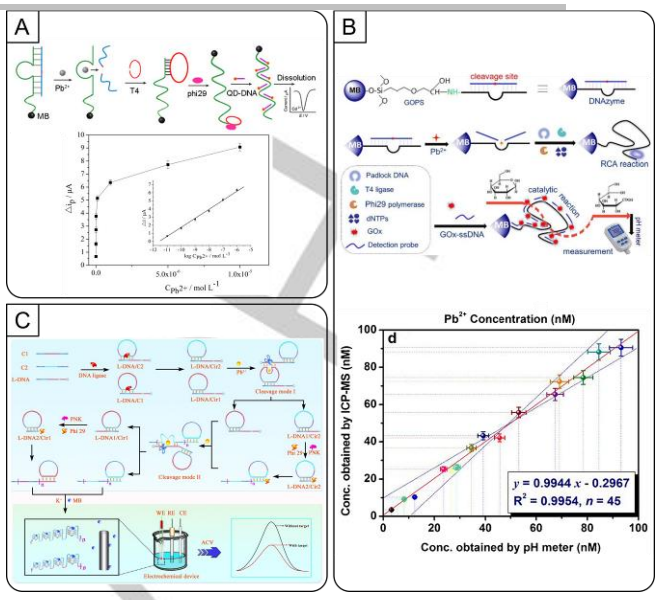

Figure 2.23. RCD-RCA assays that use electrochemical detection. (A) Electrochemical aptasensor based on Pb^{2+}-DNAzyme cleavage–triggered RCA and quantum dot-tagging. (B) Carbon fiber microelectrode (CFME) detection of a dual Pb^{2+}-DNAzyme assistant feedback amplification strategy. (C) Magnetic bead-bound Pb^{2+}-DNAzyme-RCA assay using pH sensing. Figures adapted from references from text.

Table 2.6. Electrochemical-based methods.

Surface Type	Detection Method	RCA Method	MRE Type	Regulation Method	Target	LOD	# Steps	Temperature	Assay Time	Ref.
solution (mag bead)	intercalating dye	enzyme-assisted	aptamer	structure-switching [PLP]	adenosine [CM]	0.032 nM	many	multiple	≥ 8 hrs	[347]
surface (microwell plate)	PMD	linear	aptamer	sandwich (apt/Ab) [PLP]	aflatoxin M1 [CM]	0.15 ng/mL.	many	multiple	≥ 6 hrs	[359]
surface (gold electrode)	PMD	linear	aptamer	structure-switching [PLP]	amyloid β oligomers [CM]	39 fg/mL	many	37 °C	≥ 5 hrs	[356]
surface	intercalating dye	linear	aptamer	structure-switching [PLP]	ATP [CM]	320 pM	many	multiple	≥ 8 hrs	[370]
solution	dNTP monitoring	enzyme-assisted	aptamer	structure-switching [PLP]	ATP [CM]	100 pM	many	multiple	≥ 4 hrs	[372]
surface (gold electrode)	cDNA (AuNP)	linear	aptamer	sandwich (apt 2x) [PLP]	CEA	6.7 pg/mL	many	multiple	≥ 6 hrs	[353]
surface (glassy carbon electrode)	intercalating dye	linear	aptamer	sandwich (apt/Ab) [PLP]	CEA [CM]	0.05 pg/mL	many	multiple	≥ 3 hrs	[289]
solution	G-quad dye	linear	aptamer	inhibition RCA [PLP]	CEA [CM]	2.6 fg/mL	many	multiple	≥ 5 hrs	[286]
surface (gold electrode)	cDNA (enzyme)	linear	aptamer	sandwich (split aptamer)	cocaine [CM]	1.3 nM	many	37 °C	≥ 3 hrs	[358]
surface (electrode)	G-quad dye	linear	aptamer	structure-switching [PLP]	C-reactive protein [CM]	16 fM	many	multiple	≥ 4 hrs	[355]
surface (gold electrode)	PMD	linear	aptamer	sandwich (apt/Ab)	*E. coli* [CM]	8 cfu / mL	many	37 °C	≥ 4 hrs	[303]
solution	PMD	linear	aptamer	sandwich (apt/Ab)	gastric cancer exosome [CM]	954 exosomes/mL	many	multiple	≥ 4 hrs	[304]
surface (glassy carbon electrode)	G-quad dye	linear	aptamer	structure-switching [PLP]	Hg^{2+} [CM]	0.684 pM	many	multiple	≥ 8 hrs	[284]
surface (gold electrode)	PMD	linear	aptamer	sandwich (1x apt, 1x cholesterol probe)	HT29 (EpCAM) [CM]	1 cell /mL	many	multiple	≥ 5 hrs	[367]
surface (gold electrode)	cDNA (AuNP, CuNP)	linear	aptamer	sandwich (apt 2x) [PLP]	LPS [CM]	4.8 fg/mL	many	multiple	≥ 4 hrs	[354]
surface (glassy carbon electrode)	PMD	linear	captamer	structure-switching	LPS	0.07 fg/mL	many	37 °C	≥ 3 hrs	[144]
surface (electrode)	cDNA (enzyme)	linear	aptamer	structure-switching [PLP]	maltathion [CM]	0.68 pg/mL	many	multiple	≥ 4 hrs	[373]
surface (electrode)	intercalating dye	linear	aptamer	sandwich (apt/Ab) [PLP]	MCF-7 (cancer cell) [CM]	1 cell /mL	many	multiple	≥ 5 hrs	[291]
surface (gold electrode)	GO@Fe3O4@Pt for peroxidase activity	linear	aptamer	sandwich (apt/Ab)	MPT64 [CM]	0.34 fg/mL	many	37 °C	≥ 3 hrs	[374]
solution	PMD	enzyme-assisted	aptamer	structure-switching [PLP]	MUC1 [CM]	0.71 fg/mL	many	multiple	≥ 7 hrs	[305]
solution	G-quad dye	enzyme-assisted	aptamer	inhibition RCA [PLP]	NF-κB p50 [CM]	3 pM	many	multiple	≥ 3 hrs	[287]
surface (gold electrode)	G-quad dye	linear	aptamer	structure-switching	NF-κB p65 [CM]	8.3 fM	many	multiple	≥ 4 hrs	[352]
surface (gold electrode)	intercalating dye	linear	aptamer	inhibition RCA [PLP]	OTA [CM]	0.065 ppt	many	multiple	≥ 2 hrs	[138]
surface (gold electrode)	intercalating dye	hyperbranched	aptamer	structure-switching [PLP]	OTA [CM]	0.02 pg/mL	many	multiple	≥ 8 hrs	[128]

surface (gold electrode)	$Fe(CN)_6^{(3-/4-)}$	linear	aptamer	inhibition RCA [PLP]	OTA [CM]	5 pM	many	multiple	≥ 4 hrs	[369]
solution	cDNA (QD)	linear	DNAzyme	RCD [PLP]	Pb^{2+} [CM]	7.8 pM	many	multiple	≥ 3 hrs	[149]
solution (mag bead)	cDNA (enzyme)	enzyme-assisted	DNAzyme	RCD [PLP]	Pb^{2+} [CM]	0.91 nM	many	r.t.	≥ 4 hrs	[261]
solution	G-quad dye	DFA	DNAzyme	RCD	Pb^{2+} [CM]	48 fM	many	multiple	≥ 2 hrs	[194]
surface (glassy carbon electrode)	PMD	linear	DNAzyme	RCD [PLP]	Pb^{2+} [CM]	3.3 fM	many	multiple	≥ 5 hrs	[361]
surface (gold electrode)	non-intercalator	linear	DNAzyme	RCD	Pb^{2+} [CM]	290 fM	many	multiple	≥ 4 hrs	[357]
surface (gold electrode)	cDNA (enzyme)	linear	aptamer	sandwich (apt/Ab) [PLP]	PDGF [CM]	10 fM	many	37 °C	≥ 5 hrs	[96]
surface (gold electrode)	intercalating dye	linear	aptamer	structure-switching [PLP]	PDGF	63 pM	many	multiple	≥ 5 hrs	[126]
surface (gold electrode)	intercalating dye	hyperbranched	aptamer	structure-switching [PLP]	PDGF	1.6 fmol/L	many	multiple	≥ 2 hrs	[185]
surface	cDNA (DNA)	linear	aptamer	structure-switching [PLP]	PDGF [CM]	8.8 pM	many [RT]	multiple	≥ 3 hrs	[371]
surface	cDNA (AuNP, CuNP)	linear	aptamer	sandwich (apt/Ab) [PLP]	PSA [CM]	20 ag/mL	many	multiple	≥ 5 hrs	[349]
solution	PMD	linear	aptamer	sandwich (apt/Ab) [PLP]	PSA [CM]	16.3 pg/ML	many	37 °C	≥ 7 hrs	[364]
surface (screen printed glass electrode)	G-quad dye (methylene blue)	linear	aptamer	inhibition RCA	PSA]	22.3 fM	many	not reported	≥ 8 hrs	[285]
surface (gold electrode)	methylene blue	enzyme-assisted	aptamer	structure-switching	*S. aureus* [CM]	9 CFU/mL	many	multiple	≥ 5 hrs	[288]
surface (gold electrode)	cDNA (enzyme)	linear	aptamer	structure-switching	*S. typhimurium* [CM]	19498 cfu/mL	many	37 °C	≥ 4 hrs	[259]
surface (gold electrode)	intercalating dye	hyperbranched	aptamer	structure-switching [PLP]	thrombin [CM]	1.2 aM	many	multiple	≥ 7 hrs	[127]
surface (glassy carbon electrode)	intercalating dye	linear	aptamer	structure-switching	thrombin [CM]	34.6 fM	many	37 °C	≥ 8 hrs	[106]
surface (gold electrode)	cDNA (AuNP)	linear	aptamer	sandwich (apt x2) [PLP]	thrombin [CM]	35 fM	many	multiple	≥ 6 hrs	[266]
surface (gold electrode)	cDNA (enzyme)	linear	aptamer	structure-switching [PLP]	thrombin [CM]	35.3 fM	many	multiple	≥ 7 hrs	[258]
surface (gold electrode)	cDNA (AuNP)	linear	aptamer	sandwich (apt/Ab)	*V. parahaemolyticus* [CM]	2 cfu/mL	many	multiple	≥ 3 hrs	[283]

[a] Table Footnote. [b] … [RT] denotes that detection was done with real-time monitoring; [PLP] denotes that the assay used a padlock probe ligation reaction; [CM] denotes that the assay was tested with complex media; “many” denotes any assay that required 4 or more steps; r.t. denotes that room temperature was used.

7. Summary and Future Outlook

A notable theme with NABs is the interchangeability of the recognition, and detection strategies. This is also evident in RCA-based FNABs as the number of possible variations of regulation, amplification, and detection strategies can be overwhelming. There is no doubt that RCA is the most prolific ITA method. Every week, new variations of FNA-based RCA methods are published, representing as much as 50% of all FNA-based ITA methods (Figure 2.24). The flexibility is a massive boon for rationally designing the most appropriate RCA assay. However, it is because there are so many choices that it is especially important to be thorough and strategic in deciding on the individual components, especially as different POC applications may have unique characteristics and demands that make certain strategies more practical than others. This is particularly true with paper-based biosensing, which comes with a host of advantages under the right conditions. As such, it is imperative that the assay requirements are well understood such that the best combinations can be selected.

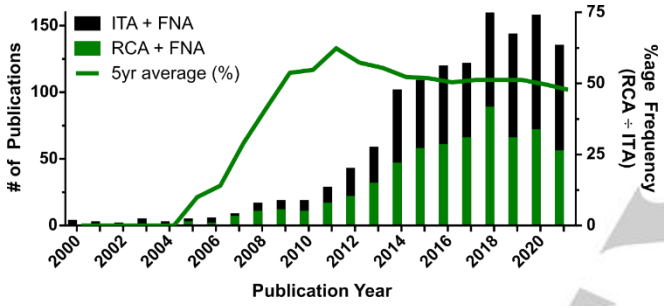

Figure 2.24. Frequency of publications mentioning RCA and FNAs compared to the frequency of publications mentioning any ITA method and FNAs as per Web of Science. The total number of publications in 2021 was estimated based on the number of publications as of June 2, 2021.

7.1 Regulation of RCA by FNAs

The first step in selecting the optimal molecular recognition strategy is determining whether to regulate the primer or CT for RCA. If real samples contain a substantial number of exonucleases or potential interferents, regulating the CT would allow one to take advantage of the exonuclease resistance properties accredited to captamers. Conversely, if the sample matrices are relatively simple, integrating a linear aptamer may be most effective as the pool of tested captamers remains limited. Another fundamental consideration is cost limitations. Incorporating rGO can be a powerful alternative to structure-switching aptamers with the added benefit of providing nuclease resistance however the high batch to batch variability may complicate its applications for low-resource.[108] Likewise, some tripartite structure-switching designs may necessitate DNA functionalization to protect from nonspecific 3'-exonuclease digestion by phi29 DP. Even the final sensitivity of the assay can be greatly affected by the recognition strategy used. Strategies utilizing target binding to inhibit RCA provide a particularly straightforward assay platform but can limit sensitivity downstream due to practical limitations of inhibitory assays. Using structure-switching aptamers can be a double-edged sword as though many creative strategies exist, poor design of the structure-switching aptamer can hamstring its apparent binding affinity.

As noted above, there are an abundance of methods available for primer regulation, using either aptamers or DNAzymes as MREs. Fewer methods exist to modulate the CT, and some of these, such as use of DNAzyme ligases or DNAzyme kinases, have relatively limited utility. In addition, methods that modulate the CT often require additional components, such as ligase enzymes, or require multiple separation or washing steps, which are challenging to integrate into simple POC devices. Even so, through careful design it is possible to design homogeneous assays using either aptamers or DNAzymes as MREs, and modulation of primer or CT availability to initiate RCA.

7.2 Amplification Methods

Luckily, any shortcomings in regulation strategies (such as binding affinities) can be mitigated with appropriate amplification strategies. When the application demands particularly sensitive detection, E-RCA techniques can improve LODs by several orders of magnitude. This can be particularly pertinent when handling complex media such as blood or stool samples which necessitate several dilutions. However, if clinically relevant or actionable amounts of analyte are easily accessible, or the sample inherently has minimal interferents, then careful optimization of the CT combined with linear RCA may be sufficient. For instance, an E-RCA method may provide a working dynamic range for early detection of disease progression, but linear RCA may be better suited for later stages of disease monitoring when the analyte is more abundant. Further, the equipment limitations of the POC setting must be considered. In a laboratory setting where high quality optical readers are abundant, linear RCA can provide sufficient RP for detection. In low-resource settings relying only on the human eye, E-RCA may be required to make the assay readout more definitive.

7.3 RCA Detection Outputs

Though the ASSURED criteria promotes POC assays that are accessible in low-resource areas with limited expertise and instrumentation, the selection of a colorimetric, fluorometric, or electrochemical approach is ultimately governed by the resources and requirements of the end-user. Colorimetric assays can be interpreted by eye, making them a popular choice for detection despite often requiring additional washing or handling steps. As colorimetric methods are fundamentally less sensitive than their fluorometric counterparts, they are best suited for applications where there is a high abundance of RP or where semi-quantitative answers are sufficient. Optical readers may improve assay sensitivity, and technological advances have made access to miniature and portable optical readers increasingly affordable especially with the increasing ubiquity of cell phones which can be used as optical devices.[205] Where fluorometric readers are available, the assays benefit from increased sensitivity and can incorporate real-time monitoring of RP generation or fluorogenic multiplexing. In the absence of significant sample handling and preparation steps, media such as blood and faecal matter can be difficult to monitor optically due to their opacity. Electrochemical strategies provide an avenue for handling complex samples while maintaining ultrasensitive assay performance with the caveat that these assays often require additional washing or handling steps in addition to readers to allow for complex media analysis. Ultimately, careful consideration of the optimal detection strategy is essential for developing POC devices and can significantly decrease assay complexity.

Whereas the strategies in Chapters 2-4 aimed to guide readers in their considerations for biosensor development, Chapter 5 detailed numerous seminal works and recent publications in the literature that

use these strategies to great effect. Though these assays may share many similarities or core schematic components, they differ greatly in assay time, sensitivities, and ease of use. Colorimetric detection methods are perhaps the most user-friendly POC detection methods for diagnostic tests as it is possible to directly visualize color changes by eye, avoiding the need for an external reader device. Though colorimetric detection is generally less sensitive than either fluorometric or electrochemical methods, its integration with ITA techniques is usually sufficient to allow detection limits in the low picomolar or even femtomolar range. Fluorometric methods require a reader to detect a signal, however, there have been many examples using either smartphones or affordable portable fluorescence readers for detection, making such assays more amenable to use in low-resource settings.[204–206] While electrochemical detection also requires a reader, there are many portable and inexpensive electrochemical readers that are compatible with the ASSURED criteria, including widely available devices such as the glucose meter.[375] While many electrochemical methods require longer operation times than other optical strategies, their incredible sensitivity and strengths with handling optically complex sample matrices makes them serious contenders for POC applications. As demonstrated, assay time can be greatly shortened by incorporating alternative assay designs which could improve its application at the POC.

To emphasize the importance of decentralizing these assays from the laboratory, we discuss assays that incorporate solution and solid-phase designs that may be more easily performed at the POC. Solution-phase assays, whether homogeneous or heterogeneous, may incorporate some amount of liquid manipulation and washing steps. Heterogeneous assays move beyond just the solution phase by incorporate particulate solids, often for MRE immobilization and washing. Solution-phase assays that minimize user interaction, such as those denoted as one-pot, act to minimize this concern central to solution-based POC analysis. Solid-phase biosensors and bioassays like those performed in microwell plates, microfluidic chips, or paper-based devices use the solid interface to manipulate the assay solution. Microfluidic devices and paper-based devices demonstrate that beyond acting as solid supports for MRE, the solid surface can be used to direct and manipulate flow and enable sequential on-device processes independent of user input.

7.4. Future Outlook

Using FNA-based strategies for regulating RCA can yield flexible and tunable platforms for biosensing. Though the antibody-antigen interaction continues to constitute the most popular mechanism of biorecognition for many biological assays, NA-based alternatives to traditional antibody-based diagnostics systems have garnered interest in part because of their expanded toolbox of analytes, as well as advantages with synthesis and handling.[4,7,376] Further, as this review has highlighted, the incorporation of RCA adds a powerful method for ultrasensitive detection of numerous analytes beyond NAs. With the emergence of RCA-linked biosensing in the late 90s, we have seen over thirty years of advancements in techniques across all stages of the assay process. Though true POC examples remain limited, great strides have been made towards this goal. Here we discuss some of the ongoing challenges facing the diagnostics field, how RCA-linked FNABs can help overcome them and highlight areas we hope to see advance.

A global interest in early disease-state biosensing in preventative healthcare measures grows in the 21st century. [377] These applications may require extremely sensitive sensing methods as analytes often exist at low concentrations at early stages of disease before clinical symptoms present. Clinical biosensors may reduce the burden on healthcare infrastructure ideally offering fast and accurate results at the POC to guide the appropriate prescription of drugs, reducing frequency and duration of clinic visits, as well as decreasing the workload of medical staff. [378–381] Perhaps most importantly, assays should strive to validate their assays' proficiency with clinically relevant matrices because despite their utility, many of the RCA methods remain untested with real samples specifically. To our benefit, creative advancements in converting linear RCA into E-RCA gives hope that some sample matrix challenges can be overcome with sample dilution and signal recovery with amplification.

While there is an application, time and place for both laboratory-based assays and POC biosensors, there is increasing interest in biosensors that compete with conventional multi-day laboratory testing. As well, reaction temperatures are equally critical. As phi29 DP is effectively able to operate at room temperature, it is pertinent to ensure that other steps are equally compatible at the same temperature. Fortunately, solutions exist for equipment-free heating elements that are compatible with POC devices.[382] These tools can help serve as a compromise as we work toward truly isothermal sensors. On-site biosensors for environmental assessment are especially useful in remote areas with the importance of monitoring water quality an ongoing pursuit. To this end, it is desirable to move POC assays from solution onto paper platforms as they are robust, cheap, and easy to store and transport. Ideally, paper-based assays should provide a procedurally simple, user-friendly, and interpretable test. Despite the many advantages, adopting RCA-based strategies to paper-based detection can be challenging. Though there are several paper-based RCA-linked FNAB examples available, the vast majority are performed in paper-based wells. At this stage, a renewed focus should be on the incorporation of lateral flow strategies to take full advantage of the inherent wicking properties of paper for sample handling.

We believe that optical detection methods, especially those that give easy to interpret real-time results, will make future RCA-based FNABs competitive on a global scale. For assay readouts, colorimetric methods such as hemin/G-quadruplex peroxidase-mimicking DNAzymes are commonly used to achieve naked-eye detection. However the peroxidase-mimicking reaction requires stringent buffer conditions making real-time monitoring challenging. We look forward to increased innovation in this portion of the field, including incorporation of real-time colorimetric sensing methods. While there are fewer examples of colorimetric detection strategies, there are numerous examples of real-time fluorogenic detection strategies for RCA. Though portable fluorescent readers are becoming increasingly prevalent, the simplicity of a test that can be interpreted by the naked eye should not be understated. As an example, real-time colorimetric monitoring has already been demonstrated for LAMP-linked NABs using crystal violet as an intercalating dye.[383,384] As DNA probe functionalization can otherwise constitute a large fraction of an assay's cost, migration of alternative real-time colorimetric monitoring techniques of NAs to RCA applications alongside other discoveries could significantly minimize the costs of optical probes.

To our knowledge, there are currently no commercially available RCA biosensors, hence there is clearly a need to produce simpler and faster RCA assays with real-world applications. The advent of the COVID-19 pandemic has put into hyper-focus the need for rapid and reliable POC testing particularly for early disease-state monitoring. This crisis has led to an enormous surge of innovation and novel ideas and we are optimistic that these efforts will propel the field of sensitive POC FNABs forward. We are confident that advancements in RCA-

linked FNABs do not necessitate reinventions of the wheel but rather finding the right vehicle to hitch our templates to.

Keywords: rolling circle amplification • aptamers • DNAzymes • POC biosensors • isothermal amplification.

8. References

[1] J. Liu, Z. Cao, Y. Lu, *Functional Nucleic Acid Sensors*, Wiley, **2009**.
[2] Y. Krishnan, F. C. Simmel, *Angew. Chemie - Int. Ed.* **2011**, *50*, 3124–3156.
[3] Y. Du, S. Dong, *Anal. Chem.* **2017**, *89*, 189–215.
[4] P. Craw, W. Balachandran, *Lab Chip* **2012**, *12*, 2469–2486.
[5] K. Janssen, K. Knez, D. Spasic, J. Lammertyn, *Sensors* **2013**, *13*, 1353–1384.
[6] Y. Zhao, F. Chen, Q. Li, L. Wang, C. Fan, *Chem. Rev.* **2015**, *115*, 12491–12545.
[7] K. S. Park, *Biosens. Bioelectron.* **2018**, *102*, 179–188.
[8] A. Dhiman, P. Kalra, V. Bansal, J. G. Bruno, T. K. Sharma, *Sensors Actuators, B Chem.* **2017**, *246*, 535–553.
[9] M. Chen, S. Bi, X. Jia, P. He, *Anal. Chim. Acta* **2014**, *837*, 44–51.
[10] C. Teller, I. Willner, *Curr. Opin. Biotechnol.* **2010**, *21*, 376–391.
[11] S. K. Silverman, *Trends Biochem. Sci.* **2016**, *41*, 595–609.
[12] I. Willner, B. Shlyahovsky, M. Zayats, B. Willner, *Chem. Soc. Rev.* **2008**, *37*, 1153–1165.
[13] Y. Lu, J. Liu, *Curr. Opin. Biotechnol.* **2006**, *17*, 580–588.
[14] W. Winkler, A. Nahvi, R. R. Breaker, *Nature* **2002**, *419*, 952–956.
[15] R. R. Breaker, *Mol. Cell* **2011**, *43*, 867–879.
[16] D. L. Robertson, G. F. Joyce, *Lett. to Nat.* **1990**, *344*, 467–468.
[17] A. D. Ellington, J. W. Szostak, *Nature* **1990**, *346*, 818–822.
[18] C. Tuerk, L. Gold, *Science (80-.).* **1990**, *249*, 505–510.
[19] R. Stoltenburg, C. Reinemann, B. Strehlitz, *Biomol. Eng.* **2007**, *24*, 381–403.
[20] M. Darmostuk, S. Rimpelova, H. Gbelcova, T. Ruml, *Biotechnol. Adv.* **2014**, *33*, 1141–1161.
[21] L. S. Green, D. Jellinek, R. Jenison, A. Östman, C. H. Heldin, N. Janjic, *Biochemistry* **1996**, *35*, 14413–14424.
[22] R. Jenison, S. Gill, A. Pardi, B. Polisky, *Science (80-.).* **2018**, *263*, 1425–1429.
[23] S. Tyagi, F. Kramer, *Nat. Biotechnol.* **1996**.
[24] M. a M. . Cooper, *Nat. Rev. Drug Discov.* **2002**, *1*, 515–528.
[25] B. Van Dorst, J. Mehta, K. Bekaert, E. Rouah-Martin, W. De Coen, P. Dubruel, R. Blust, J. Robbens, *Biosens. Bioelectron.* **2010**, *26*, 1178–1194.
[26] E. Luzi, M. Minunni, S. Tombelli, M. Mascini, *TrAC Trends Anal. Chem.* **2003**, *22*, 810–818.
[27] D. S. Wilson, J. W. Szostak, *Annu. Rev. Biochem.* **1999**, *68*, 611–647.
[28] J. C. Cox, A. D. Ellington, *Bioorganic Med. Chem.* **2001**, *9*, 2525–2531.
[29] M. Jing, M. T. Bowser, *Anal. Chim. Acta* **2011**, *686*, 9–18.
[30] A. Sassolas, B. Leca-Bouvier, L. Blum, *Chem. Rev.* **2008**.
[31] M. Bauer, M. Strom, D. S. Hammond, S. Shigdar, *Molecules* **2019**, *24*, 4377.
[32] F. Kleinjung, S. Klussmann, V. A. Erdmann, F. W. Scheller, J. P. Fürste, F. F. Bier, *Anal. Chem.* **1998**, *70*, 328–331.
[33] R. R. Breaker, G. F. Joyce, *Chem. Biol.* **1994**, *1*, 223–229.
[34] S. K. Silverman, *Acc. Chem. Res.* **2009**, *42*, 1521–1531.
[35] D. E. Huizenga, J. W. Szostak, *Biochemistry* **1995**, *34*, 656–665.
[36] A. Flynn-Charlebois, Y. Wang, T. K. Prior, I. Rashid, K. A. Hoadley, R. L. Coppins, A. C. Wolf, S. K. Silverman, *J. Am. Chem. Soc.* **2003**, *125*, 2444–2454.
[37] M. Chandra, A. Sachdeva, S. K. Silverman, *Nat. Chem. Biol.* **2009**, *5*, 718–720.
[38] H. Gu, K. Furukawa, Z. Weinberg, D. F. Berenson, R. R. Breaker, *J. Am. Chem. Soc.* **2013**, *135*, 9121–9129.
[39] D. J. Parker, Y. Xiao, J. M. Aguilar, S. K. Silverman, *J. Am. Chem. Soc.* **2013**, *135*, 8472–8475.
[40] Y. Li, R. R. Breaker, *Proc. Natl. Acad. Sci. U. S. A.* **1999**, *96*, 2746–2751.
[41] Y. Li, Y. Liu, R. R. Breaker, *Biochemistry* **2000**, *39*, 3106–3114.
[42] T. L. Sheppard, P. Ordoukhanian, G. F. Joyce, *Proc. Natl. Acad. Sci. U. S. A.* **2000**, *97*, 7802–7807.
[43] P. Travascio, Y. Li, D. Sen, *Chem. Biol.* **1998**, *5*, 505–517.
[44] M. Famulok, J. S. Hartig, G. Mayer, *Chem. Rev.* **2007**, *107*, 3715–3743.
[45] M. M. Ali, S. D. Aguirre, H. Lazim, Y. Li, *Angew. Chemie - Int. Ed.* **2011**, *50*, 3751–3754.
[46] Z. Shen, Z. Wu, D. Chang, W. Zhang, K. Tram, C. Lee, P. Kim, B. J. Salena, Y. Li, *Angew. Chemie* **2016**, *128*, 2477–2480.
[47] M. Mauk, J. Song, H. H. Bau, R. Gross, F. D. Bushman, R. G. Collman, C. Liu, *Lab Chip* **2017**, *17*, 382–394.
[48] J. R. Choi, K. W. Yong, R. Tang, Y. Gong, T. Wen, F. Li, B. Pingguan-Murphy, D. Bai, F. Xu, *TrAC - Trends Anal. Chem.* **2017**, *93*, 37–50.
[49] E. M. McConnell, I. Cozma, Q. Mou, J. D. Brennan, Y. Lu, Y. Li, *Chem. Soc. Rev.* **2021**, DOI 10.1039/D1CS00240F.
[50] D. Mabey, R. W. Peeling, A. Ustianowski, M. D. Perkins, *Nat. Rev. Microbiol.* **2004**, *2*, 231–240.
[51] M. Urdea, L. A. Penny, S. S. Olmsted, M. Y. Giovanni, P. Kaspar, A. Shepherd, P. Wilson, C. A. Dahl, S. Buchsbaum, G. Moeller, D. C. Hay Burgess, *Nature* **2006**, *444 Suppl*, 73–79.
[52] P. Yager, G. J. Domingo, J. Gerdes, *Annu. Rev. Biomed. Eng.* **2008**, *10*, 107–144.
[53] A. W. Martinez, S. T. Phillips, G. M. Whitesides, E. Carrilho, *Anal. Chem.* **2010**, *82*, 3–10.
[54] W. Zhou, P. J. Jimmy Huang, J. Ding, J. Liu, *Analyst* **2014**, *139*, 2627–2640.
[55] C. Jung, A. D. Ellington, *Acc. Chem. Res.* **2014**, *47*, 1825–1835.
[56] K. B. Mullis, F. A. Faloona, in *Methods Enzymol.*, **1987**, pp. 335–350.
[57] L. Yan, J. Zhou, Y. Zheng, A. S. Gamson, B. T. Roembke, S. Nakayama, H. O. Sintim, *Mol. Biosyst.* **2014**, *10*, 970–1003.
[58] G. T. Walker, M. S. Fraiser, J. L. Schram, M. C. Little, J. G. Nadeau, D. P. Malinowski, *Nucleic Acids Res.* **1992**, *20*, 1691–1696.
[59] P. Gill, A. Ghaemi, *Nucleosides. Nucleotides Nucleic Acids* **2008**, *27*, 224–43.
[60] O. Piepenburg, C. H. Williams, D. L. Stemple, N. A. Armes, *PLoS Biol.* **2006**, *4*, 1115–1121.
[61] S. Lutz, P. Weber, M. Focke, B. Faltin, J. Hoffmann, C. Müller, D. Mark, G. Roth, P. Munday, N. Armes, O. Piepenburg, R. Zengerle, F. Von Stetten, *Lab Chip* **2010**, *10*, 887–893.
[62] R. K. Daher, G. Stewart, M. Boissinot, M. G. Bergeron, *Clin. Chem.* **2016**, *62*, 947–958.
[63] T. Notomi, *Nucleic Acids Res.* **2000**, *28*, 63e – 63.
[64] N. Tomita, Y. Mori, H. Kanda, T. Notomi, *Nat. Protoc.* **2008**, *3*, 877–882.
[65] T. Notomi, Y. Mori, N. Tomita, H. Kanda, *J. Microbiol.* **2015**, *53*, 1–5.
[66] J. T. Connelly, J. P. Rolland, G. M. Whitesides, *Anal. Chem.* **2015**, *87*, 7595–7601.
[67] M. Vincent, Y. Xu, H. Kong, *EMBO Rep.* **2004**, *5*, 795–800.
[68] Y.-J. Jeong, K. Park, D.-E. Kim, *Cell. Mol. Life Sci.* **2009**, *66*, 3325–3336.
[69] P. J. Asiello, A. J. Baeumner, *Lab Chip* **2011**, *11*, 1420–1430.
[70] S. Barreda-García, R. Miranda-Castro, N. de-los-Santos-Álvarez, A. J. Miranda-Ordieres, M. J. Lobo-Castañón, *Anal. Bioanal. Chem.* **2018**, *410*, 679–693.
[71] R. M. Dirks, N. A. Pierce, *Proc. Natl. Acad. Sci. U. S. A.* **2004**, *101*, 15275–15278.
[72] S. Bi, S. Yue, S. Zhang, *Chem. Soc. Rev.* **2017**, *46*, 4281–4298.
[73] W. Zhao, M. M. Ali, M. A. Brook, Y. Li, *Angew. Chemie - Int. Ed.* **2008**, *47*, 6330–6337.

[74] M. M. Ali, F. Li, Z. Zhang, K. Zhang, D.-K. Kang, J. A. Ankrum, X. C. Le, W. Zhao, *Chem. Soc. Rev.* **2014**, *43*, 3324.

[75] L. Gu, W. Yan, L. Liu, S. Wang, X. Zhang, M. Lyu, *Pharmaceuticals* **2018**, *11*, 1–19.

[76] S. Yue, Y. Li, Z. Qiao, W. Song, S. Bi, *Trends Biotechnol.* **2021**, 1–13.

[77] X. Xu, Y. Su, Y. Zhang, X. Wang, H. Tian, X. Ma, H. Chu, W. Xu, *TrAC - Trends Anal. Chem.* **2021**, *141*, 116293.

[78] L. Xu, J. Duan, J. Chen, S. Ding, W. Cheng, *Anal. Chim. Acta* **2021**, *1148*, 238187.

[79] H. Shi, J. Cui, H. Sulemana, W. Wang, L. Gao, *Luminescence* **2021**, *36*, 842–848.

[80] M. G. Mohsen, E. T. Kool, *Acc. Chem. Res.* **2016**, *49*, 2540–2550.

[81] E. T. Kool, *J. Am. Chem. Soc.* **1991**, *113*, 6265–6266.

[82] G. Prakash, E. T. Kool, *J. Chem. Soc. Chem. Commun.* **1991**, *176*, 1161.

[83] D. Liu, S. L. Daubendiek, M. A. Zillman, K. Ryan, E. T. Kool, *J. Am. Chem. Soc.* **1996**, *118*, 1587–1594.

[84] V. V. Demidov, *Expert Rev. Mol. Diagn.* **2002**, *2*, 542–548.

[85] P. M. Lizardi, X. Huang, Z. Zhu, P. Bray-Ward, D. C. Thomas, D. C. Ward, *Nat. Genet.* **1998**, *19*, 225–232.

[86] O. Söderberg, M. Gullberg, M. Jarvius, K. Ridderstråle, K. J. Leuchowius, J. Jarvius, K. Wester, P. Hydbring, F. Bahram, L. G. Larsson, U. Landegren, K. Wester, P. Hydbring, F. Bahram, L. G. Larsson, U. Landegren, *Nat. Methods* **2006**, *3*, 995–1000.

[87] J. Jarvius, J. Melin, J. Göransson, J. Stenberg, S. Fredriksson, C. Gonzalez-Rey, S. Bertilsson, M. Nilsson, S. Bertilsson, M. Nilsson, *Nat. Methods* **2006**, *3*, 725–727.

[88] K. Sato, R. Ishii, N. Sasaki, K. Sato, M. Nilsson, *Anal. Biochem.* **2013**, *437*, 43–45.

[89] C. Larsson, J. Koch, A. Nygren, G. Janssen, A. K. Raap, U. Landegren, M. Nilsson, *Nat. Methods* **2004**, *1*, 227–232.

[90] F. Dahl, J. Baner, M. Gullberg, M. Mendel-Hartvig, U. Landegren, M. Nilsson, J. Banér, M. Gullberg, M. Mendel-Hartvig, U. Landegren, M. Nilsson, J. Baner, M. Gullberg, M. Mendel-Hartvig, U. Landegren, M. Nilsson, *Proc. Natl. Acad. Sci.* **2004**, *101*, 4548–4553.

[91] Q. Ma, Z. Gao, *Anal. Bioanal. Chem.* **2018**, *410*, 3093–3100.

[92] B. Schweitzer, S. Wiltshire, J. Lambert, S. O'Malley, K. Kukanskis, Z. Zhu, D. C. Ward, S. O'Malley, K. Kukanskis, Z. Zhu, S. F. Kingsmore, P. M. Lizardi, D. C. Ward, *Proc. Natl. Acad. Sci. U. S. A.* **2000**, *97*, 10113–10119.

[93] B. Schweitzer, S. Roberts, B. Grimwade, W. Shao, M. Wang, Q. Fu, Q. Shu, I. Laroche, Z. Zhou, V. T. Tchernev, J. Christiansen, S. F. Kingsmore, *Nat. Biotechnol.* **2002**, *20*, 359–365.

[94] M. C. Mullenix, R. Sivakamasundari, W. J. Feaver, R. M. Krishna, M. P. Sorette, H. J. Datta, D. M. Morosan, S. P. Piccoli, *Clin. Chem.* **2002**, *48*, 1855–1858.

[95] A. Raghunathan, M. P. Sorette, H. R. Ferguson, S. P. Piccoli, *Clin. Chem.* **2002**, *48*, 1853–1855.

[96] L. Zhou, L.-J. Ou, X. Chu, G.-L. Shen, R.-Q. Yu, *Anal. Chem.* **2007**, *79*, 7492–7500.

[97] F. Akter, M. Mie, E. Kobatake, *Anal. Biochem.* **2011**, *416*, 174–179.

[98] M. Liu, C. Y. Hui, Q. Zhang, J. Gu, B. Kannan, S. Jahanshahi-Anbuhi, C. D. M. M. M. Filipe, J. D. Brennan, Y. Li, C. D. M. M. M. Filipe, J. D. Brennan, Y. Li, *Angew. Chemie - Int. Ed.* **2016**, *55*, 2709–2713.

[99] A. K. Yetisen, M. S. Akram, C. R. Lowe, *Lab Chip* **2013**, *13*, 2210–2251.

[100] J. Méndez, L. Blanco, M. Salas, *EMBO J.* **1997**, *16*, 2519–2527.

[101] R. M. Bialy, M. M. Ali, Y. Li, J. D. Brennan, *Chem. – A Eur. J.* **2020**, *26*, 5085–5092.

[102] R. Nutiu, Y. Li, **2003**, DOI 10.1021/ja028962o.

[103] R. Nutiu, Y. Li, *Angew. Chemie - Int. Ed.* **2005**, *44*, 1061–1065.

[104] P. S. Lau, B. K. Coombes, Y. Li, *Angew. Chemie Int. Ed.* **2010**, *49*, 7938–7942.

[105] P. S. Lau, Y. Li, in *Biosens. Based Aptamers Enzym.*, **2013**, pp. 69–92.

[106] T. Hu, Y. N. Zheng, M. J. Li, W. B. W. B. Liang, Y. Q. Chai, R. Yuan, *Anal. Chem.* **2018**, *90*, 6096–6101.

[107] X. Liu, F. Yang, D. Li, R. Yuan, Y. Xiang, *Sensors Actuators, B Chem.* **2020**, *305*, 127405.

[108] M. Liu, W. Zhang, D. Chang, Q. Zhang, J. D. Brennan, Y. Li, *TrAC - Trends Anal. Chem.* **2015**, *74*, 120–129.

[109] C. H. Lu, H. H. Yang, C. L. Zhu, X. Chen, G. N. Chen, *Angew. Chemie - Int. Ed.* **2009**, *48*, 4785–4787.

[110] M. Liu, J. Song, S. Shuang, C. Dong, J. D. Brennan, Y. Li, *ACS Nano* **2014**, *8*, 5564–5573.

[111] Y. Mao, M. Liu, K. Tram, J. Gu, B. J. Salena, Y. Jiang, Y. Li, *Chem. - A Eur. J.* **2015**, *21*, 8069–8074.

[112] C. Y. Hui, M. Liu, Y. Li, J. D. Brennan, *Angew. Chemie Int. Ed.* **2018**, *57*, 4549–4553.

[113] M. Liu, Q. Yin, Y. Chang, Q. Zhang, J. D. Brennan, Y. Li, *Angew. Chemie - Int. Ed.* **2019**, *58*, 8013–8017.

[114] X. Li, X. He, Q. Zhang, Y. Chang, M. Liu, *Anal. Methods* **2019**, *11*, 4328–4333.

[115] W. Cheng, L. Ding, Y. Chen, F. Yan, H. Ju, Y. Yin, *Chem. Commun.* **2010**, *46*, 6720–6722.

[116] M. Liu, W. Zhang, Q. Zhang, J. D. Brennan, Y. Li, *Angew. Chemie Int. Ed.* **2015**, *54*, 9637–9641.

[117] J. Wang, Y. Wang, S. Liu, H. Wang, X. Zhang, X. Song, J. Huang, *Anal. Chim. Acta* **2019**, *1060*, 79–87.

[118] R. M. Bialy, Y. Li, J. D. Brennan, *Chem. Eur. J.* **2021**, *(Accepted)*, 1–7.

[119] R. Deng, Y. Dong, X. Xia, Y. Dai, K. Zhang, Q. He, W. C. Zeng, X. Ren, J. Li, *Anal. Chem.* **2018**, *90*, 14347–14354.

[120] M. M. Ali, Y. Li, *Angew. Chemie Int. Ed.* **2009**, *48*, 3512–3515.

[121] M. Liu, Q. Zhang, D. Chang, J. Gu, J. D. Brennan, Y. Li, *Angew. Chemie Int. Ed.* **2017**, 1–6.

[122] L. Blanco, A. Bernad, J. M. Lazaro, G. Martin, C. Garmendia, M. Salas, *J. Biol. Chem.* **1989**, *264*, 8935–8940.

[123] J. Banér, M. Nilsson, M. Mendel-Hartvig, U. Landegren, *Nucleic Acids Res.* **1998**, *26*, 5073–5078.

[124] M. Nilsson, H. Malmgren, M. Samiotaki, M. Kwiatkowski, B. Chowdhary, U. Landegren, *Science (80-.).* **1994**, *265*, 2085–2088.

[125] L. Yang, C. W. Fung, J. C. Eun, A. D. Ellington, *Anal. Chem.* **2007**, *79*, 3320–3329.

[126] Z.-S. Wu, H. Zhou, S. Zhang, G. Shen, R. Yu, *Anal. Chem.* **2010**, *82*, 2282–2289.

[127] G. Jin, C. Wang, L. Yang, X. Li, L. Guo, B. Qiu, G. Chen, Z. Lin, G. Chen, *Biosens. Bioelectron.* **2015**, *63*, 166–171.

[128] L. Yang, Y. Zhang, R. Li, C. Lin, L. Guo, B. Qiu, Z. Lin, G. Chen, *Biosens. Bioelectron.* **2015**, *70*, 268–274.

[129] Z. Qiu, J. Shu, Y. He, Z. Lin, K. Zhang, S. Lv, D. Tang, *Biosens. Bioelectron.* **2017**, *87*, 18–24.

[130] Y. Jiang, S. Zou, X. Cao, *Sensors Actuators, B Chem.* **2017**, *251*, 976–984.

[131] L. Xu, Z. Jiang, Y. Mu, Y. Zhang, Q. Zhan, J. Cui, W. Cheng, S. Ding, *Sensors Actuators, B Chem.* **2018**, *259*, 596–603.

[132] R. Huang, L. He, S. Li, H. Liu, L. Jin, Z. Chen, N. He, Y. Zhao, Z. Li, Y. Deng, N. He, *Nanoscale* **2020**, *12*, 2445–2451.

[133] S. Niazi, I. M. Khan, Y. Yu, I. Pasha, Y. Lv, A. Mohsin, B. S. Mushtaq, Z. Wang, *Sensors Actuators, B Chem.* **2020**, *315*, 1–10.

[134] S. Bi, L. Li, S. Zhang, *Anal. Chem.* **2010**, *82*, 9447–9454.

[135] C. Ma, W. Wang, Q. Yang, C. Shi, L. Cao, *Biosens. Bioelectron.* **2011**, *26*, 3309–3312.

[136] P. Tong, W.-W. W. Zhao, L. Zhang, J.-J. J. Xu, H.-Y. Y. Chen, *Biosens. Bioelectron.* **2012**, *33*, 146–151.

[137] C. Ding, N. Wang, J. Zhang, Z. Wang, *Biosens. Bioelectron.* **2013**, *42*, 486–491.

[138] L. Huang, J. Wu, L. Zheng, H. Qian, F. Xue, Y. Wu, D. Pan, S. B. Adeloju, W. Chen, *Anal. Chem.* **2013**, *85*, 10842–10849.

[139] K. Liang, S. Zhai, Z. Zhang, X. Fu, J. Shao, Z. Lin, B. Qiu, G. N. Chen, B. Qiu, G. N. Chen, *Analyst* **2014**, *139*, 4330–4334.

[140] X. Lin, Q. Chen, W. Liu, H. Li, J. M. J.-M. M. J.-M. M. Lin, *Biosens. Bioelectron.* **2014**, *56*, 71–76.

[141] P. He, L. Liu, W. Qiao, S. Zhang, *Chem. Commun.* **2014**, *50*, 1481–1484.

[142] J. Li, M. Mohammed-Elsabagh, F. Paczkowski, Y. Li, *ChemBioChem* **2020**, DOI 10.1002/cbic.202000003.
[143] D. A. Di Giusto, W. A. Wlassoff, J. J. Gooding, B. A. Messerle, G. C. King, **n.d.**, DOI 10.1093/nar/gni063.
[144] M. Zhao, A. Y. Chen, D. Huang, Y. Q. Chai, Y. Zhuo, R. Yuan, *Anal. Chem.* **2017**, *89*, 8335–8342.
[145] L. Wang, K. Tram, M. M. Ali, B. J. Salena, J. Li, Y. Li, *Chem. Eur. J.* **2014**, *20*, 2420–4.
[146] S. Wang, S. Bi, Z. Wang, J. Xia, F. Zhang, M. Yang, R. Gui, Y. Li, Y. Xia, *Chem. Commun.* **2015**, *51*, 7927–7930.
[147] E. J. Cho, L. Yang, M. Levy, A. D. Ellington, *J. Am. Chem. Soc.* **2005**, *127*, 2022–3.
[148] S. A. McManus, Y. Li, *J. Am. Chem. Soc.* **2013**, *135*, 7181–7186.
[149] S. Tang, P. Tong, H. Li, J. Tang, L. Zhang, *Biosens. Bioelectron.* **2013**, *42*, 608–611.
[150] K. Tram, P. Kanda, Y. Li, *J. Nucleic Acids* **2012**, *1*, 958683.
[151] M. Liu, Q. Zhang, Z. Li, J. Gu, J. D. Brennan, Y. Li, *Nat. Commun.* **2016**, *7*, 1–7.
[152] F. B. Dean, *Genome Res.* **2001**, *11*, 1095–1099.
[153] F. B. Dean, S. Hosono, L. Fang, X. Wu, A. F. Faruqi, P. Bray-Ward, R. S. Lasken, Z. Sun, Q. Zong, Y. Du, J. Du, M. Driscoll, W. Song, S. F. Kingsmore, M. Egholm, R. S. Lasken, *Proc. Natl. Acad. Sci.* **2002**, *99*, 5261–5266.
[154] S. Tabor, H. E. Huber, C. C. Richardson, *J. Biol. Chem.* **1987**, *262*, 16212–23.
[155] H. E. Huber, S. Tabor, C. C. Richardson, *J. Biol. Chem.* **1987**, *262*, 16224–16232.
[156] S. Kamtekar, A. J. Berman, J. Wang, J. M. Lázaro, M. de Vega, L. Blanco, M. Salas, T. . T. a. Steitz, M. Vega, L. Blanco, T. . T. a. Steitz, *Mol. Cell* **2004**, *16*, 609–618.
[157] A. J. Berman, S. Kamtekar, J. L. Goodman, J. M. Lázaro, M. de Vega, L. Blanco, M. Salas, T. A. Steitz, M. Vega, L. Blanco, T. A. Steitz, *EMBO J.* **2007**, *26*, 3494–3505.
[158] B. D. Harfe, S. Jinks-Robertson, *Annu. Rev. Genet.* **2000**, *34*, 359–399.
[159] I. V. Shevelev, U. Hübscher, *Nat. Rev. Mol. Cell Biol.* **2002**, *3*, 364–375.
[160] I. Rodríguez, J. M. Lázaro, L. Blanco, S. Kamtekar, A. J. Berman, J. Wang, M. Vega, T. a Steitz, M. Salas, M. de Vega, I. Rodriguez, J. M. Lazaro, L. Blanco, S. Kamtekar, A. J. Berman, J. Wang, T. a Steitz, M. Salas, M. de Vega, I. Rodríguez, J. M. Lázaro, L. Blanco, S. Kamtekar, A. J. Berman, J. Wang, T. a Steitz, M. Salas, M. de Vega, I. Rodriguez, J. M. Lazaro, L. Blanco, S. Kamtekar, A. J. Berman, J. Wang, T. a Steitz, M. Salas, M. de Vega, I. Rodríguez, J. M. Lázaro, L. Blanco, S. Kamtekar, A. J. Berman, J. Wang, T. a Steitz, M. Salas, M. de Vega, *Proc. Natl. Acad. Sci.* **2005**, *102*, 6407–6412.
[161] L. Blanco, M. Salas, *Nucleic Acids Res.* **1985**, *13*, 1239–1249.
[162] V. Khare, K. A. Eckert, *Mutat. Res. Mol. Mech. Mutagen.* **2002**, *510*, 45–54.
[163] B. Joffroy, Y. O. Uca, D. Prešern, J. P. K. Doye, T. L. Schmidt, *Nucleic Acids Res.* **2018**, *46*, 538–545.
[164] J. Björkesten, S. Patil, C. Fredolini, P. Lönn, U. Landegren, *Nucleic Acids Res.* **2020**, *48*, DOI 10.1093/nar/gkaa419.
[165] A. S. Fauci, D. M. Morens, *N. Engl. J. Med.* **2012**, *366*, 454–461.
[166] O. Lazcka, F. J. Del Campo, F. X. Muñoz, *Biosens. Bioelectron.* **2007**, *22*, 1205–1217.
[167] M. Mascini, S. Tombelli, *Biomarkers* **2008**, *13*, 637–657.
[168] K. S. McKeating, A. Aubé, J. F. Masson, *Analyst* **2016**, *141*, 429–449.
[169] M. U. Ahmed, I. Saaem, P. C. Wu, A. S. Brown, *Crit. Rev. Biotechnol.* **2014**, *34*, 180–196.
[170] A. P. Dhawan, in *IEEE J. Transl. Eng. Heal. Med.*, Institute Of Electrical And Electronics Engineers Inc., **2016**.
[171] S. R. Corrie, J. W. Coffey, J. Islam, K. A. Markey, M. A. F. Kendall, *Analyst* **2015**, *140*, 4350–4364.
[172] T. Murakami, J. Sumaoka, M. Komiyama, *Nucleic Acids Res.* **2009**, *37*, DOI 10.1093/nar/gkn1014.
[173] X. Y. Li, Y. C. Du, Y. P. Zhang, D. M. Kong, *Sci. Rep.* **2017**, *7*, 1–10.
[174] W. Tian, P. Li, W. He, C. Liu, Z. Li, *Biosens. Bioelectron.* **2019**, *128*, 17–22.
[175] J. Y. Marciniak, A. C. Kummel, S. C. Esener, M. J. Heller, B. T. Messmer, *Biotechniques* **2008**, *45*, 275–280.
[176] J. Zhuang, W. Lai, G. Chen, D. Tang, *Chem. Commun.* **2014**, *50*, 2935–2938.
[177] Q. Li, F. Zeng, N. Lyu, J. Liang, *Analyst* **2018**, *143*, 2304–2309.
[178] H. Xu, Y. Zhang, S. Zhang, M. Sun, W. Li, Y. Jiang, Z. S. Wu, *Anal. Chim. Acta* **2019**, *1047*, 172–178.
[179] H. Xu, D. Wu, Y. Zhang, H. Shi, C. Ouyang, F. Li, L. Jia, S. Yu, Z. S. Wu, *Sensors Actuators, B Chem.* **2018**, *258*, 470–477.
[180] D. Y. Zhang, W. Zhang, X. Li, Y. Konomi, *Detection of Rare DNA Targets by Isothermal Ramification Amplification*, **n.d.**
[181] X. Zhu, H. Xu, H. Zheng, G. Yang, Z. Lin, B. Qiu, L. Guo, Y. Chi, G. Chen, L. Guo, Y. Chi, G. Chen, *Chem. Commun.* **2013**, *49*, 10115–10117.
[182] Y. Zhang, L. Yang, C. Lin, L. Guo, B. Qiu, Z. Lin, G. Chen, *Anal. Methods* **2015**, *7*, 6109–6113.
[183] F. Wu, W. Liu, S. Yang, Q. Yao, Y. Chen, X. Weng, X. Zhou, *J. Photochem. Photobiol. A Chem.* **2018**, *355*, 114–119.
[184] X. Miao, Z. Zhu, H. Jia, C. Lu, X. Liu, D. Mao, G. Chen, *Sensors Actuators, B Chem.* **2020**, *320*, 128435.
[185] Q. Wang, H. Zheng, X. Gao, Z. Lin, G. Chen, *Chem. Commun.* **2013**, *49*, 11418–11420.
[186] X. Zhu, C. Feng, B. Zhang, H. Tong, T. Gao, G. Li, *Analyst* **2015**, *140*, 74–78.
[187] C. Feng, X. Mao, H. Shi, B. Bo, X. Chen, T. Chen, X. Zhu, G. Li, *Anal. Chem.* **2017**, *89*, 6631–6636.
[188] C. Feng, B. Bo, X. Mao, H. Shi, X. Zhu, G. Li, *Theranostics* **2017**, *7*, DOI 10.7150/thno.16671.
[189] F. Wang, C. H. Lu, X. Liu, L. Freage, I. Willner, *Anal. Chem.* **2014**, *86*, 1614–1621.
[190] H. Fujita, Y. Kataoka, S. Tobita, M. Kuwahara, N. Sugimoto, *Anal. Chem.* **2016**, *88*, 7137–7144.
[191] J. Wang, Y. Wang, S. Liu, H. Wang, X. Zhang, X. Song, J. Yu, J. Huang, *Analyst* **2019**, *144*, 3389–3397.
[192] M. Liu, Q. Yin, E. M. McConnell, Y. Chang, J. D. Brennan, Y. Li, *Chem. – A Eur. J.* **2018**, *24*, 4473–4479.
[193] Y. Gu, T. T. Zhang, Z. F. Huang, S. W. Hu, W. Zhao, J. J. Xu, H. Y. Chen, *Chem. Sci.* **2018**, *9*, 3517–3522.
[194] W. Cai, S. Xie, J. Zhang, D. Tang, Y. Tang, *Biosens. Bioelectron.* **2018**, *117*, 312–318.
[195] Y. Li, R. R. Breaker, *J. Am. Chem. Soc.* **1999**, *121*, 5364–5372.
[196] T. Konry, I. Smolina, J. M. Yarmush, D. Irimia, M. L. Yarmush, *Small* **2011**, *7*, 395–400.
[197] C. Carrasquilla, J. R. L. Little, Y. Li, J. D. Brennan, *Chem. - A Eur. J.* **2015**, *21*, 7369–7373.
[198] M. Liu, Q. Zhang, B. Kannan, G. A. Botton, J. Yang, L. Soleymani, J. D. Brennan, Y. Li, *Angew. Chemie - Int. Ed.* **2018**, *57*, 12440–12443.
[199] W. Zhao, C. H. Cui, S. Bose, D. Guo, C. Shen, W. P. Wong, K. Halvorsen, O. C. Farokhzad, G. S. L. Teo, J. A. Phillips, D. M. Dorfman, R. Karnik, J. M. Karp, *Proc. Natl. Acad. Sci. U. S. A.* **2012**, *109*, 19626–19631.
[200] J. Li, L. Lin, J. Yu, S. Zhai, G. Liu, L. Tian, *ACS Appl. Bio Mater.* **2019**, *2*, 4106–4120.
[201] H. Gu, L. Hao, N. Duan, S. Wu, Y. Xia, X. Ma, Z. Wang, *Microchim. Acta* **2017**, *184*, 2893–2899.
[202] S. Li, Y. Jiang, X. Yang, M. Lin, H. Dan, S. Zou, X. Cao, *Anal. Chim. Acta* **2021**, *1150*, DOI 10.1016/j.aca.2021.338229.
[203] G. Zhu, R. Hu, Z. Zhao, Z. Chen, X. Zhang, W. Tan, *J. Am. Chem. Soc.* **2013**, *135*, 16438–16445.
[204] E. Petryayeva, W. R. Algar, *RSC Adv.* **2015**, *5*, 22256–22282.
[205] X. Huang, D. Xu, J. Chen, J. Liu, Y. Li, J. Song, X. Ma, J. Guo, *Analyst* **2018**, *143*, 5339–5351.
[206] M. Mayer, A. J. Baeumner, *Chem. Rev.* **2019**, *119*, 7996–8027.
[207] C. Feng, X. Mao, Y. Yang, X. Zhu, Y. Yin, G. Li, *J. Electroanal. Chem.* **2016**, *781*, 223–232.
[208] R. Lorenzo-Gómez, N. Fernández-Alonso, R. Miranda-Castro, N. de-los-Santos-Álvarez, M. J. Lobo-Castañón, *Talanta* **2019**, *197*, 406–412.
[209] H. Chen, Y. Hou, F. Qi, J. Zhang, K. Koh, Z. Shen, G. Li, *Biosens. Bioelectron.* **2014**, *61*, 83–87.

[210] P. He, W. Qiao, L. Liu, S. Zhang, *Chem. Commun.* **2014**, *50*, 10718–10721.
[211] X. Li, L. Wang, C. Li, *Chem. - A Eur. J.* **2015**, *21*, 6817–6822.
[212] F. Gao, L. Du, D. Tang, Y. Lu, Y. Zhang, L. Zhang, *Biosens. Bioelectron.* **2015**, *66*, 423–430.
[213] L. Yao, Y. Ye, J. Teng, F. Xue, D. Pan, B. Li, W. Chen, *Anal. Chem.* **2017**, *89*, 9775–9780.
[214] X. Zhang, J. Chen, H. Liu, S. Zhang, *Biosens. Bioelectron.* **2015**, *65*, 341–345.
[215] W. Sun, W. Song, X. Guo, Z. Wang, *Anal. Chim. Acta* **2017**, *978*, 42–47.
[216] A. J. Berdis, *Chem. Rev.* **2009**, *109*, 2862–2879.
[217] S. V. Hamidi, J. Perreault, *Talanta* **2019**, *201*, 419–425.
[218] K. Tram, P. Kanda, B. J. Salena, S. Huan, Y. Li, *Angew. Chemie - Int. Ed.* **2014**, *53*, 12799–12802.
[219] M. M. Ali, M. Wolfe, K. Tram, J. Gu, C. D. M. Filipe, Y. Li, J. D. Brennan, *Angew. Chemie - Int. Ed.* **2019**, *58*, 9907–9911.
[220] S. V. Hamidi, H. Ghourchian, *Biosens. Bioelectron.* **2015**, *72*, 121–126.
[221] Q. Ma, P. Li, Z. Gao, S. F. Yau Li, *Sensors Actuators, B Chem.* **2019**, *281*, 424–431.
[222] L. Linck, E. Reiß, F. Bier, U. Resch-Genger, *Anal. Methods* **2012**, *4*, 1215–1220.
[223] X. J. Yang, K. Zhang, J. J. Xu, H. Y. Chen, *Anal. Chem.* **2018**, *90*, 6199–6205.
[224] L. Hao, W. Wang, X. Shen, S. Wang, Q. Li, F. An, S. Wu, *J. Agric. Food Chem.* **2020**, *68*, 369–375.
[225] A. N. Glazer, H. S. Rye, *Nature* **1992**, *359*, 859–861.
[226] A. S. Biebricher, I. Heller, R. F. H. Roijmans, T. P. Hoekstra, E. J. G. Peterman, G. J. L. Wuite, *Nat. Commun.* **2015**, *6*, DOI 10.1038/ncomms8304.
[227] C. Hong, X. Zhang, S. Ye, H. Yang, Z. Huang, D. Yang, R. Cai, W. Tan, *ACS Appl. Mater. Interfaces* **2021**, *13*, 19695–19700.
[228] S. Jiang, M. Liu, W. Tantai, Q. Xu, X. Zou, F. Ma, C. Y. Zhang, *Chem. Commun.* **2021**, *57*, 2041–2044.
[229] N. O. Fischer, T. M. Tarasow, J. B. H. H. Tok, *Anal. Biochem.* **2008**, *373*, 121–128.
[230] M. Wang, I. Dilek, B. A. Armitage, *Langmuir* **2003**, *19*, 6449–6455.
[231] J. O. Smith, D. A. Olson, B. A. Armitage, *J. Am. Chem. Soc.* **1999**, *121*, 2686–2695.
[232] V. V. Demidov, V. N. Potaman, M. D. Frank-Kamenetskil, M. Egholm, O. Buchard, S. H. Sönnichsen, P. E. Nlelsen, *Biochem. Pharmacol.* **1994**, *48*, 1310–1313.
[233] T. Y. Kim, M. C. Lim, M. A. Woo, B. H. Jun, *Nanomaterials* **2018**, *8*, 1–13.
[234] H. Jans, Q. Huo, *Chem. Soc. Rev.* **2012**, *41*, 2849–2866.
[235] W. Zhou, X. Gao, D. Liu, X. Chen, *Chem. Rev.* **2015**, *115*, 10575–10636.
[236] W. Zhao, M. A. Brook, Y. Li, *ChemBioChem* **2008**, *9*, 2363–2371.
[237] E. Boisselier, D. Astruc, *Chem. Soc. Rev.* **2009**, *38*, 1759–1782.
[238] R. Elghanian, J. J. Storhoff, R. C. Mucic, R. L. Letsinger, C. A. Mirkin, *Science (80-.).* **1997**, *277*, 1078–1081.
[239] M. M. Ali, S. D. Aguirre, Y. Xu, C. D. M. M. Filipe, R. Pelton, Y. Li, *Chem. Commun.* **2009**, 6640–6642.
[240] C. Hong, A. Baek, S. S. Hah, W. Jung, D. E. Kim, *Anal. Chem.* **2016**, *88*, 2999–3003.
[241] K. Liang, H. Wang, P. Li, Y. Zhu, J. Liu, B. Tang, *Talanta* **2020**, *207*, 120285.
[242] X. Sun, Y. Wang, L. Zhang, S. Liu, M. Zhang, J. Wang, B. Ning, Y. Peng, J. He, Y. Hu, Z. Gao, *Anal. Chem.* **2020**, *92*, 3032–3041.
[243] Y. Zhang, L. Chen, K. Hsieh, T. H. Wang, *Anal. Chem.* **2018**, *90*, 12180–12186.
[244] C. Larsson, I. Grundberg, O. Söderberg, M. Nilsson, *Nat. Methods* **2010**, *7*, 395–397.
[245] L. Yao, Y. Chen, J. Teng, W. Zheng, J. Wu, S. B. Adeloju, D. Pan, W. Chen, D. Pan, W. Chen, *Biosens. Bioelectron.* **2015**, *74*, 534–538.
[246] Y. Jiang, Z. Qiu, T. Le, S. Zou, X. Cao, *Anal. Chim. Acta* **2020**, *1127*, 79–88.
[247] D. Zhu, Y. Yan, P. Lei, B. Shen, W. Cheng, H. Ju, S. Ding, *Anal. Chim. Acta* **2014**, *846*, 44–50.
[248] S. Tyagi, F. R. Kramer, *Nat. Publ. Gr.* **1996**, *14*, 303–308.
[249] Z.-S. Wu, S. Zhang, H. Zhou, G.-L. Shen, R. Yu, *Anal. Chem.* **2010**, *82*, 2221–2227.
[250] J. Wang, H. yan H. ya. H. yan Dong, Y. Zhou, L. yu L. y. Han, T. Zhang, M. Lin, C. Wang, H. Xu, Z. S. Wu, L. Jia, C. Wang, H. Xu, Z. S. Wu, L. Jia, *Biosens. Bioelectron.* **2018**, *122*, 239–246.
[251] N. Li, L. Yi, Z. He, W. Zhang, H. Li, J. M. Lin, *Analyst* **2017**, *142*, 634–640.
[252] T. Gao, B. Wang, L. Shi, X. Zhu, Y. Xiang, J. I. Anzai, G. Li, *Anal. Chem.* **2017**, *89*, 10776–10782.
[253] J. Bai, Z. Gao, W. Wang, Y. Peng, J. Wu, M. Zhang, Q. Li, Z. Zhao, M. Liu, J. Wang, G. Cao, J. Bai, Z. Gao, W. Wang, Y. Peng, J. Wu, M. Zhang, Q. Li, Z. Zhao, M. Liu, J. Wang, G. Cao, *Anal. Chem.* **2021**, *93*, 4488–4496.
[254] M. Nilsson, M. Gullberg, F. Dahl, K. Szuhai, A. K. Raap, *Nucleic Acids Res.* **2002**, *30*, 66e – 66.
[255] L. Lv, L. Guo, Q. Zhao, *Anal. Methods* **2015**, *7*, 1855–1859.
[256] Z. Zhan, H. Li, J. Liu, G. Xie, F. Xiao, X. Wu, Z. P. Aguilar, H. Xu, *Food Control* **2020**, *107*, 106806.
[257] S. Wu, Q. Yu, C. He, N. Duan, *Spectrochim. Acta - Part A Mol. Biomol. Spectrosc.* **2020**, *224*, 117387.
[258] Z. W. Wu, X. C. Xie, H. R. Guo, H. Xia, K. J. Huang, *Anal. Bioanal. Chem.* **2020**, *412*, 915–922.
[259] C. Ge, R. Yuan, L. Yi, J. Yang, H. Zhang, L. Li, G. Yi, W. Nian, G. Yi, *J. Electroanal. Chem.* **2018**, *826*, 174–180.
[260] S. Ciftci, R. Cánovas, F. Neumann, T. Paulraj, M. Nilsson, G. A. Crespo, N. Madaboosi, *Biosens. Bioelectron.* **2020**, *151*, DOI 10.1016/j.bios.2019.112002.
[261] D. Tang, B. Xia, Y. Tang, J. Zhang, Q. Zhou, *Microchim. Acta* **2019**, *186*, DOI 10.1007/s00604-019-3454-1.
[262] Y. Jia, F. Sun, N. Na, J. Ouyang, *Anal. Chim. Acta* **2019**, *1060*, 64–70.
[263] F. Sun, X. Sun, Y. Jia, Z. Hu, S. Xu, L. Li, N. Na, J. Ouyang, *Analyst* **2019**, *144*, 6019–6024.
[264] L. Ge, B. Li, H. Xu, W. Pu, H. F. Kwok, *Biosens. Bioelectron.* **2019**, *132*, 210–216.
[265] L. Huang, D. B. Wang, N. Singh, F. Yang, N. Gu, X. E. Zhang, *Nanoscale* **2018**, *10*, 20289–20295.
[266] T. Fan, Y. Du, Y. Yao, J. Wu, S. Meng, J. Luo, F. Gao, X. Zhang, D. Yang, C. Wang, Y. Qian, F. Gao, *Sensors Actuators, B Chem.* **2018**, *266*, 9–18.
[267] G. Yao, H. Pei, J. Li, Y. Zhao, D. Zhu, Y. Zhang, Y. Lin, Q. Huang, C. Fan, *NPG Asia Mater.* **2015**, *7*, e159.
[268] B. T. Roembke, S. Nakayama, H. O. Sintim, *Methods* **2013**, *64*, 185–198.
[269] D. Sen, W. Gilbert, *Nature* **1988**, *334*, 364–366.
[270] B. R. Vummidi, J. Alzeer, N. W. Luedtke, *ChemBioChem* **2013**, *14*, 540–558.
[271] P. Chilka, N. Desai, B. Datta, *Molecules* **2019**, *24*, 752.
[272] Y. Guo, W. Yao, Y. Xie, X. Zhou, J. Hu, R. Pei, *Microchim. Acta* **2016**, *183*, 21–34.
[273] H. X. Jiang, Z. Z. Liang, Y. H. Ma, D. M. Kong, Z. Y. Hong, *Anal. Chim. Acta* **2016**, *943*, 114–122.
[274] X. Y. Li, Y. C. Du, Y. P. Zhang, D. M. Kong, *Sci. Rep.* **2017**, *7*, 6263.
[275] X. Xu, H. Wei, W. Jiang, *Analyst* **2017**, *142*, 2247–2252.
[276] I. J. Lee, N. I. Goo, D. E. Kim, *Analyst* **2016**, *141*, 6503–6506.
[277] W. Li, W. Jiang, L. Wang, *Anal. Chim. Acta* **2016**, *940*, 1–7.
[278] X. Zheng, L. Niu, D. Wei, X. Li, S. Zhang, *Sci. Rep.* **2016**, *6*, 2–7.
[279] W. Li, L. Wang, Y. Wang, W. Jiang, *Talanta* **2018**, *189*, 383–388.
[280] X. Li, J. Song, Q. W. Xue, F. H. You, X. Lu, Y. C. Kong, S. Y. Ma, W. Jiang, C. Z. Li, *Nanomaterials* **2016**, *6*, 1–10.
[281] F. Yang, X. Li, J. Li, Y. Xiang, R. Yuan, *Talanta* **2019**, *204*, 812–816.
[282] J. Li, F. Yang, B. Jiang, W. Zhou, Y. Xiang, R. Yuan, *Analyst* **2020**, DOI 10.1039/d0an01491e.
[283] J. Teng, Y. Ye, L. Yao, C. Yan, K. Cheng, F. Xue, D. Pan, B. Li, W. Chen, *Microchim. Acta* **2017**, *184*, 3477–3485.
[284] J. Lv, S. Xie, W. Cai, J. Zhang, D. Tang, Y. Tang, *Analyst* **2017**, *142*, 4708–4714.
[285] C. Y. Lee, H. T. Fan, Y. Z. Hsieh, *Sensors Actuators, B Chem.* **2018**, *255*, 341–347.

[286] T. Liu, D. Sun, M. Gu, X. Wu, G. L. Wang, *Sensors Actuators, B Chem.* **2020**, *317*, 128210.
[287] M. Gu, D. Sun, T. Liu, X. Wu, G. L. Wang, *Sensors Actuators, B Chem.* **2020**, *324*, 128660.
[288] R. Cai, S. Zhang, L. Chen, M. Li, Y. Zhang, N. Zhou, *ACS Appl. Mater. Interfaces* **2021**, *13*, 4905–4914.
[289] W. Jiang, L. Liu, L. Zhang, Q. Guo, Y. Cui, M. Yang, *Microchim. Acta* **2017**, *184*, 4757–4763.
[290] W. Xiang, G. Wang, S. Cao, Q. Wang, X. Xiao, T. Li, M. Yang, *Microchim. Acta* **2018**, *185*, DOI 10.1007/s00604-018-2867-6.
[291] C. Shen, S. Liu, X. Li, M. Yang, *Anal. Chem.* **2019**, *91*, 11614–11619.
[292] C. Shen, S. Liu, X. Li, D. Zhao, M. Yang, *Microchim. Acta* **2018**, *185*, DOI 10.1007/s00604-018-3086-x.
[293] Q. Wang, B. Jiang, J. Xie, Y. Xiang, R. Yuan, Y. Chai, *Analyst* **2013**, *138*, 5751–5756.
[294] P. Miao, L. Ning, X. Li, P. Li, G. Li, *Bioconjug. Chem.* **2012**, *23*, 141–145.
[295] X. Cheng, X. Liu, T. Bing, Z. Cao, D. Shangguan, *Biochemistry* **2009**, *48*, 7817–7823.
[296] J. Kosman, B. Juskowiak, *Anal. Chim. Acta* **2011**, *707*, 7–17.
[297] S. Bi, Y. Cui, Y. Dong, N. Zhang, *Biosens. Bioelectron.* **2014**, *53*, 207–213.
[298] J. W. Lim, T. Y. Kim, S. W. Choi, M. A. Woo, *Food Chem.* **2019**, *300*, 125177.
[299] J. W. Lim, T. Y. Kim, M. C. Lim, S. W. Choi, M. A. Woo, *Biochip J.* **2020**, *14*, 169–178.
[300] S. Song, X. Wang, K. Xu, G. Xia, X. Yang, *J. Agric. Food Chem.* **2019**, *67*, 1244–1253.
[301] E. Santovito, D. Greco, V. D'Ascanio, S. M. Sanzani, G. Avantaggiato, *Anal. Chim. Acta* **2020**, *1133*, 20–29.
[302] P. Yan, Y. Hao, Z. Shu, C. Gu, X. Zhou, X. Liu, H. Xiang, *Microchim. Acta* **2018**, *185*, DOI 10.1007/s00604-018-2839-x.
[303] Y. Guo, Y. Wang, S. Liu, J. Yu, H. Wang, Y. Wang, J. Huang, *Biosens. Bioelectron.* **2016**, *75*, 315–319.
[304] R. Huang, L. He, Y. Xia, H. Xu, C. Liu, H. Xie, S. Wang, L. Peng, Y. Y. Y. Liu, Y. Y. Y. Liu, N. He, Z. Li, S. Wang, L. Peng, Y. Y. Y. Liu, Y. Y. Y. Liu, N. He, Z. Li, S. Wang, L. Peng, Y. Y. Y. Liu, Y. Y. Y. Liu, N. He, Z. Li, *Small* **2019**, *15*, 1–7.
[305] S. K. Li, A. Y. Chen, Y. Q. Chai, R. Yuan, Y. Zhuo, *Electrochim. Acta* **2016**, *212*, 767–774.
[306] F. Li, H. Zhang, Z. Wang, A. M. Newbigging, M. S. Reid, X.-F. Li, X. C. Le, *Anal. Chem.* **2014**, *87*, 274–292.
[307] H. Zhang, F. Li, B. Dever, X. F. Li, X. C. Le, *Chem. Rev.* **2013**, *113*, 2812–2841.
[308] M. Liu, D. Chang, Y. Li, *Acc. Chem. Res.* **2017**, *50*, 2273–2283.
[309] D. Morrison, M. Rothenbroker, Y. Li, D. Morrison, M. Rothenbroker, Y. Li, **2018**, DOI 10.1002/smtd.201700319.
[310] Y. Sun, Y. Chang, Q. Zhang, M. Liu, *Micromachines* **2019**, *10*, 531.
[311] J. Li, F. Yang, B. Jiang, W. Zhou, Y. Xiang, R. Yuan, *Analyst* **2020**, *145*, 7858–7863.
[312] R. M. Bialy, M. M. Ali, Y. Li, J. D. Brennan, *Chem. – A Eur. J.* **2020**, *26*, 5085–5092.
[313] L. Tang, Y. Liu, M. M. Ali, D. K. Kang, W. Zhao, J. Li, *Anal. Chem.* **2012**, *84*, 4711–4717.
[314] K. Abnous, N. M. Danesh, M. Ramezani, M. Alibolandi, M. A. Nameghi, T. S. Zavvar, S. M. Taghdisi, *Anal. Chim. Acta* **2021**, *1165*, 338549.
[315] L. Xu, Q. Dai, Z. Shi, X. Liu, L. Gao, Z. Wang, X. Zhu, Z. Li, *J. Microbiol. Methods* **2020**, *173*, 105917.
[316] D. Gou, G. Xie, Y. Li, X. Zhang, H. Chen, *Microchim. Acta* **2018**, *185*, DOI 10.1007/s00604-018-2972-6.
[317] K. Abnous, N. M. Danesh, M. Ramezani, M. Alibolandi, M. A. Nameghi, T. S. Zavvar, S. M. Taghdisi, *Anal. Chim. Acta* **2021**, *1165*, 338549.
[318] S. Lv, K. Zhang, D. Tang, *Analyst* **2019**, *144*, 3716–3720.
[319] S. M. Russell, R. De La Rica, *ACS Sensors* **2018**, *3*, 1059–1068.
[320] N. Convery, N. Gadegaard, *Micro Nano Eng.* **2019**, *2*, 76–91.
[321] S. Feng, S. Mao, J. Dou, W. Li, H. Li, J. M. Lin, *Chem. Sci.* **2019**, *10*, 8571–8576.
[322] L. He, Z. Shen, J. Wang, J. Zeng, W. Wang, H. Wu, Q. Wang, N. Gan, *Microchim. Acta* **2020**, *187*, 176.
[323] L. He, Z. Shen, Y. Cao, T. Li, D. Wu, Y. Dong, N. Gan, *Analyst* **2019**, *144*, 2755–2764.
[324] L. Lv, L. Guo, Q. Zhao, *Anal. Methods* **2015**, *7*, 1855–1859.
[325] L. Guo, L. Hao, Q. Zhao, *Anal. Bioanal. Chem.* **2016**, *408*, 4715–4722.
[326] Y. Li, W. Dai, X. Lv, Y. Deng, *Anal. Methods* **2018**, *10*, 1767–1773.
[327] W. Zhang, Z. He, L. Yi, S. Mao, H. Li, J. M. Lin, *Biosens. Bioelectron.* **2018**, *102*, 652–660.
[328] S. Feng, S. Mao, J. Dou, W. Li, H. Li, J. M. Lin, *Chem. Sci.* **2019**, *10*, 8571–8576.
[329] J. Credou, T. Berthelot, *J. Mater. Chem. B* **2014**, *2*, 4767–4788.
[330] S. Jahanshahi-Anbuhi, K. Pennings, V. Leung, M. Liu, C. Carrasquilla, B. Kannan, Y. Li, R. Pelton, J. D. Brennan, C. D. M. Filipe, *Angew. Chemie Int. Ed.* **2014**, *53*, 6155–6158.
[331] B. Kannan, S. Jahanshahi-Anbuhi, R. H. Pelton, Y. Li, C. D. M. Filipe, J. D. Brennan, *Anal. Chem.* **2015**, *87*, 9288–9293.
[332] S. Jahanshahi-Anbuhi, B. Kannan, V. Leung, K. Pennings, M. Liu, C. Carrasquilla, D. White, Y. Li, R. H. Pelton, J. D. Brennan, C. D. M. Filipe, *Chem. Sci.* **2016**, *7*, 2342–2346.
[333] M. M. Ali, C. L. Brown, S. Jahanshahi-Anbuhi, B. Kannan, Y. Li, C. D. M. Filipe, J. D. Brennan, *Sci. Rep.* **2017**, *7*, 1–10.
[334] M. Liu, J. Wang, Y. Chang, Q. Zhang, D. Chang, C. Y. Hui, J. D. Brennan, Y. Li, *Angew. Chemie - Int. Ed.* **2020**, *59*, 7706–7710.
[335] W. Chiuman, Y. Li, *PLoS One* **2007**, *2*, 1224.
[336] Y. Li, D. Sen, *Nat. Struct. Biol.* **1996**, *3*, 743–747.
[337] P. Travascio, P. K. Witting, A. G. Mauk, D. Sen, *J. Am. Chem. Soc.* **2001**, *123*, 1337–1348.
[338] Z. Cheglakov, Y. Weizmann, B. Basnar, I. Willner, *Org. Biomol. Chem.* **2007**, *5*, 223–225.
[339] Y. Tian, Y. He, C. Mao, *Chembiochem* **2006**, *7*, 1862–4.
[340] M. Yao, X. Lv, Y. Deng, M. Rasheed, *Anal. Chim. Acta* **2019**, *1055*, 115–125.
[341] A. R. Pavankumar, A. Engström, J. Liu, D. Herthnek, M. Nilsson, *Anal. Chem.* **2016**, *88*, 4277–4284.
[342] Y. Sun, Y. Chang, Q. Zhang, M. Liu, *Micromachines* **2019**, *10*, 531.
[343] E. Paleček, M. Bartošík, *Chem. Rev.* **2012**, *112*, 3427–3481.
[344] E. Paleček, F. Jelen, *Crit. Rev. Anal. Chem.* **2002**, *32*, 261–270.
[345] A. M. Chiorcea-Paquim, R. Eritja, A. M. Oliveira-Brett, *J. Nucleic Acids* **2018**, *2018*, DOI 10.1155/2018/5307106.
[346] T. Goda, M. Tabata, Y. Miyahara, *Front. Bioeng. Biotechnol.* **2015**, *3*, 29.
[347] J. Shen, H. Wang, C. Li, Y. Zhao, X. Yu, X. Luo, *Biosens. Bioelectron.* **2017**, *90*, 356–362.
[348] D. Sun, J. Lu, Z. Luo, L. Zhang, P. Liu, Z. Chen, **2018**, DOI 10.1016/j.bios.2018.08.002.
[349] Y. Zhu, H. Wang, L. Wang, J. Zhu, W. Jiang, *ACS Appl. Mater. Interfaces* **2016**, *8*, 2573–2581.
[350] R. A. Marcus, *Annu. Rev. Phys. Chem.* **1964**, *15*, 155–196.
[351] D. I. Li, S. Song, C. Fan, **2010**, DOI 10.1021/ar900245u.
[352] K. Deng, C. Li, H. Huang, X. Li, *Sensors Actuators, B Chem.* **2017**, *238*, 1302–1308.
[353] S. Lv, K. Zhang, Q. Zhou, D. Tang, *Sensors Actuators, B Chem.* **2020**, *310*, 127874.
[354] S. Xie, J. Zhang, L. Teng, W. Yuan, Y. Tang, Q. Peng, Q. Tang, *Sensors Actuators, B Chem.* **2019**, *301*, 127072.
[355] M. J. Li, H. J. Wang, R. Yuan, Y. Q. Chai, *Chem. Commun.* **2019**, *55*, 10772–10775.
[356] X. Liao, C. Zhang, Z. Shi, H. Shi, Y. Qian, F. Gao, *J. Electroanal. Chem.* **2020**, *878*, 114604.
[357] Y. Peng, L. Li, X. Yi, L. Guo, *Biosens. Bioelectron.* **2014**, *59*, 314–320.
[358] B. Shen, J. Li, W. Cheng, Y. Yan, R. Tang, Y. Li, H. Ju, S. Ding, *Microchim. Acta* **2015**, *182*, 361–367.
[359] Y. H. Pang, L. L. Guo, X. F. Shen, N. C. Yang, C. Yang, *Electrochim. Acta* **2020**, *341*, 136055.
[360] J. Tang, J. Li, P. Xiong, Y. Sun, Z. Zeng, X. Tian, D. Tang,

Microchim. Acta **2020**, *187*, DOI 10.1007/s00604-020-04434-0.
[361] M. Qing, Y. Yuan, W. Cai, S. Xie, Y. Tang, R. Yuan, J. Zhang, *Sensors Actuators B* **2018**, *263*, 469–475.
[362] L. Y. Yao, X. Q. Yu, Y. J. Zhao, A. P. Fan, *Anal. Methods* **2015**, *7*, 8786–8792.
[363] J. Zhang, J. Shi, H. Zhang, Y. Zhu, W. Liu, K. Zhang, Z. Zhang, *J. Extracell. Vesicles* **2020**, *10*, DOI 10.1002/jev2.12025.
[364] K. Zhang, S. Lv, M. Lu, D. Tang, *Biosens. Bioelectron.* **2018**, *117*, 590–596.
[365] H. Pei, F. Li, Y. Wan, M. Wei, H. Liu, Y. Su, N. Chen, Q. Huang, C. Fan, *J. Am. Chem. Soc.* **2012**, *134*, 11876–11879.
[366] D. Zhu, P. Song, J. Shen, S. Su, J. Chao, A. Aldalbahi, Z. Zhou, S. Song, C. Fan, X. Zuo, Y. Tian, L. Wang, H. Pei, *Anal. Chem.* **2016**, *88*, 4949–4954.
[367] A. Bagheri Hashkavayi, B. S. Cha, S. H. Hwang, J. Kim, K. S. Park, *Sensors Actuators, B Chem.* **2021**, *343*, 130087.
[368] Y. Guo, X. Sun, G. Yang, J. Liu, *Chem. Commun.* **2014**, *50*, 7659–7662.
[369] S. M. Taghdisi, N. M. Danesh, M. Ramezani, M. Alibolandi, M. A. Nameghi, G. Gerayelou, K. Abnous, *Talanta* **2021**, *223*, 121705.
[370] X. Yi, L. Li, Y. Peng, L. Guo, *Biosens. Bioelectron.* **2014**, *57*, 103–109.
[371] M. Y. Lin, W. Y. Hsu, Y. S. Yang, J. W. Huang, Y. L. Chung, H. Chen, *Anal. Bioanal. Chem.* **2016**, *408*, 4785–4797.
[372] Y. Guo, X. Sun, G. Yang, J. Liu, *Chem. Commun.* **2014**, *50*, 7659–7662.
[373] J. Tang, J. Li, P. Xiong, Y. Sun, Z. Zeng, X. Tian, D. Tang, *Microchim. Acta* **2020**, *187*, 450.
[374] D. Gou, G. Xie, Y. Li, X. Zhang, H. Chen, *Microchim. Acta* **2018**, *185*, 436.
[375] J. Wang, *TrAC - Trends Anal. Chem.* **2002**, *21*, 226–232.
[376] A. Chen, S. Yang, *Biosens. Bioelectron.* **2015**, *71*, 230–242.
[377] A. Leaf, *J. Am. Med. Assoc.* **1993**, *269*, 616.
[378] A. P. Dhawan, W. J. Heetderks, M. Pavel, S. Acharya, M. Akay, A. Mairal, B. Wheeler, C. C. Dacso, T. Sunder, N. Lovell, M. Gerber, M. Shah, S. G. Senthilvel, M. D. Wang, B. Bhargava, *IEEE J. Transl. Eng. Heal. Med.* **2015**, *3*, 1–10.
[379] D. A. Giljohann, C. A. Mirkin, *Nature* **2009**, *462*, 461–464.
[380] C. P. Price, *BMJ* **2001**, *322*, 1285–8.
[381] C. P. Price, *Clin. Chem. Lab. Med.* **2002**, *40*, 246–251.
[382] B. Udugama, P. Kadhiresan, W. C. W. Chan, *Proc. Natl. Acad. Sci. U. S. A.* **2020**, *117*, 4632–4641.
[383] S. Miyamoto, S. Sano, K. Takahashi, T. Jikihara, *Anal. Biochem.* **2015**, *473*, 28–33.
[384] S. Roy, N. F. Mohd-Naim, M. Safavieh, M. U. Ahmed, *ACS Sensors* **2017**, *2*, 1713–1720.

CHAPTER 3 | EXPERIMENTAL

3.1. Materials.

DNA Oligonucleotides. All DNA oligonucleotides were obtained from Integrated DNA Technologies (IDT; Coralville, IA). All sequences are shown in Table 3.1. The 28-nt substrate strand (FS28) contains a chimeric riboadenosine nucleotide (rA) that is positioned between a fluorescein-dT (F) and dabacyl-dT(Q). All sequences were purified by 10% dPAGE (8 M urea) before use. Concentrations of all purified oligonucleotides were confirmed spectroscopically.

Enzymes and chemicals. T4 polynucleotide kinase (PNK; with 10× reaction buffer A), T4 DNA ligase (with 10× T4 DNA ligase buffer), phi29 DNA polymerase (with 10× phi29 DNA polymerase buffer), FastDigest Taq1, deoxyribonucleaoside 5'triphosphate mixture (dNTPs), polyethylene glycol (PEG) 4000, adenosine 5'-triphosphate (ATP) solution, 10 000× SYBR Gold DNA stain, and GeneRuler™ 1 kb Plus DNA ladder were all purchased from Thermo Fisher (USA). All other reagents were purchased from Bioshop Canada or from Sigma-Aldrich without further purification, analytical grade, and used as directed. Water was purified with a Milli-Q Synthesis A10 water purification system and subsequently autoclaved.

3.2 Bacterial Strains and Growth Conditions

Bacterial cells. Helicobacter pylori (J99) (HP), *Escherichia coli* O157:H7 (EC), *Clostridium difficile* (CD), *Bacillus subtilis* (BS), *Listeria monocytogenes* (LM), and *Salmonella serovar typhimurium* (ST) are routinely maintained in our lab (originally from ATCC). Bacteria for selectivity assays were prepared in the original work[1] and stored at -20 °C until used.

Preparation of Crude Extracellular Mixtures (CEMs). H. pylori CEMs were prepared as follows. Individual culture tubes were used to grow the bacteria in 3 mL autoclaved tryptic soy

broth (TSB) with continuous shaking at 37 °C and 250 rpm. Where specified, 2% v/v of sheep's blood, human blood, or human serum was added at the beginning of incubation. While 2% v/v sheep's blood was used in the original procedure, we noted it was not necessary to generate a target-producing bacterial culture. After centrifugation at 11,000 g for 5 minutes at room temperature, the cells were separated from the supernatant using a 0.2 micron molecular size filter, aliquoted into microcentrifuge tubes (100 µL) and stored at -20 °C until use.

Quantification of Cell Count. H. pylori (J99) was grown in individual culture tubes in 3 mL tryptic soy broth (TSB) including 2% sheep blood with continuous shaking at 37 °C and 250 rpm. This solution was then serially diluted with TSB. The 6^{th}, 7^{th}, and 8^{th} ten-fold dilutions (100 µL) were spread in tryptic soy agar (TSA) plates, performed in triplicate. The plates were incubated at 37 °C for 18 h and the colonies were counted. From these values, the original cell concentration of the culture was determined.

3.3 DNA Modifications

DNAzyme Ligation. The substrate sequence (FS28) was first phosphorylated as follows in a total volume of 100 µL: 1 nmol linear oligonucleotide, 150 nmol adenosine 5'triphosphate, 20 U T4 polynucleotide kinase (PNK) in a 1x PNK buffer A (50 mM Tris-HCl, pH 7.6 at 25 ˚C, 10 mM $MgCl_2$, 5 mM DDT, 0.1 mM spermidine). The solution was heated at 37 °C for 45 minutes, then heated at 90 °C for 5 minutes. A ligation template oligonucleotide (1.1 nmol) and the evolved DNAzyme sequence (Dhp3t4, 1 nmol) were added to the solution, heated to 90 °C for one minute, and allowed to cool to room temperature. The phosphorylated sequences were circularized in a volume of 300 µL containing: 30 µL PEG4000, 30 U T4 DNA Ligase, in a 1x T4 DNA Ligase Buffer (400 mM Tris-HCl, 100 mM $MgCl_2$, 100 mM DDT, 5 mM ATP, pH 7.8

at 25 °C). The solution was incubated at room temperature for 2 hours. DNA circles were then purified by dPAGE and stored at -20 °C until use.

Circular DNA Ligation. Linear single stranded DNA (ssDNA) sequences were first phosphorylated as follows in a total volume of 100 μL: 1 nmol linear oligonucleotide, 150 nmol adenosine 5'triphosphate, 20 U T4 polynucleotide kinase (PNK) in a 1x PNK buffer A (50 mM Tris-HCl, pH 7.6 at 25 °C, 10 mM $MgCl_2$, 5 mM DDT, 0.1 mM spermidine). The solution was heated at 37 °C for 45 minutes, then heated at 90 °C for 5 minutes. A ligation template oligonucleotide (1.1 nmol) was added to the solution, heated to 90 °C for one minute, and allowed to cool. The phosphorylated sequences were circularized in a volume of 300 μL containing: 30 μL PEG4000, 30 U T4 DNA Ligase, in a 1x T4 DNA Ligase Buffer (400 mM Tris-HCl, 100 mM $MgCl_2$, 100 mM DDT, 5 mM ATP, pH 7.8 at 25 °C). The solution was incubated at room temperature for 2 hours. DNA circles were then ethanol precipitated, purified by dPAGE and another ethanol precipitation, and stored at -20 °C until use.

Catenane Ligation. The ssDNA sequence for $CT_{ii\text{-}R}$ was first phosphorylated and ligated as described above, and subsequently purified by dPAGE. Next, the ssDNA sequence for CT_i was phosphorylated as above and incubated at a 1:1 ratio with $CT_{ii\text{-}R}$ and a ligation template oligonucleotide. The phosphorylated sequences were circularized in a volume of 300 μL containing: 30 μL PEG4000, 30 U T4 DNA Ligase, in a 1x T4 DNA Ligase Buffer (400 mM Tris-HCl, 100 mM $MgCl_2$, 100 mM DDT, 5 mM ATP, pH 7.8 at 25 °C). The solution was incubated at room temperature for 2 hours. The resultant catenane was then ethanol precipitated, purified by dPAGE and another ethanol precipitation, and stored at -20 °C until use.

*Gel analysis***.** Agarose, dPAGE, and nPAGE gels were all visualized on a Bio-Rad Chemidoc Imaging system and quantified with using ImageLab software and ImageJ processing.

For dPAGE gels where noted, SYBR Gold staining occurred in a 200 mL 0.5x SYBR Gold solution for 15 minutes and rinsed with purified MilliQ water at least three times before imaging. For agarose gels, imaging was performed using 0.5x Gel Red gel for imaging.

3.4 Gel and Microplate-Based Assays and Analysis

Kinetic fluorescence experiments in solution, RCD-substrate. Microplate fluorescent analysis was all performed using a Tecan Spark M1000 plate reader at an excitation wavelength of 506 nm and emission wavelength of 522 nm in 96-well plates at 25 °C unless otherwise specified. Baseline fluorescence was determined by measuring fluorescence at 1-minute intervals for three minutes unless otherwise specified. All fluorescence measurements are reported as F/F_0 or $F-F_0$ for a comparison to the original work, where F is the final fluorescence intensity and F_0 is the initial fluorescent intensity prior to the addition of the amplification reaction.

DNAzyme Cleavage, cis-RCDs. 3 µL of the CEM was mixed with 5 µL of 2x SB and 1 µL (5 µM stock) of the DNAzyme and diluted to 10 µL. The reaction mixture was incubated at room temperature for 30 min unless otherwise listed. Where specified, 1 uL of PNK (10 U/µL) was added and incubated at 37 °C for 30 minutes. This reaction was quenched by adding 10 µL of 2x GLB, and then subjected to 10% dPAGE analysis.

DNAzyme Cleavage, catenane. 3 µL of the CEM was mixed with 5 µL of 2x SB, 1 µL (1 µM stock) of the DNAzyme, and 1 µL (50 µM stock) of the *trans*-DNAzyme to a final volume of 10 µL. The reaction mixture was incubated at room temperature for 30 min unless otherwise listed. Where specified, 1 uL of PNK (10 U/µL) was added and incubated at 37 °C for 30 minutes. This reaction was quenched by adding 10 µL of 2x GLB, and then subjected to 10% dPAGE analysis.

Kinetic Fluorescence Experiments, Selectivity Tests. To compare DNAzyme activity with other potential contaminant bacterial species, 10 µL of this CEM was mixed with 25 µL 2x selection buffer (SB) and diluted to 40 µL. Fluorimetric measurements were taken with the following parameters: shaken for 5 seconds prior to insertion, excitation 506 nm, emission 556 nm, reading from the bottom, gain 150, signal acquisition every minute for a 5 minute duration. After, 10 µL (1 µM stock) of the noted DNAzyme was added to the wells and monitored fluorometrically every minute for 60 minutes. This data was processed using Microsoft Excel.

RCA Reaction, Proof-of-Concept. A 20 µL solution containing 1 pmol of circularized oligonucleotide and 1 pmol of primer was heated to 90 °C for one minute and allowed to cool for 15 minutes. To this solution, 5.0 µL of 10x Buffer for phi29 DNA Polymerase, 2.5 µL dNTPs (100 mM), and 1.0 µL phi29 DNA polymerase (10 U/ µL) and diluted to a final volume of 50 µL. This was incubated at ambient room temperature for the specified time.

RCD-Substrate RCA Initiation Reaction. 3 µL of the CEM was mixed with 5 µL of 2x SB and 1 µL (5 µM stock) of the DNAzyme and diluted to 10 µL. The reaction mixture was incubated at room temperature for 30 min unless otherwise listed. Where specified, 1 uL of PNK (10 U/µL) was added and incubated at 37 °C for 30 minutes. This was added to a reaction mixture containing 1 pmol of the denoted CT, 5.0 µL of 10x Buffer for phi29 DNA Polymerase, 2.5 µL dNTPs (100 mM), and 1.0 µL phi29 DNA polymerase (10 U/ µL) and diluted to a final volume of 50 µL. Where kinetic fluorescence was monitored, this final volume had a concentration of SYBR Gold of 0.5x. This reaction incubated at ambient room temperature for the specified time.

Kinetic fluorescence experiments in solution, RCA detection with intercalating dyes. Microplate fluorescent analysis was all performed using a Tecan Spark M1000 plate reader at an

excitation wavelength of 506 nm and 522 nm for emission in 96-well plates at 25 °C unless otherwise specified. Baseline fluorescence was determined by measuring fluorescence at 1-minute intervals for three minutes unless otherwise specified. All fluorescence measurements are reported as F/F_0 where F is the final fluorescence intensity and F_0 is the initial fluorescent intensity prior to the addition of the amplification reaction.

Table 3.1. Nucleic acid sequences used in this work.

Iteration	**Label**	**Sequence (5' -> 3')**
Catenane Design	**CT_i** Template for rolling circle amplification. CT_i is produced via circularization using CT_i-LT as the template.	
	Linear CT_i	CGCGGCGCCC TTTCTTTCTG ACTACCTAGG ATACTTGACT GATTTCTTCC GCTTCTGTCC ACGAATCAG
	CT_i-LT	GCGCCGCGCT GATTCG
	$CT_{ii\text{-}R}$ Template for DNAzyme cleavage and subsequent creation of a rolling circle amplification primer. Linear $CT_{ii\text{-}R}$ is produced by ligating CT_{ii}FS to CT_{ii}Ext using CT_{ii}LT1 as the template, then circularizing using CT_{ii}LT2 as the template to produce $CT_{ii\text{-}R}$	
	FS	CTATGAACTG ACQRFGACCT CACTACCAAG
	CT_{ii}Ext	TCTCTCTCTC TCTCTCTCTC AGAAATCAGT CAAGTATCCT AGGTTCTCTC TCTCTCTCTC TCTC
	CT_{ii}LT1	AGAGAGAGAT CTTGATCG
	CT_{ii}LT2	AGGAAGAGTG AGAGAGAG
	RCA Primer i	CTG ATT CGT GGA CAG AAG
	RCA Primer ii	GAG ACT TGG TAG TGA GGT
Original ***Cis*-DNAzyme**	**Forward *cis*-DNAzyme** The linear DNAzyme is produced via ligation of FS28 to DHp3t4(idT) using FSDZ-LT as the template.	
	Ligated Forward *cis*-DNAzyme	CTATGAACTG AC**QRF**GACCTCA CTACCAAGAT GCCATCGATG GTCTTTGGTA TGTGGGGTCC GAGGGTAGAG CTCTGAACTCG /3InvdT/
	FS28	CTATGAACTG AC**QRF**GACCTCA CTACCAAG
	DHp3t4(idT)	ATGCCATCGA TGGTCTTTGG TATGTGGGGT CCGAGGGTAG AGCTCTGAAC TCG /3InvdT/
	FSDZ-LT	CATCGATGGC ATCTTGGTAGTG AG
	CT-Forward Template for rolling circle amplification. CT-forward is produced via circularization using CT-forward-LT as the template.	
	CT-forward	TGTGATGCGA TTGCCCGAAA AAGACAGTAG GTACTCATTA GGATCCTGTT TGTAATCAGT TCCTTTTGAG CTAAGACGGC GTC
	CT-forward-LT	AACAGGATCC TAATGAGTACC
	RCA Primer	
	RCA Monomer	GACGCCGTCT TAGCTCAAA AGGAACTGAT TACAAACAGG ATCCTAATGA GTACCTACTG TCTTTTTCGG GCAATCGCAT CACA

Reverse	**Reverse *cis*-DNAzyme**	
	The linear DNAzyme is produced via ligation of DHp3t4 to FS28(idT) using DZFS-LT as the template.	
***cis*-DNAzyme**	Reverse *cis*-DNAzyme	ATGCCATCGA TGGTCTTTGG TATGTGGGGT CCGAGGGTAG AGCTCTGAAC TCGCTATGAA CTGAC**QRF**GA CCTCACTACC AAG /3InvdT/
	FS28 (idT)	CTATGAACTG AC**QRF**GACCTCA CTACCAAG /3InvdT/
	DHp3t4	ATGCCATCGA TGGTCTTTGG TATGTGGGGT CCGAGGGTAG AGCTCTGAAC TCG
	DZFS-LT	AGTTCATAGC GAGTTCAG
	LrgClv -1nt(3')	ATGCCATCGA TGGTCTTTGG TATGTGGGGT CCGAGGGTAG AGCTCTGAAC TCGCTATGAA CTGA
	LrgClv -2nt(3')	ATGCCATCGA TGGTCTTTGG TATGTGGGGT CCGAGGGTAG AGCTCTGAAC TCGCTATGAA CTG
	LrgClv -3nt(3')	ATGCCATCGA TGGTCTTTGG TATGTGGGGT CCGAGGGTAG AGCTCTGAAC TCGCTATGAA CT
	LrgClv -4nt(3')	ATGCCATCGA TGGTCTTTGG TATGTGGGGT CCGAGGGTAG AGCTCTGAAC TCGCTATGAA C
	LrgClv -5nt(3')	ATGCCATCGA TGGTCTTTGG TATGTGGGGT CCGAGGGTAG AGCTCTGAAC TCGCTATGAA
	LrgClv -6nt(3')	ATGCCATCGA TGGTCTTTGG TATGTGGGGT CCGAGGGTAG AGCTCTGAAC TCGCTATGA
	LrgClv -7nt(3')	ATGCCATCGA TGGTCTTTGG TATGTGGGGT CCGAGGGTAG AGCTCTGAAC TCGCTATG
	LrgClv -8nt(3')	ATGCCATCGA TGGTCTTTGG TATGTGGGGT CCGAGGGTAG AGCTCTGAAC TCGCTAT
RCA	**CT-Reverse**	
	Template for rolling circle amplification. CT-Reverse is produced via circularization using CT-reverse-LT as the template.	
	CT1	ATCTCGACTA GTCAGCACAC CCAAAGACCA TCGATGGCAT AACTACCACA ATACTACAAC
	CT2	ATCTCGACTA GTCAGCACAC ACATACCAAA GACCATCGAT AACTACCACA ATACTACAAC
	CT3	ATCTCGACTA GTCAGCACAC ACCCCACATA CCAAAGACCA AACTACCACA ATACTACAAC
	CT4	ATCTCGACTA GTCAGCACAC CTCGGACCCC ACATACCAAA AACTACCACA ATACTACAAC
	CT5	ATCTCGACTA GTCAGCACAC CTACCCTCGG ACCCCACATA AACTACCACA ATACTACAAC
	CT6	ATCTCGACTA GTCAGCACAC GAGCTCTACC CTCGGACCCC AACTACCACA ATACTACAAC
	CT7	ATCTCGACTA GTCAGCACAC GTTCAGAGCT CTACCCTCGG AACTACCACA

		ATACTACAAC
	CT8	ATCTCGACTA GTCAGCACAC AGCGAGTTCA GAGCTCTACC AACTACCACA ATACTACAAC
	CT9	ATCTCGACTA GTCAGCACAC TTCATAGCGA GTTCAGAGCT AACTACCACA ATACTACAAC
	CT10	ATCTCGACTA GTCAGCACAC GTCAGTTCAT AGCGAGTTCA AACTACCACA ATACTACAAC
	CT-LT	TAGTCGAGAT GTTGTAGTAT

Q = dabcyl-dT; R = adenine ribonucleotide; F = Fluorescein-dT

4.1 5'-Substrate-RCD-inverted-dT-3' Primer Release

The first RCD primer-release strategy was based on the original DHp3t4 *cis*-DNAzyme reported in 2019,[1] which featured a *cis*-RCD with the FS28 fluorgenic substrate ligated to the 5' terminus of the DNAzyme (5'-Substrate-RCD-inverted-dT-3', see Table 3.1 and Figure 4.1A). For this work, the 3' end of the *cis*-RCD was modified by adding an inverted dT unit to prevent amplification or digestion by phi29 DP.[3] As shown in Figure 4.1B, target-triggered cleavage is expected to liberate a small quencher-labelled strand from the larger RCD strand, accompanied by an increase of fluorescence, allowing the unprotected 3'-cleavage fragment to bind to a complementary CT and thus act as a primer for RCA.

As a first step toward developing the amplification system, an 83-nt CT was designed

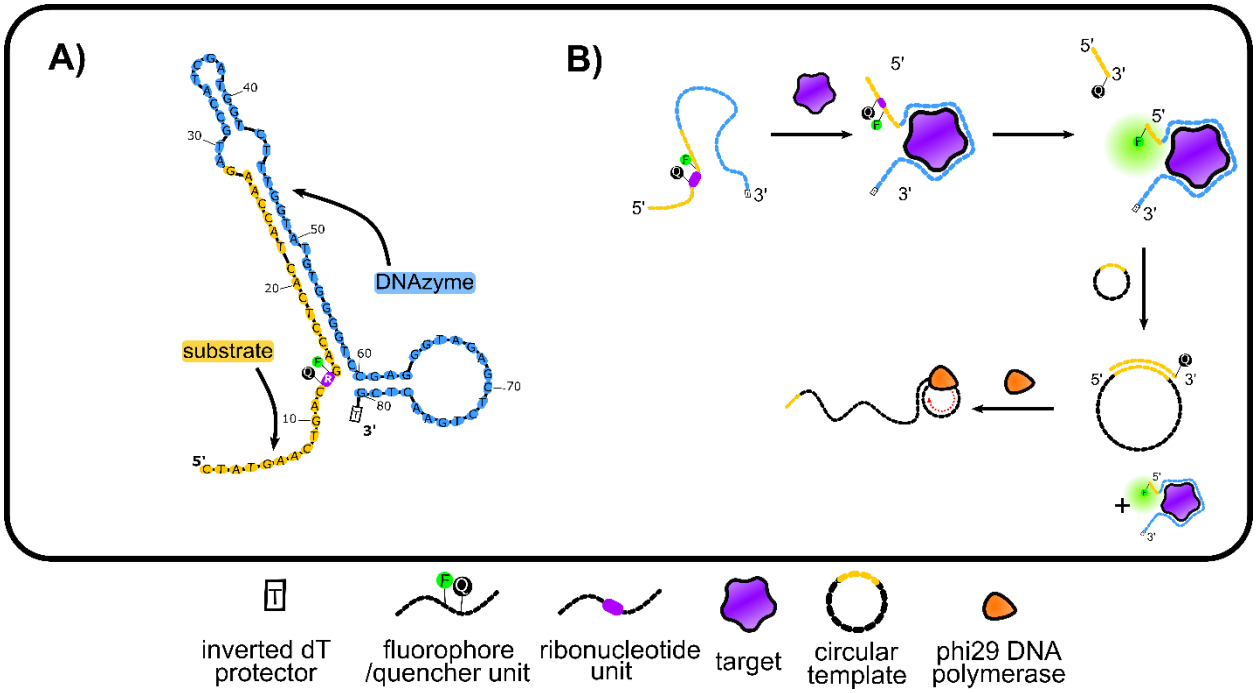

Figure 4.1 A) The mfold web server for computational molecular biology was used to predict the secondary structures of the RCD (5'-Substrate-RCD-inverted-dT-3') with the lowest ΔG. B) Schematic of target-triggered *cis*-RCD cleavage leading to amplification of a CT with RCA.

such that the resulting RP would contain repeats of a Taq1 restriction site that would allow for RP monomerization, allowing for detection of monomeric units as opposed to the large polymeric RP, and helping to further confirm production of the expected RP (see Figure 4.2A).

To determine if the primer produced from RCD cleavage could induce amplification, the CT was incubated with 1 pmol of a synthetic 20-nt DNA primer sequence that was identical to that expected to be released from the RCD, and which was fully complementary to the recognition region of the CT (yellow section in Figure 4.1B). Using agarose gel electrophoresis, the reaction products were observed at various RCA reaction times up to 60 min, and clearly showed an increasingly intense band at the expected high molecular weight region of the RCA product, which should be several thousand nucleotides in length (Figure 4.2A). Successful amplification was further conformed by using Taq1 to digest the large RP to produce shorter digestion products. As shown in Figure 4.2B, dPAGE of the digestion products produced the expected ladder pattern with each band representing one or more repeats (dimer, trimer, etc.) of the original 83 nt output sequence, confirming the presence of the restriction sites in the RP. Overall, these results indicate that the primer was readily amplified when the complementary CT was present, indicating that the primer released by the RCD should be able to initiate RCA.

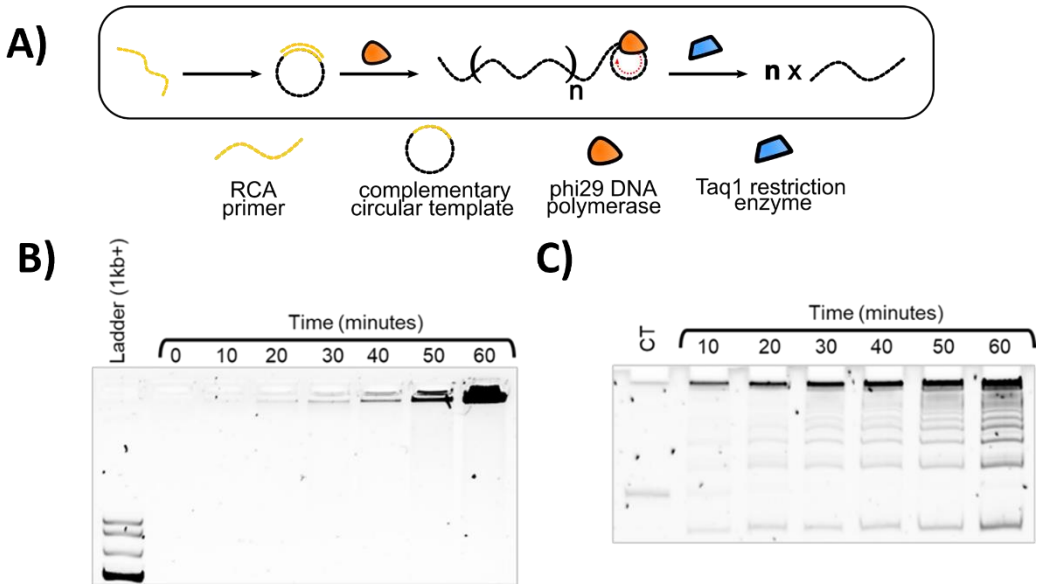

Figure 4.2. Proof of concept amplification using a basic 83-nt CT; sequence given in Table 3.1 A) A basic schematic depicting polymeric RP and its Taq1 monomerized equivalent B) Agarose gel analysis of polymeric RP generated using 1 pmol primer with 1 pmol CT. C) dPAGE gel analysis of the same RP digested with Taq1 for 15 minutes.

We next aimed to confirm that the RCD cleavage product could act as a primer for RCA while the intact RCD would not produce any amplification. The initial assay utilized NaOH to cleave the RCD, which produced the two expected cleavage fragments, as visualized by SYBR Gold staining of a dPAGE gel (Figure 4.3B, marker lane) showed the expected band for the short primer along with the larger cleavage fragment for the remaining RCD. Note that the intact RCD as well as the longer cleavage fragment can also be visualized directly by monitoring the fluorescein-dT, although the shorter cleavage fragment that acts as the primer has no fluorophore attached and thus can only be visualized by staining. RCA experiments using the intact RCD demonstrated that the full sequence was unable to initiate RCA, as expected (see Figure 4.3C below). On the other hand, the shorter cleavage fragment generated by NaOH derived cleavage was able to initiate RCA, indicating that the system should be able to produce cleavage-initiated RCA with minimal background.

We then examined the ability to produce the short cleavage fragment using cleavage of the RCD with *H. pylori* CEM, as monitored using dPAGE with imaging of the fluorescein label in the RCD. As shown in Figure 4.3A the HP CEM resulted in time-dependent cleavage, which resulted in an increase in the intensity of the cleavage band associated with the larger fluorescein-labelled product. In this case the smaller primer fragment could not be visualized owing to the lack of a fluorescein label. We also note that rather than having a single cleavage band, the RCD produced two closely spaced bands in the gel, consistent with the presence of two cleavage products, likely attributable to cleavage at the ribo-linkage as well as cleavage 2-3 nucleotides to the 5' end of the ribo-linkage. In order to visualize the smaller unlabelled cleavage fragment, the dPAGE gel was stained with SYBR Gold. However, as shown in Figure 4.3B, there was no band present at the expected location of this cleavage fragment (see marker lane), and instead there was a time-dependent increase in a band at the bottom of the gel that was indicative of monomeric nucleotides, which would be produced by digestion of the shorter cleavage fragment. We confirmed that the intact RCD would not produce RP whereas a NaOH-liberated primer could in Figure 4.3C, leading us to conclude that an absence of RP could indicate the absence of generated primer in the reaction mixture.

To confirm that the digestion of the short cleavage fragment, we used gel elution to sequester and concentrate any cleavage product within the expected region of the dPAGE cleavage band, as well as for lower regions of the gel that could contain shorter fragments and labelled these A-E (where A would contain the full-length cleavage fragment and E would contain fragments smaller than 10-nt). In each case, the total material from ten cleavage reactions was pooled and concentrated and a CT completely complementary to the shorter cleavage product was incubated with this concentrated solution along with phi29 DP to initiate RCA. In several trials, a PNK step was also added to account for the possibility that the cleavage

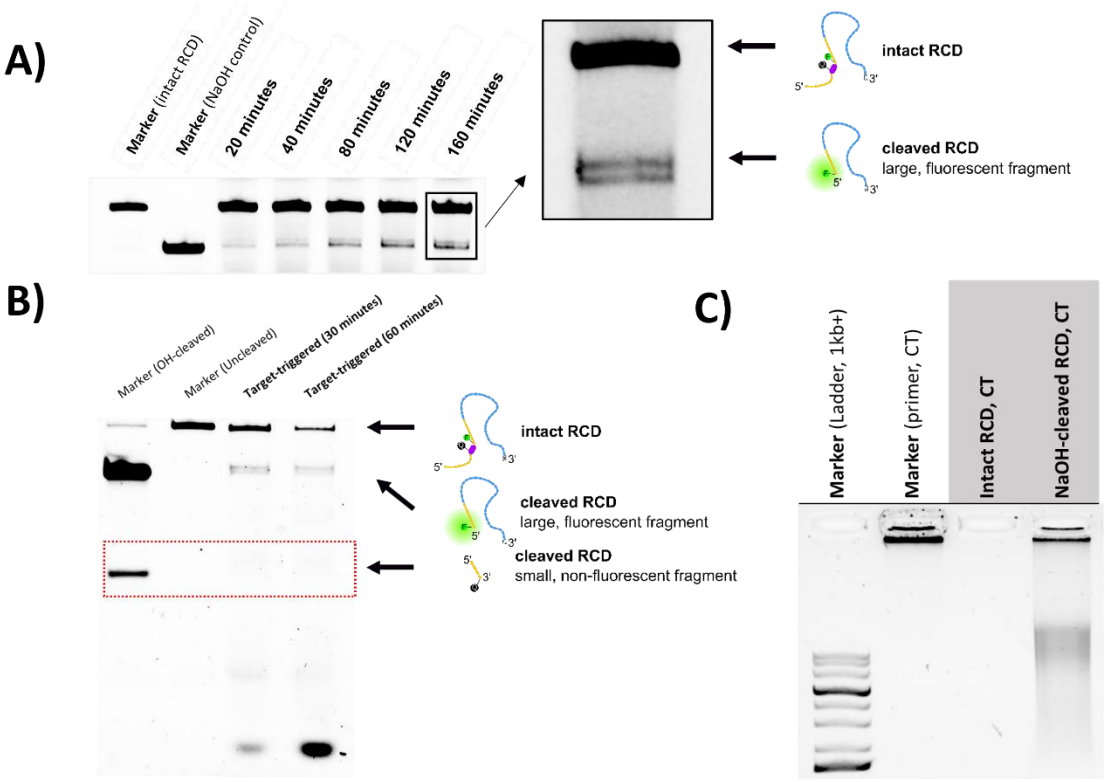

Figure 4.3. A) Target -triggered cleavage of 2.5 pmol of the original *cis*-RCD incubated with 3 µL of undiluted *H. pylori* CEM as measured over several periods of time. dPAGE gel imaging indicaties where the larger, fluorescent target-triggered cleavage product is easily visualized with fluorescence imaging. B) Target -triggered cleavage of 2.5 pmol of the original *cis*-RCD incubated with 3 µL of undiluted *H. pylori* CEM after 30- and 60-minutes. dPAGE gel imaging indicates where the small, non-fluorescent target-triggered cleavage product is visualized with SYBR Gold staining. C) Fluorescence detection of RP generated over 60 minutes using a complementary primer, intact RCD, and NaOH-cleaved RCD (2.5 pmol each) and CT (1pmol).

product might carry a terminal 2'3'-cyclic phosphate. Ultimately, these experiments indicated that the no fragment on the dPAGE gel was able to trigger amplification (Figure 4.4A), implying that there was no cleavage fragment longer that the minimal length of 6-nt required to initiate RCA.[2] This further supports the hypothesis that the shorter cleavage product was digested completely by nucleases endogenous to the CEM (Figure 4.4B). We suspect that the liberated primer with a free 3' terminus would be susceptible to digestion by any 3'-exonucleases present in the HP CEM – we note that the larger cleavage fragment remains intact owing to the presence of the inverted 3'-dT.[3] We note that there was a faint band present at the expected location of the shorter cleavage fragment after 30 min of digestion, which was completely absent after 60

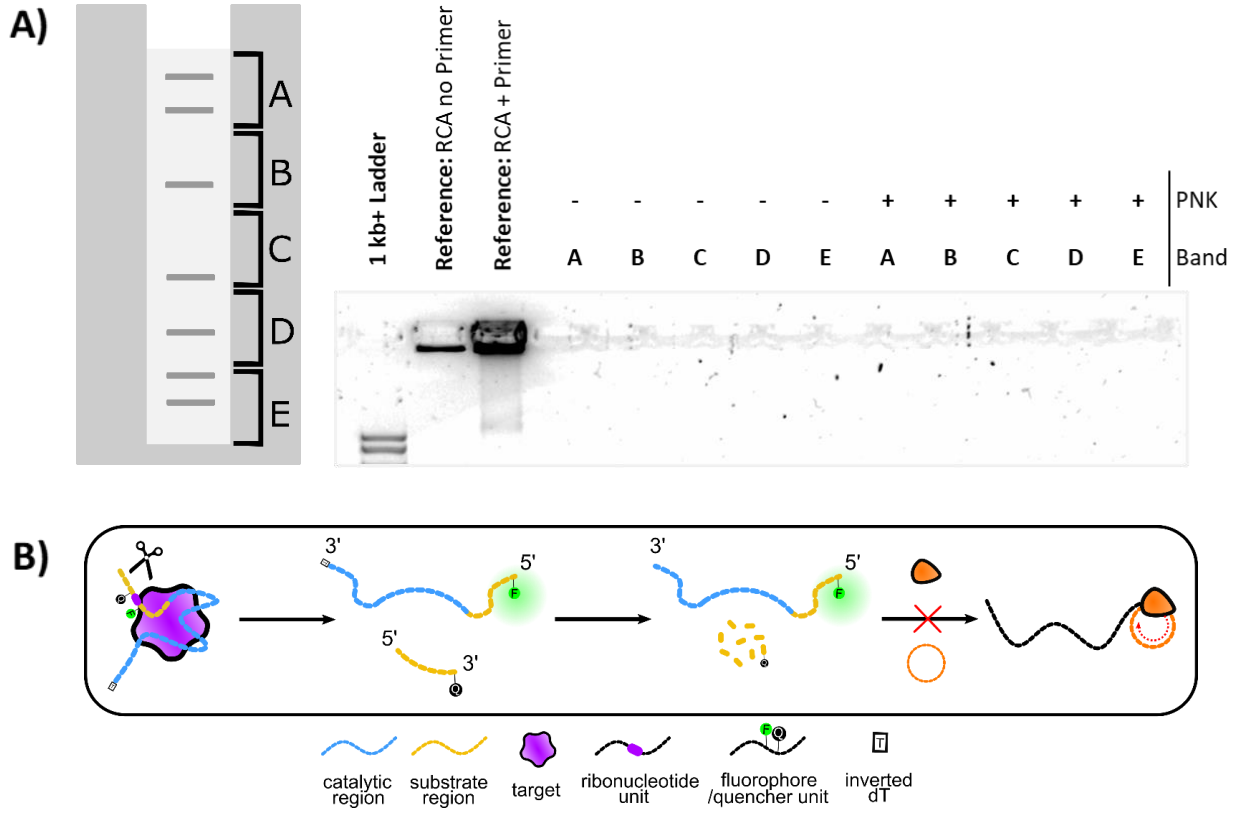

Figure 4.4. A) Agarose gel analysis of a 60-minute RCA reaction initiated with concentrated cleavage products of various lengths, both with and without PNK treatment. In accordance with the label, lane A would contain RCA reaction initiated by the larger potential fragments and E would contain RP initiated by nucleic acids <10-nt. B) Schematic of the suspected digestion process that prevented RCA initiation.

minutes (Figure 4.3B). Hence, it is possible that a 30-minute cleavage reaction might reduce overall digestion and allow for priming of the RCA reaction, though a shorter digestion time produced less initial cleavage product, and thus would likely affect sensitivity of assays using this primer.

In summary, the *cis*-RCD primer-release strategy was initially pursued as it allowed use of the original RCD sequence reported in 2019. However, while the RCD was clearly able to be cleaved by the HP CEM, the resulting short cleavage fragment that was to be used as the primer for RCA was found to be digested by nucleases that were endogenous to the HP CEM, with current evidence supporting the presence of an endonuclease with 3' exonucleic action. As a

result, this MRE design was abandoned in pursuit of an alternative strategy designed specifically to avoid the possibility of primer digestion.

4.2 trans-RCD Catenane Primer Release

The second strategy explored for RCD primer release was based on a catenated design initially reported by Liu *et al.* involving the use of a topologically constrainted nanostructure consisting of two interlocked ssDNA rings (Figure 4.5).[17] In this strategy, the one circle acts as the normal circular template for RCA (denoted as CT_i), while the second is a circularized sequence containing the substrate for the RCD, including the fluorophore and quencher flanking a single ribonucleotide (denoted as $CT_{ii\text{-}R}$). By circularizing the substrate and producing a strong region of hybridization with the CT, the cleavage of the ribo-linkage will produce a 3' fragment that can only be digested up to the point where the hybridization with the CT begins, at which point RCA can be initiated by phi29 DP.[4] For the HP DNAzyme system, a 24-bp complementary duplex was used to interlock the two rings, which is expected to prevent RCA from proceeding along either CT. The long complementary region also prevents both CT_i and $CT_{ii\text{-}R}$ from rotating independent of each other by interlocking and hybridizing the circular ssDNA strands. The use of a circular substrate also removes any 3' terminus and hence prevents digestion of $CT_{ii\text{-}R}$.

We synthesized a catenane wherein CT_i was the amplification template, which was 69-nt long and contained a 24-nt binding region identical to that of the CT used in the original report on the use of catenated circles. A complementary 24-nt region was inserted into the sequence of $CT_{ii\text{-}R}$, along with the substrate sequence for the DHp3t4 DNAzyme (Figure 4.5A).[15] In addition, two spacer regions were inserted between the substrate and the linking regions to reduce strain on $CT_{ii\text{-}R}$. The expected reaction is shown in Figure 4.5B. Here, a *trans*-version of

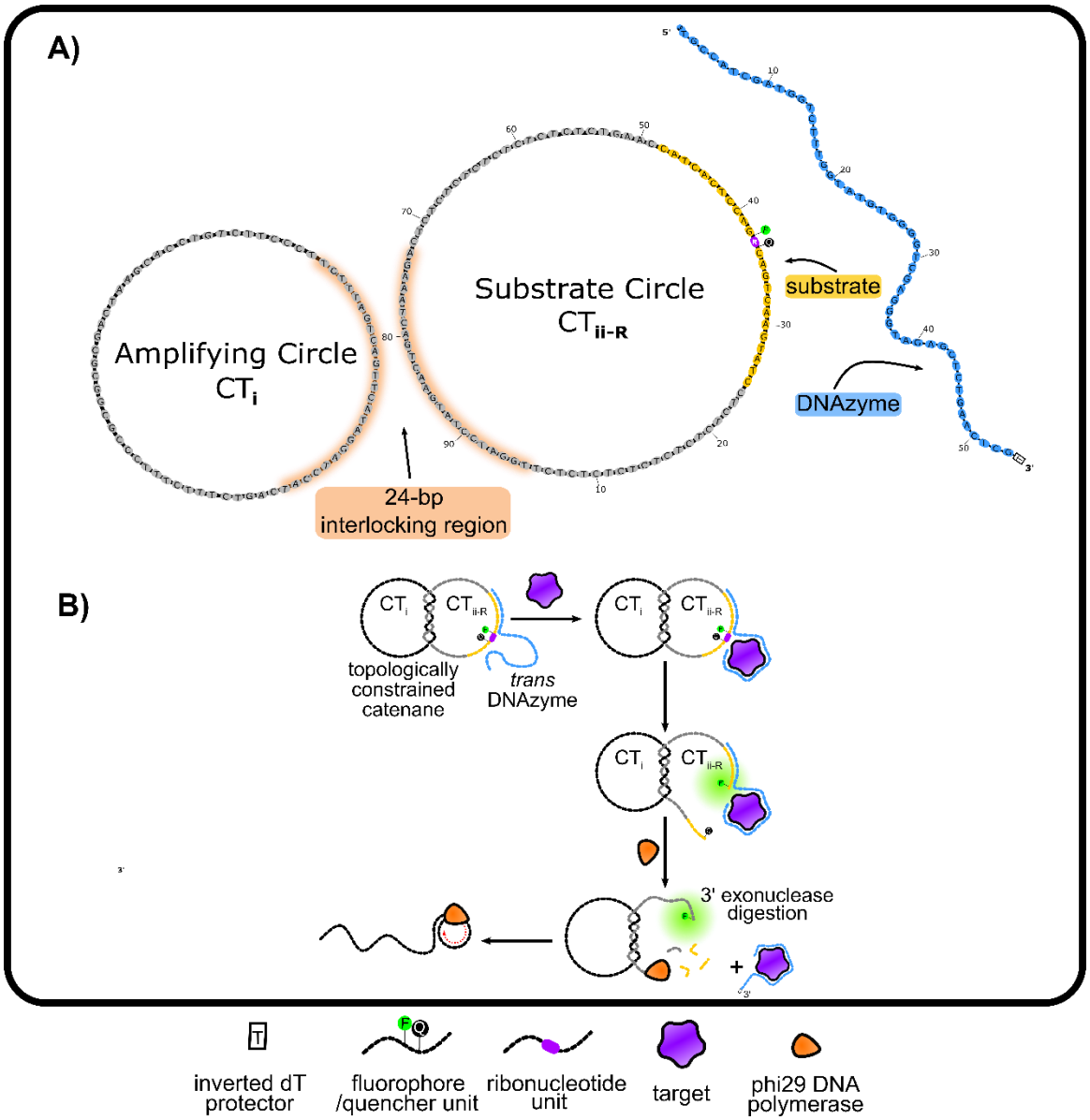

Figure 4.5. A) Sequences of the interlocked nanostructure and *trans*-RCD as detailed in Table 3.1: fluorescein-dT; Q: dabcyl-dT; R: adenosine ribonucleotide. B) Schematic of target-triggered *trans*-RCD catenane cleavage leading to amplification with the CT.

the RCD acts upon the catenated cirular substrate, cleaving the $CT_{ii\text{-}R}$ at the embedded ribo-linkage, and producing a increase in emission intensity due to dequenching. The resultant 3'-terminus of the cleaved substrate is then digested by phi29 DP (and possibly endogenous exonucleases in the HP CEM) up to the point where the strong interlocking region begins. At this point the remaining sequence is comlementary to CT_i, and thus can be amplified by phi29 DP to produce RCA reaction products.

We first investigated whether it was possible to form the catenated structure with the two circles, and whether this structure could be cleaved by a *trans*-form of the original *cis*-DNAzyme. To confirm that a catenane nanostructure had been formed, a dPAGE (8M urea) was performed to investigate the ssDNA species after ligation and gel purification (Figure 4.6A). Lanes 1-4 contain reference bands for individual NA species (linear CT_i, circularized CT_i, linear $CT_{ii\text{-}R}$, circularized $CT_{ii\text{-}R}$). The catenane species in lane 5 migrated through the dPAGE gel much more slowly during electrophoresis, suggesting that the larger catenane structure had been formed. If the ssDNA rings had not been interlocked, dPAGE analysis would have revealed two circularized products. To further confirm that ligation had yielded the interlocked nanostructure, we used hydrolytic cleavage of the ribonucleotide unit to determine the expected cleavage products. If the correct catenane structure was indeed formed, this would yield a linearized substrate strand (linear $CT_{ii\text{-}R}$) and circularized CT_i. Incubation at 90 ˚C for 5 minutes in basic solution (0.25M NaOH) was expected to hydrolytically cleave the ribonucleotide unit, resulting in two nucleic acid species. In comparing these new cleavage strands to the reference bands in lanes 1-4, they were identified as circular CT_i and linearized $CT_{ii\text{-}R}$. This indicated that synthesis successfully yielded the ssDNA nanostructure, and that the ribo-linkage in the $CT_{ii\text{-}R}$ could be cleaved to linearize the substate strand.

To prove that the interaction between the two ssDNA rings acts to mechanically lock them and prevent spurious amplification, we first confirmed that each ssDNA ring could act as a template for amplification independently (Figure 4.6B). To do so, we designed two 16-nt primers (P1 and P2) where each primer was 100% complementary to one of the two catenane circles (CT_i and $CT_{ii\text{-}R}$, respectively). While CT_i is the only ssDNA ring that acts as a template for amplification in the assay design, the circular nature of $CT_{ii\text{-}R}$ indicates that it is possible it could also act as a template for RP generation. We confirmed that the amplification template CT_i amplified as expected. However, $CT_{ii\text{-}R}$ showed no ability to generate RP, presumably owing to the presence of the ribonucleotide within the DNA sequence and/or the presence of the fluorophore and quencher. To confirm this hypothesis, an identical all-DNA CT_{ii} was used as a

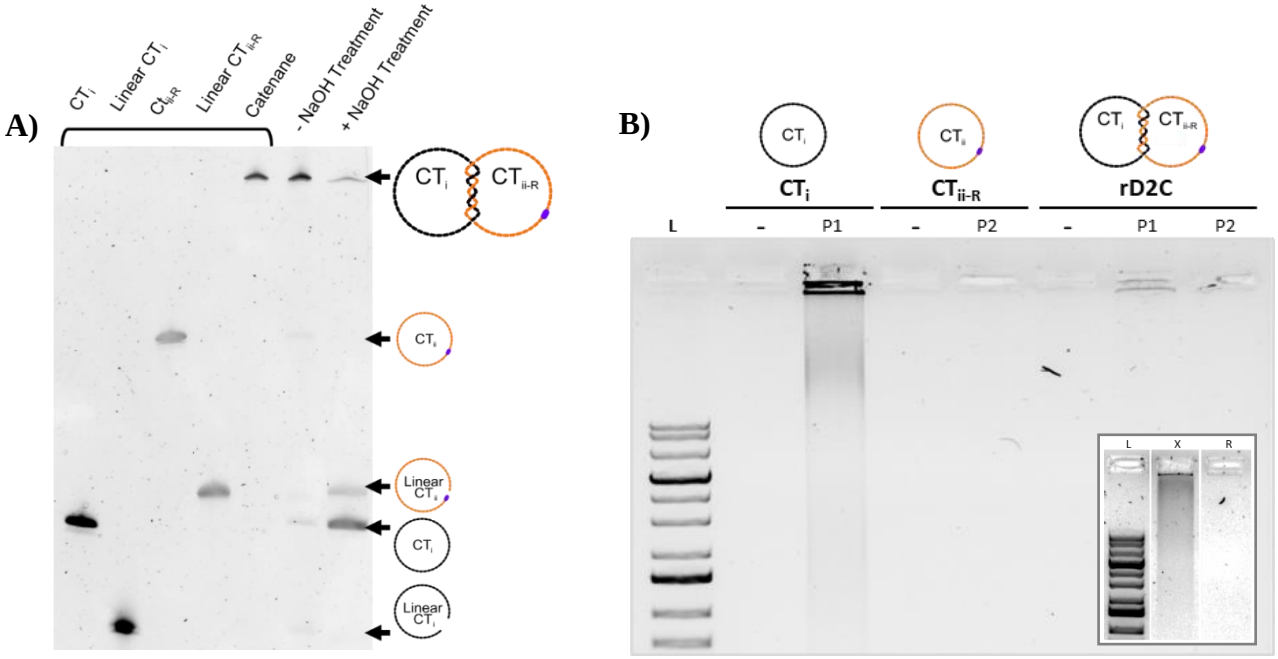

Figure 4.6. A) dPAGE visualization of synthesis reagents and RNA cleavage products. Synthesis of the topologically constrained nanostructure proceeded by circularizing $CT_{ii\text{-}R}$, followed by circularization of CT_{ii}. The five leftmost lanes include the individual components both linearized and circularized. The two rightmost lanes show the resultant bands from ribonucleotide cleavage, linearized $CT_{ii\text{-}R}$ and circular CT_i. B) Agarose detection of RP from CT_i, $CT_{ii\text{-}R}$, (1 pmol, respectively) and the catenane using P1 and P2 as primers (1 pmol). Lane L, 1 kb+ ladder. Inset: Limited RCA capabilities of the ribonucleotide-containing circle ($CT_{ii\text{-}R}$). Lane L, 1 kb+ ladder. Lane X, CT_{ii} RP (no ribonucleotide). Lane R, $CT_{ii\text{-}R}$ (with ribonucleotide).

template, and could be easily amplified (Figure 4.6B(inset)). The catenated structure, denoted as rD2C, was also investigated as a template for RCA. A small amount of amplification could be seen with rD2C, suggesting that a small amount of CT_i may remain uncatenated, and can thus contribute to the overall background signal. It may also be possible that phi29 DNA polymerase can read through the interlocked region as it extends P1, because the primer is entirely and exclusively complementary to a region of the CT opposite the 24-bp interlocking region.

Following the characterization of the catenanted substrate, we next evaluated the ability of the *trans*-RCD to cleave the circularized substrate. In this case, the *trans*-RCD was redesigned (see Table 3.1) to contain a terminal sequence that could hybridize to CTii-R via a 14-nt nucleotide region. Unfortunately, the *trans*-RCD was not able to effectively cleave $CT_{ii\text{-}R}$ during incubation with HP CEM (Figure 4.7A). dPAGE analysis revealed that incubation failed to release CT_i and that no new fluorescent species corresponding to a linearized form of $CT_{ii\text{-}R}$ could be detected to indicate the cleavage of $CT_{ii\text{-}R}$. In order to account for possible interference resuting from ring strain in the catenated substrate, the *trans*-RCD was also used in conjuction with the uncomplexed $CT_{ii\text{-}R}$. However, the *trans*-RCD showed poor cleavage performance even with the free circularized substrate, when an equal amount of the free circle was incubated with target (Figure 4.7B). These results indicate that the *trans*-RCD may not be able to access the ribonucleodide linkage in the $CT_{ii\text{-}R}$ substrate, either due to a sterically strained ssDNA inducing a conformation change that blocked the cleavage site, or possibly insufficient hybridization of the *trans*-RCD to $CT_{ii\text{-}R}$ owing to the relative short 14-nt hybridization region. As expected, the lack of a cleavage producte also resulted in an inabilty to obtain any amplification when using target-triggered cleavage of the catenane species (Figure 4.7C). To improve this DNAzyme performance, it is likely that either a larger $CT_{ii\text{-}R}$ with longer unstructured regions joining the substate and interlocking regions, or a longer hybridization region on the RCD, or both, may be

needed achieve cleavage with the *trans*-RCD. However, it is also possible that substatial re-engineering of the RCD and substrate sequences may be needed to avoid secondary structures, particularly stems in the RCD, that might prevent operation of the RCD in the *trans* form.

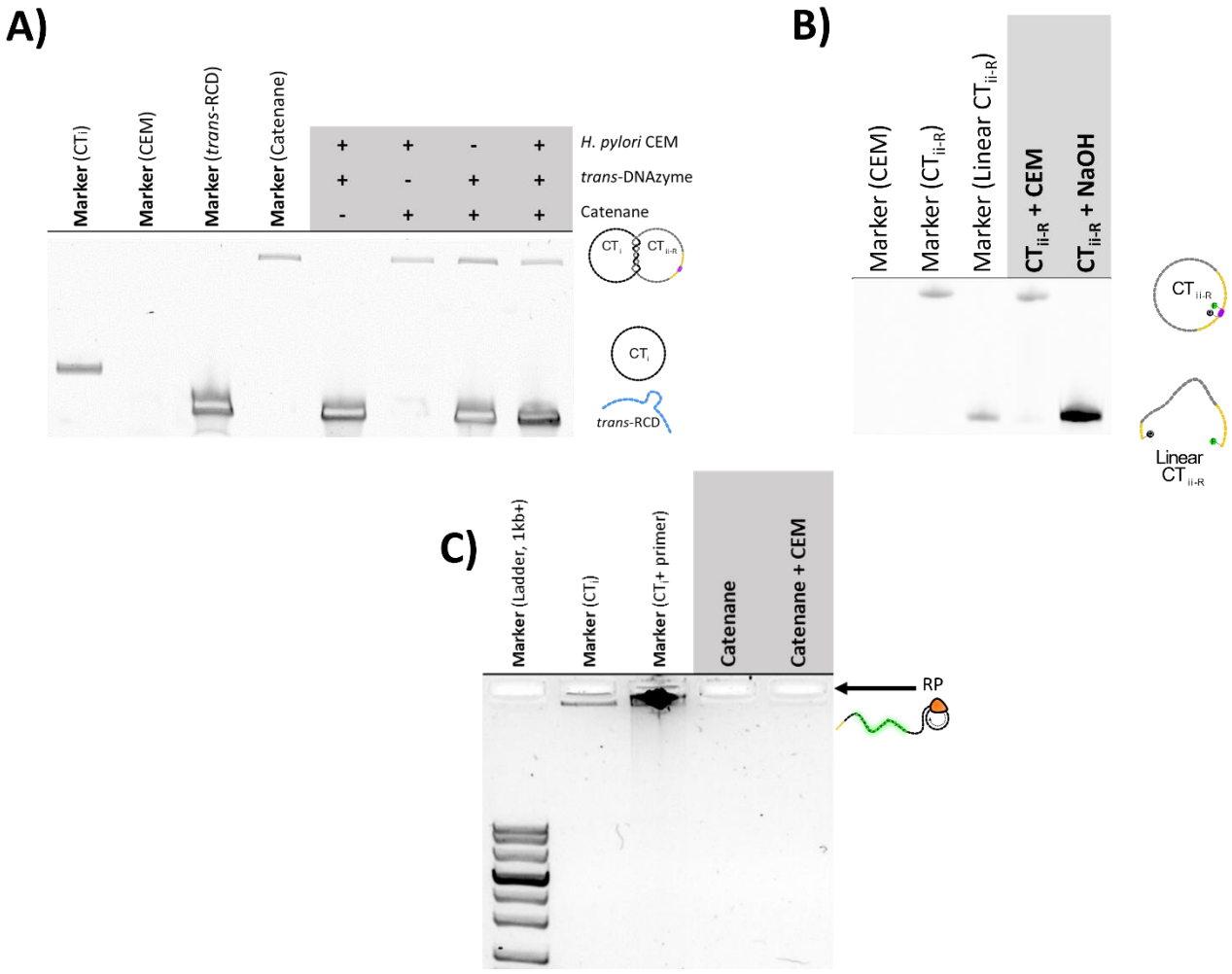

Figure 4.7. A) SYBR Gold stained-dPAGE gel depicting various incubation conditions for the *trans* system. Note that the concentration of the *trans*-RCD (50 pmol in a 50 µL reaction volume) is 50x the concentration of the catenane species (1 pmol), as per the original paper. B) SYBR Gold stained-dPAGE gel comparing the cleavage performance of free $CT_{ii\text{-}R}$ (5 pmol) C) Agarose detection of RP from RP generated using CT_i and the assembled catenane (5 pmol, respectively). SYBR Gold staining was used to visualize the RP with fluorescence scanning.

4.3 5'-RCD-Substrate-inverted dT-3' Primer Release

In the final approach to develop a primer-release strategy using the *H. pylori* RCD, we opted to revert to the original *cis*-form of the RCD but to reverse the order of the substrate and catalytic units and thus utilize the larger cleavage product as a primer. While the original RCD had the substrate sequence ligated to the 5' end of the RCD (5'-Substrate-RCD-inverted-dT-3',

denoted as **substrate-RCD**), the new design had the catalytic region at the 5' end of the overall sequence, ligated to the 5' end of the substrate, which was terminated with an inverted dT at its 3' end (5'-RCD-Substrate-inverted dT-3', denoted as **RCD-substrate**), as shown in Figure 4.8A. In this configuration, the cleavage should result in a short cleavage product with an inverted dT at the 3' end that cannot initiate RCA, and a longer 3' terminated RCD that can bind to an

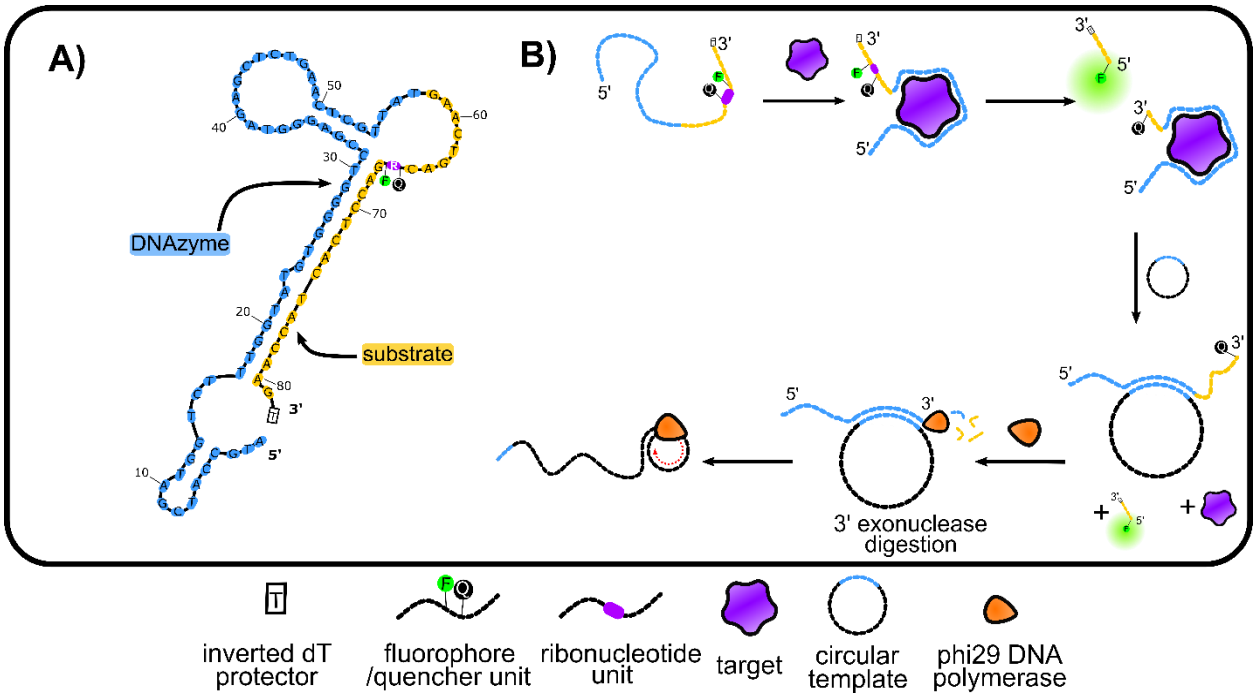

Figure 4.8. A) The *mfold* web server for computational molecular biology was used to predict the secondary structures of the final *cis*-RCD (5'-Substrate-RCD-inverted-dT-3') with the lowest ΔG. B) Schematic of target-triggered *cis*-RCD cleavage leading to amplification with the CT.

appropriate CT to initiate RCA, as shown in Figure 4.8B.

The use of the longer primer, coupled with the possibility of a bound target, was expected to reduce the rate of digestion by endogenous nucleases in the HP CEM, facilitating initiation of RCA. However, it is also possible that using the RCD as the primer may require that the target can be displaced from the RCD to allow polymerization to proceed, though this will depend on

the specific region of the RCD primer that binds to the CT, where binding of the CT closer to the 3' end may avoid the need to displace the target to achieve amplification.

To our knowledge, this is the first time a *cis*-DNAzyme has been reorganized to move the substrate sequence to the opposite end relative to the sequence derived from the SELEX process and subsequently been used to trigger RCA. Hence, the first objective was to determine if the reorganized *cis*-RCD could still produce cleavage products in the presence of HP CEM, and whether the cleavage reaction retained similar sensitivity and selectivity for HP CEM. As shown in Figure 4.9, the SYBR Gold stained dPAGE gel clearly indicated that addition of 10^8 CFU/mL of HP CEM led to a time dependent cleavage of the RCD to produce a long cleavage product, along with increased amounts of shorter digestion products at longer reaction times, confirming both that cleavage activity was retained, and that the digestion of the RCD-based primer was much slower than was observed for the short primer liberated by the original RCD.

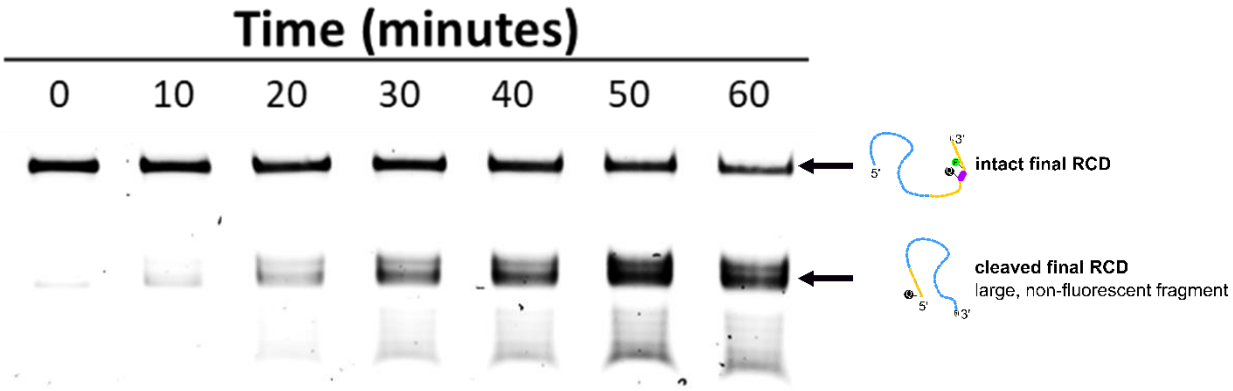

Figure 4.9. Stained dPAGE images of target-triggered RCD cleavage over time, highlighting the appearance of smaller oligonucleotides in the reaction mixture that increase in intensity over time. Cleavage followed the procedure noted in the experimental.

A comparison of the cleavage rates for the rearranged RCD relative to the original RCD indicated that the rearranged RCD cleaved at a rate that was similar to the originally selected *cis*-DNAzyme, and hence would be expected to demonstrate a similar sensitivity. Thus, the data clearly show that it is possible to reverse the order of the RCD and substrate in a *cis*-DNAzyme and retain cleavage activity, providing the ability to generate different primer outputs that can be evaluated for initiation of RCA. Evaluation of the selectivity of the cleavage reaction (Figure 4.10) revealed that the reversed RCD also retained selectivity against several gram positive and gram negative bacteria, similar to the original *cis*-RCD.

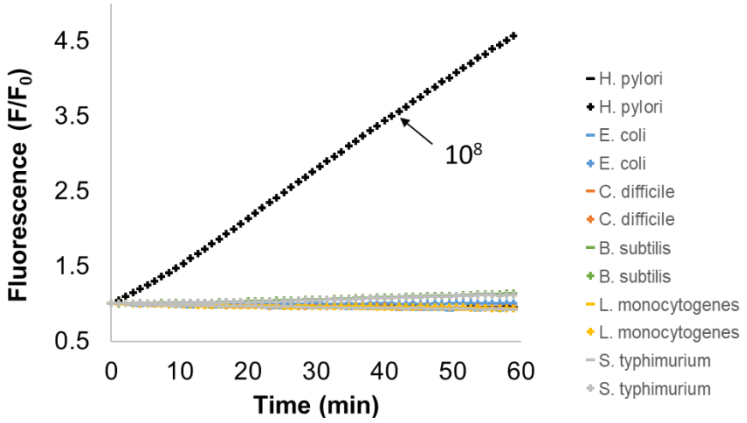

Figure 4.10. Analysis of cleavage specificity by monitoring real-time fluorescence after bacterial CEM incubation using the final, reorganized *cis*-RCD. In this assay, HP = *Helicobacter pylori*, EC = *Escherichia coli* O157:H7, CD = *Clostridium difficile*, BS = *Bacillus subtilis*, LM = *Listeria mono.* (Insert) Sensitivity data from the original paper following an identical procedure.

As noted above, the original **substrate-RCD** DNAzyme was observed to produce two cleavage fragments, suggesting that cleavage could occur both at the ribo-linkage and at a DNA junction upstream of the ribo-linkage to produce a shorter fragment. To determine if this behaviour was retained for the rearranged **RCD-substrate** DNAzyme, the cleavage products obtained from NaOH cleavage (which should cleave solely at the ribo-linkage) were compared to

those obtained with HP CEM, with cleavage fragments visualized using SYBR Gold staining. As shown in Figure 4.11A, the RCD primer strand obtained using HP CEM was in fact several nucleotides shorter in length than was obtained using NaOH cleavage, indicating that a series of 3' termini might be produced. A higher resolution dPAGE gel (Figure 4.11B) revealed that the expected 65-nt cleavage fragment (left lane) was in fact not present in the HP CEM cleavage product, while both a 63-nt and 60-nt cleavage fragment were produced, with the 60-nt fragment being the prominent fragment within the series of bands. Such DNA-DNA cleavage has been reported previously for the Cu(II) dependent DNA-cleaving DNAzyme (CuDD),[5] but has not been previously reported for a bacteria-specific DNAzyme. Such a cleavage product may not include a 2'3'cyclic phosphate on the 3' terminus, avoiding the need for PNK to allow initiation of RCA, as discussed in more detail below. More importantly, the removal of the 5 NA from the 3'-terminus requires that the CT be designed to bind upstream of the 3' terminus to ensure strong binding of the primer to the CT.

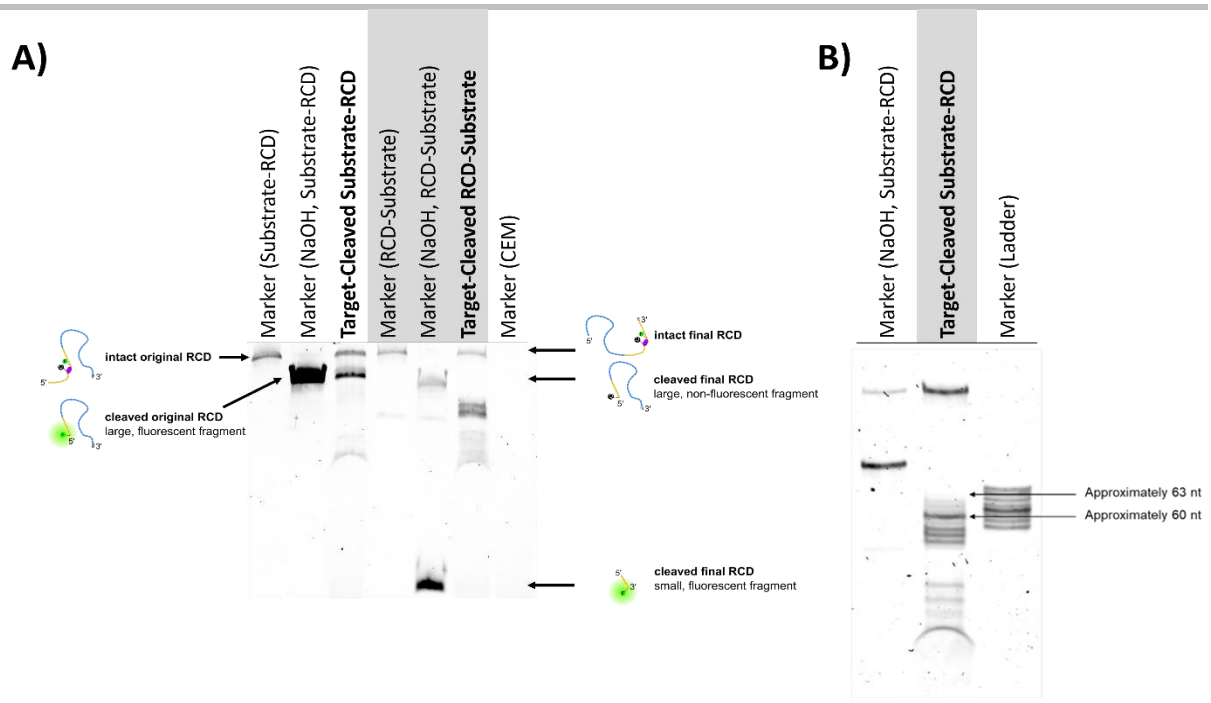

Figure 4.11. A) Comparing the cleavage modes of the forward and reverse DNAzymes. Lanes labelled with NaOH have undergone digestion to cleave at the ribonucleotide unit. Equal concentrations of RCD (2.5 pmol) and undiluted CEM (3 µL) were used in each experiment . B) dPAGE visualization of various cleavage bands for the reverse DNAzyme. The lane labelled Ladder contains eight sequences ranging from 56 – 64 nt.

4.4 Rolling Circle Amplification

The use of the RCD as a primer for RCA requires that two main issues be addressed. First, the CT must be able to compete effectively with the target for binding with the cleaved RCD, as target binding has previously been shown to inhibit RCA when using aptamers as primers.[8] Secondly, the rate of digestion of the cleaved product by endogenous nucleases in the CEM must be slow enough to allow the cleavage fragment to bind to the CT to initiate RCA. For both of these reasons, the specific binding region between the cleavage fragment and CT must be carefully optimized. For this reason, we evaluated a series of circular templates that all had 20-nt complementary regions to the release primer, but that bound at different regions in the cleavage fragment each separated by 5-nt, as shown in Figure 4.12A. Here, the cleavage

fragment is drawn in the 5' – 3' direction, and the schematic shows a series of CTs designed to bind from the 5' to the 3' end. In cases where the CT bound far from the 3' end, it was expected that phi29 DP would digest the 3' overhang and thus initiate RCA from the mature primer, which should avoid any issues with partial digestion of the pre-primer by endogenous nucleases in the HP CEM (Figure 4.12B).

Several additional factors were considered in designing the CT to maximize amplification efficiency. First, a CT size of 68-nt was chosen as it is sufficiently short to maximize amplification while containing an odd number of helical half-turns to maximize strain.[6] Second, sequence composition was skewed to contain more adenosine and cytosine nucleotides (65%-80 % adenosine and cytosine) based on the work by Mao *et al*.[7] Finally, as noted above, several CTs were complementary to internal sequences of the primer, which may be expected to aid in effectively displacing the bound target so that RCA was not inhibited.

A total of 10 CT sequences that were complementary to a distinct 20-nt portion of the cleavage product were evaluated both for their ability to bind to the cleavage product and their ability to initiate RCA. Figure 4.13A shows dPAGE gels that were used to assess the formation of a complex between the CT and the cleavage product. Interestingly, binding of the CT to either of the terminal ends seemed to be inhibited, as both CT1-CT3 and CT7-CT10 showed a substantial amount of free cleavage product and only very faint bands that would correspond to at complex, indicating that the CT was not able to form a primer-CT duplex in these cases. This may be due to the presence of secondary structure in the primer, which prevented binding of the CT1-CT3, or digestion of the 3' terminus which may prevent binding of CT7-CT 10. On the other hand, CT4 and CT5 do not result in a significant amount of free cleavage product, and the band associated with the free CT is shifted upward, providing evidence for complex formation.

It is also noted that CT1-CT3 also displayed and upward shift in the CT band, which likely indicates that the CTs with binding regions towards the 5' end of the primer may be better suited for this amplification assay.

To finalize CT selection, we compared the RCA-generated RP of the ten CTs during target-triggered cleavage for a defined period of time (1 hour), with the RP being detected by binding of the SYBR Gold intercalating dye. The RCA data shown in Figure 4.13B reveals two key trends. First, a trend of increasing RP production was observed going from CT1 to CT5, with CT5 generating the highest signal of any of the CTs. This roughly follows the trend observed in the formation of the CT-primer complex, and may indicate that CTs that bind closer to the centre of the primer are better able to compete with and thus displace the target from the primer. Second, the CTs all contain binding regions closer to the 5' end of the cleavage product, which is also the region that does not participate in substrate-strand annealing. Second, CT6-CT10 all produced low levels of RP, save for CT9 which showed high variance between amplification experiments. This trend suggests that CTs that target the 3' end of the primer likely cannot initiate RCA either owing to digestion of the binding region or an inability of the CT to displace the bound target, both of which will lead to an inability to generate a CT-primer complex. Based on these results CT5 was selected as the circular template for the remaining RCA experiments.

Following CT optimization several experiments were done to further optimize the performance of target-triggered amplification reaction. These included i) incorporating a 45-

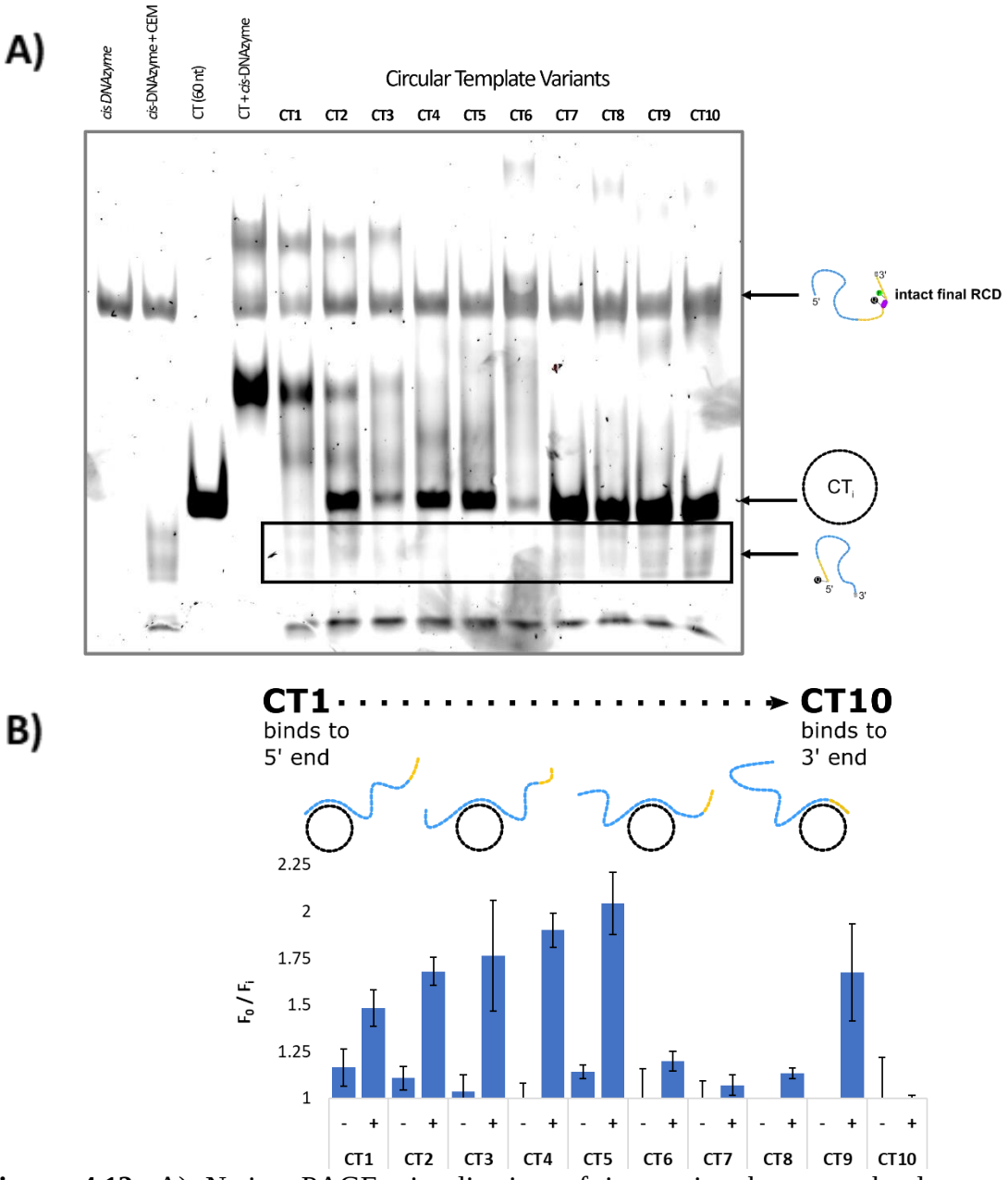

Figure 4.12. A) Native PAGE visualization of interaction between the large target-cleaved DNAzyme fragment (from 1 pmol intact RCD) and the ten (10) CT variants (2.5 pmol). The dotted box indicates where the free cleavage product that acts as a primer appears when unbound to the CT. B) Fluorescence response RP generated using ten (10) circular templates (5 pmol), assessed using SYBR Gold. (-) indicates a TSB blank, (+) indicates TSB-based CEM.

second 90°C heating step to aid in displacement of the bound target and annealing between the cleavage product and complementary CT, followed by room temperature RCA; ii) a 30- minute incubation with 1 μL 10 U/μL PNK at 37°C to remove any 2'-3' cyclic phosphate on the 3' terminus, which could inhibit RCA; iii) a combination of these two steps; or, iv) no post-cleavage steps. As shown in Figure 4.13A, no additional post-cleavage steps were required to obtain efficient amplification, indicating that the CT was able to displace any bound target, and further indicating that at least some fraction of the cleavage products did not contain the 2',3'-cyclic phosphate that could prevents amplification, supported by the presence of the shorter cleavage products observed in Figure 4.11. The ability to obtain amplification without additional processing steps makes the assay more straightforward and reduces user steps and the potential for user error.

Figure 4.13B compares the performance of equal amounts of a synthetic 20-nt primer and target-cleaved RCDs, along with a control using the uncleaved RCD. As expected, the free primer produced the highest rate of amplification, while the cleavage product showed slower amplification and the uncleaved RCD produced very little amplification. The lower rate for the cleavage product relative to the free primer is likely due to the need to both digest the 3' terminus prior to initiation of the RCA reaction, and possibly also the need to displace any bound target, which would be expected to retard the RCA reaction. Even so, the cleavage product clearly produced significant amounts of reaction product, while the intact RCD does not, leading to a useful platform for HP detection using the reversed RCD.

Finally, we evaluated the concentration dependence of RCA using CT5 as a template. As shown in Figure 4.13C, the assay provides a detection limit of at least 10^6 CFU/mL using a 40 min cleavage time followed by a 50 min amplification time, for a total assay time of 90 minutes.

These results are not competitive with previously reported RCA based assays for bacteria, which typically demonstrated LOD values of 1 – 1000 cfu/mL (though many of these used significantly longer amplification times), and in fact is on par with the unamplified fluorescence assay using the original HP RCD. Additional work will be required to further evaluate and optimized the RCA reaction, and incorporation of an exponential RCA method may be required to further decease the LOD.

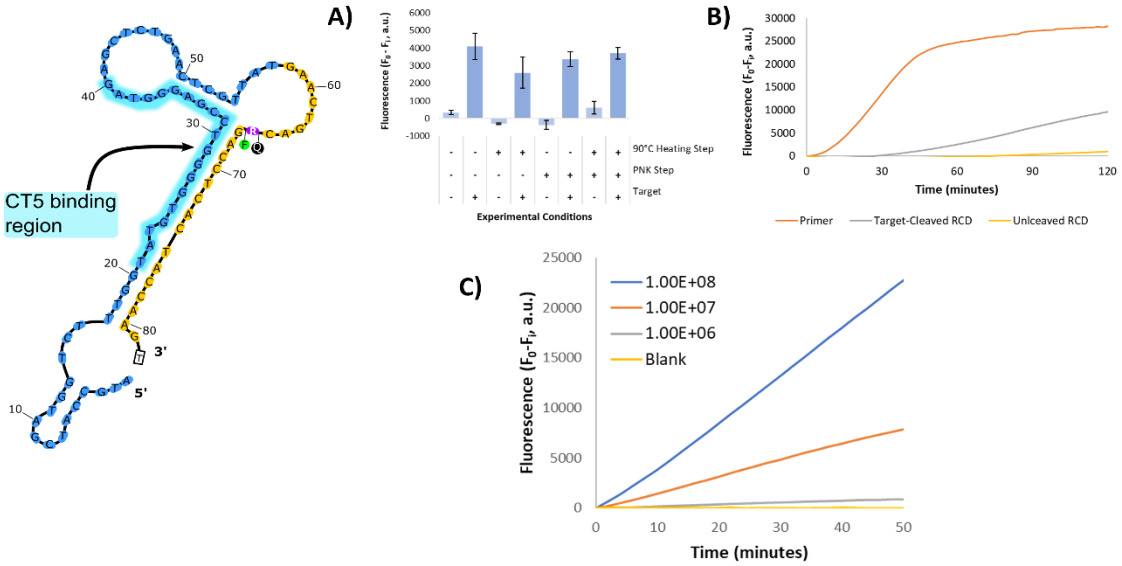

Figure 4.13. Fluorescence measurements of CT5 RP accumulation using SYBR Gold. A) Comparing the impact of post-cleavage treatment on RCA performance after 60-minutes. B) Real-time kinetic fluorescence data for the amplification reaction (1 pmol CT5, 2.5 mol RCD). This data compares the performance of equal concentrations of free primer (2.5 pmol, orange), RCD incubated with CEM (gray), and RCD incubated with TSB (yellow). C) Real-time kinetic fluorescence data indicating the increase in fluorescence during target-triggered RCD cleavage (1 pmol).

A further point to note is that we observed highly variable cleavage activity from different cultures of HP, which could also be a key factor impacting the LOD of the RCA reaction shown above. Bacterial culturing experiments used to generate target-rich CEM indicated that surprisingly, not every culturing procedure and resultant CEM could be used

induce significant cleavage of the optimized DNAzyme. Our culturing experiments indicated that many factors, including the bacterial strain, culture time, and presence of growth factors could impact the concentration of the specific DNAzyme target within a bacterial culture. Indeed, this work suggests that HP CEM may be far more sensitive to culturing conditions relative to previous CEMs for bacteria such as E. coli, which has been observed to display cleavage activity for the EC1 DNAzyme that is essentially insensitive to culture conditions.[9,10] The sensitivity of target generation to culture conditions has not yet been widely examined as a factor controlling cleavage of bacterial DNAzymes, and clearly shows that further work is needed to identify the specific targets that are activating DNAzymes within CEMs. In addition, these findings indicate that the culturing conditions of bacteria used for DNAzyme selection must be well controlled to ensure that: i) the culturing conditions reproducibly induce clinically relevant biomarkers and ii) these biomarkers are proportional to cell concentration and therefore can be used to quantify the analyte.

[1] M. M. Ali, M. Wolfe, K. Tram, J. Gu, C. D. M. Filipe, Y. Li, J. D. Brennan, *Angew. Chemie Int. Ed.* **2019**, *58*, 9907–9911.

[2] J. Méndez, L. Blanco, M. Salas, *EMBO J.* **1997**, *16*, 2519–2527.

[3] J. Zhang, *Catal. 2018, Vol. 8, Page 550* **2018**, *8*, 550.

[4] M. Liu, Q. Zhang, Z. Li, J. Gu, J. D. Brennan, Y. Li, *Nat. Commun.* **2016**, *7*, 12074.

[5] N. Carmi, L. A. Shultz, R. R. Breaker, *Chem. Biol.* **1996**, *3*, 1039–1046.

[6] B. Joffroy, Y. O. Uca, D. Prešern, J. P. K. Doye, T. L. Schmidt, *Nucleic Acids Res.* **2018**, *46*, 538–545.

[7] Y. Mao, M. Liu, K. Tram, J. Gu, B. J. Salena, Y. Jiang, Y. Li, *Chem. - A Eur. J.* **2015**, *21*, 8069–8074.

[8] R. M. Bialy, M. M. Ali, Y. Li, J. D. Brennan, *Chem. - A Eur. J.* **2020**, *26*, 5085–5092.

[9] Z. Shen, Z. Wu, D. Chang, W. Zhang, K. Tram, C. Lee, P. Kim, B. J. Salena, Y. Li, *Angew. Chemie Int. Ed.* **2016**, *55*, 2431–2434.

[10] I. Cozma, E. M. McConnell, J. D. Brennan, Y. Li, *Biosens. Bioelectron.* **2021**, *177*, 112972.

CHAPTER 5 | CONCLUSION AND FUTURE WORK

The key goal of this thesis was to utilize the *H. pylori* RCD previously developed within this laboratory to regulate the initiation of rolling circle amplification as a way to improve the original limit of detection reported using unamplified fluorescence-based assays. A total of three different approaches were investigated to regulate RCA through RCD-mediated primer release. The first approach utilized a *cis*-RCD design that was essentially identical to that explored in the original work. The expectation was that the smaller of the two cleavage products could be utilized as a primer for RCA, however the results indicated that there the primer was rapidly digested upon formation, likely due to endogenous nucleases present in the *H. pylori* CEM.

To address the above issue with primer degradation we modified the RCD design into a *trans* arrangement, with the substrate sequence being circularized and catenated with the circular template in a topologically constrained structure. We anticipated that the cleavage of the circularized substrate would produce a pre-primer that could be digested by phi29 DP to produce a mature primer that would be able to initiate RCA using the bound CT. However, we found that the *trans*-RCD was unable to cleave the circular ssDNA substrate, and thus did not produce observable RCA.

A final method, which was able to produce robust RCA, utilized a redesigned *cis*-RCD wherein the substrate region was moved from the 5’ end of the original RCD to the 3’ end of the new RCD. For the first time, we showed that a *cis*-RCD can feature the substrate strand on either terminal end of the RCD, regardless of its location during *cis*-DNAzyme selection, and then used to initiate RCA. Evaluation of this RCD demonstrated that the RCD was able to cleave the substrate in a target-dependent manner, and that the long cleavage fragment, which contained

the original RCD and possibly the bound target, was able to regulate a target-dependant RCA reaction. These results are the first to show that a RCD sequence can act as a primer for RCA, and also demonstrated that this longer primer was not susceptible to digestion by nucleases within the HP CEM, overcoming the issues with the original RCD. In addition, the use of the longer RCD fragment avoided the need for either heating steps or PNK treatment that have previously been required for other DNAzyme-regulated RCA assays. However, preliminary data on the sensitivity of the RCA-based assay for HP did not provide an improved detection limit relative to the original unamplified fluorescence assay, indicating that further optimization of the reaction conditions will be required.

While it was possible to design a DNAzyme-regulated RCA assay using the HP DNAzyme, several challenges were identified in this work. Firstly, this work was the first to identify potential issues with nucleases present in bacterial CEM. While it is generally expected that the SELEX process will tend to identify DNAzymes that are nuclease resistant, the selection method is not designed to prevent digestion of cleavage fragments, which in this work negated the ability to use a short cleavage fragment as a primer for RCA. Secondly, this work clearly revealed the challenges related to moving from an original *cis*-RCD to a *trans*-form of the RCD. It is clear that substantial re-optimization of the *trans*-RCD is likely to be required to produce substantial cleavage activity, a process that would likely be extremely time-consuming. In the work presented here, the most reasonable alteration to the *trans*-RCD would likely be incorporation of a longer binding arm on the RCD to aid in hybridization to the circularized substrate. However, other modifications including redesign of the circular substrate may also be needed, making optimization challenging. Third, while the rearranged *cis*-RCD was able to produce the desired cleavage fragment that could regulate RCA, the data presented herein

suggest that the RCA-based assay did not result in improved detection limits, which could indicate slower cleavage, a reduced rate of primer binding to the CT (owing to the need to remove the bound target), or slower processing of the phi29 DP. While these possibilities were not explored in detail, there is a need to better understand each of these steps in order to optimize the RCA reaction. Finally, this work was the first to demonstrate that the concentration of target in a CEM can be sensitive to the specific culturing conditions used to produce the CEM. It was observed that in some cases the CEM did not produce any cleavage of the RCD, bringing into question the use of unknown targets as markers to quantify bacterial concentration, and clearly demonstrating the need for additional work to identify RCD-activating targets within CEMs.

To further improve sensitivity, future work could include modifying the RCA step to include an exponential amplification process (E-RCA), which could improve detection limits by 3 or more orders of magnitude. Additionally, as described in Chapter 2, it is possible to use a different output method, which could include colorimetric or electrochemical outputs, that may aid in improving detection limits. In addition, the RCA assay could be integrated with a device such as a paper-based sensor or microfluidic device to aid in sample processing or other steps that would be needed to more easily assess clinical samples, as was reported in the original report on the HP DNAzyme. Such studies will be the basis of future work in our group.